NASA CR - 182148

NASA

SPACE PLASMA CONTACTOR RESEARCH - 1987

Prepared for

LEWIS RESEARCH CENTER

NATIONAL AERONAUTICS AND SPACE ADMINISTRATION

Grant NAG3-776

Annual Report

January 1988

Paul J. Wilbur
Department of Mechanical Engineering
Colorado State University
Fort Collins, CO 80523

1. Report No.	2. Government Accession No.	3. Recipient's Catalog No.
NASA CR-182148		

4. Title and Subtitle	5. Report Date
SPACE PLASMA CONTACTOR RESEARCH - 1987	Jan. 1988
	6. Performing Organization Code

7. Author(s)	8. Performing Organization Report No.
Paul J. Wilbur	10. Work Unit No.

9. Performing Organization Name and Address	11. Contract or Grant No.
Department of Mechanical Engineering Colorado State University Fort Collins, CO 80523	NAG3-776
	13. Type of Report and Period Covered Annual Jan. 1, 1987-Jan. 1, 1988
12. Sponsoring Agency Name and Address	14. Sponsoring Agency Code
National Aeronautics and Space Administration Washington, D.C. 20546	

15. Supplementary Notes

Grant Monitor - Michael Patterson, NASA Lewis Research Center
Cleveland, Ohio 44135

16. Abstract

A simple model describing the process of electron collection from a low pressure ambient plasma in the absence of magnetic field and contactor velocity effects is presented. Experimental measurements of the plasma surrounding the contactor are used to demonstrate that a double-sheath generally develops and separates the ambient plasma from a higher density, anode plasma located adjacent to the contactor. Agreement between the predictions of the model and experimental measurements obtained at electron collection current levels ranging to 1 A suggests 1) the surface area at the ambient plasma boundary of the double-sheath is equal to the electron current being collected divided by the ambient plasma random electron current density, 2) the surface area of the higher density anode plasma boundary of the double-sheath is equal to the ion current being emitted across this boundary divided by the ion current density required to sustain a stable sheath, and 3) the voltage drop across the sheath is determined by the requirement that the ion and electron currents counterflowing across the boundaries be at space-charge limited levels.

The efficiency of contactor operation is shown to improve when significant ionization and excitation is induced by electrons that stream from the ambient plasma through the double-sheath and collide with neutral atoms being supplied through the hollow cathode. Deficiencies that develop in the model, when tests are conducted at different neutral atom and plasma densities and at higher electron collection currents than those used for the bulk of the tests, are pointed out.

17. Key Words (Suggested by Author(s))	18. Distribution Statement
Hollow Cathode Electrodynamic Tether Plasma Contactor	Unclassified-Unlimited

19. Security Classif. (of this report)	20. Security Classif. (of this page)	21. No. of pages	22. Price*
Unclassified	Unclassified	83	

*For sale by the National Technical Information Service, Springfield, Virginia 22161

TABLE OF CONTENTS

LIST OF FIGURES

ELECTRODYNAMIC TETHER PLASMA CONTACTOR RESEARCH

John D. Williams

INTRODUCTION

Two critical components of an electrodynamic tether system are the plasma contactors located at opposite ends of the tether itself. They provide the electrical connection to the ionosphere, one emitting electrons and collecting ions and the other collecting electrons and emitting ions. Contactors should provide a good connection to the space plasma because a voltage drop between either contactor and the space plasma that is comparable to the voltage drop across the system load will cause a substantial degradation in system efficiency. In order to be able to design contactors with low voltage drops so high efficiencies can be assured it is necessary to understand how changes in operating parameters can change contactor performance. One obvious way to study plasma contactors and as a result develop this understanding is to conduct tests in ground-based vacuum facilities in which ionospheric conditions are simulated. Models can then be developed that describe results obtained in these tests. Unfortunately, one cannot adequately simulate the very low plasma density, diverse composition and large extent of typical ionospheric plasmas in currently available laboratory facilities. If models of the plasma contacting process are used to normalize experimental results, however, valuable insights into this process can be obtained from such ground-based tests. Once these models have been developed and then verified in space tests, they can be used to design and predict the performance of space-based contactors.

The specific objective of the work to be described here has been to develop an understanding of the "near-field" plasma contacting process

that can be applied to ambient space plasma conditions to predict how plasma contactors should perform in space. This understanding should not only facilitate the design of efficient plasma contacting devices suitable for specific electrodynamic tether systems, but it should also suggest how contactor operating parameters might be adjusted to effect system control. The term "near-field" is applied here because the theory being developed is based on experimental observations obtained in an environment where no significant magnetic fields are present and the contactor is stationary relative to the ambient space plasma. It is expected that such a model describes phenomena that occur in the region close to the contactor where the effects of magnetic field and plasma velocity are shielded out. The task of merging this model with one that describes far-field phenomena where magnetic field and plasma velocity effects are important[1] remains to be done.

THEORY

The manner in which a hollow cathode-based plasma contactor couples to an ambient plasma can be described by considering three separate regions which are associated with the plasma contacting process.[2] The first of these regions is in intimate contact with the plasma contactor and is termed the "high density plume region". This term is used to suggest that the plasma density, which is sustained by ionization occurring close to the contactor, generally exceeds the density of the ambient plasma with which contactor is exchanging charge. This "ambient plasma," which would be the ionospheric plasma for a contactor being used in a space application, will be assumed to have uniform plasma properties that are not perturbed significantly by current flowing to or from the contactor. Separating the ambient plasma and high density

plume regions is a double-sheath region, across which a voltage drop is sustained and through which the current being conducted between the high density plume and ambient plasma regions flows. The current flowing through the double-sheath region will be assumed to be limited by space-charge effects at both the ambient plasma and high density plume boundaries. Assuming that the contactor couples to the ambient plasma in a spherical geometry as suggested by Fig. 1, simple models of the plasma contacting process can be developed which have been shown to be in reasonable agreement with experimental results.[2,3] Figure 1 actually shows the contactor operating in the electron collection mode (i.e. the mode in which electrons flow from the ambient plasma to the high density plume and ions flow from the high density plume to the ambient plasma). The contactor can also be operated in the electron emission mode in which electrons flow from the contactor to the ambient plasma and ions counterflow from the ambient plasma to the high density plume and then to a contactor surface. It has been shown in a space environment that large electron currents can be easily emitted to an ambient plasma from a hollow cathode at relatively low potential differences[4] and, consequently, this research program has focused primarily on the electron collection mode. A model of the process of collecting electrons from a uniform ambient plasma using a hollow cathode plasma contactor was proposed during the grant period covered by this report. The details of this model together with descriptions of experiments conducted to verify it were organized into two formal papers that are reproduced in Appendices A and B of this report and the detailed information they contain will only be summarized and cited in the body of this report. The most complete description of the model as it has been developed up to this point is contained in Appendix A while the

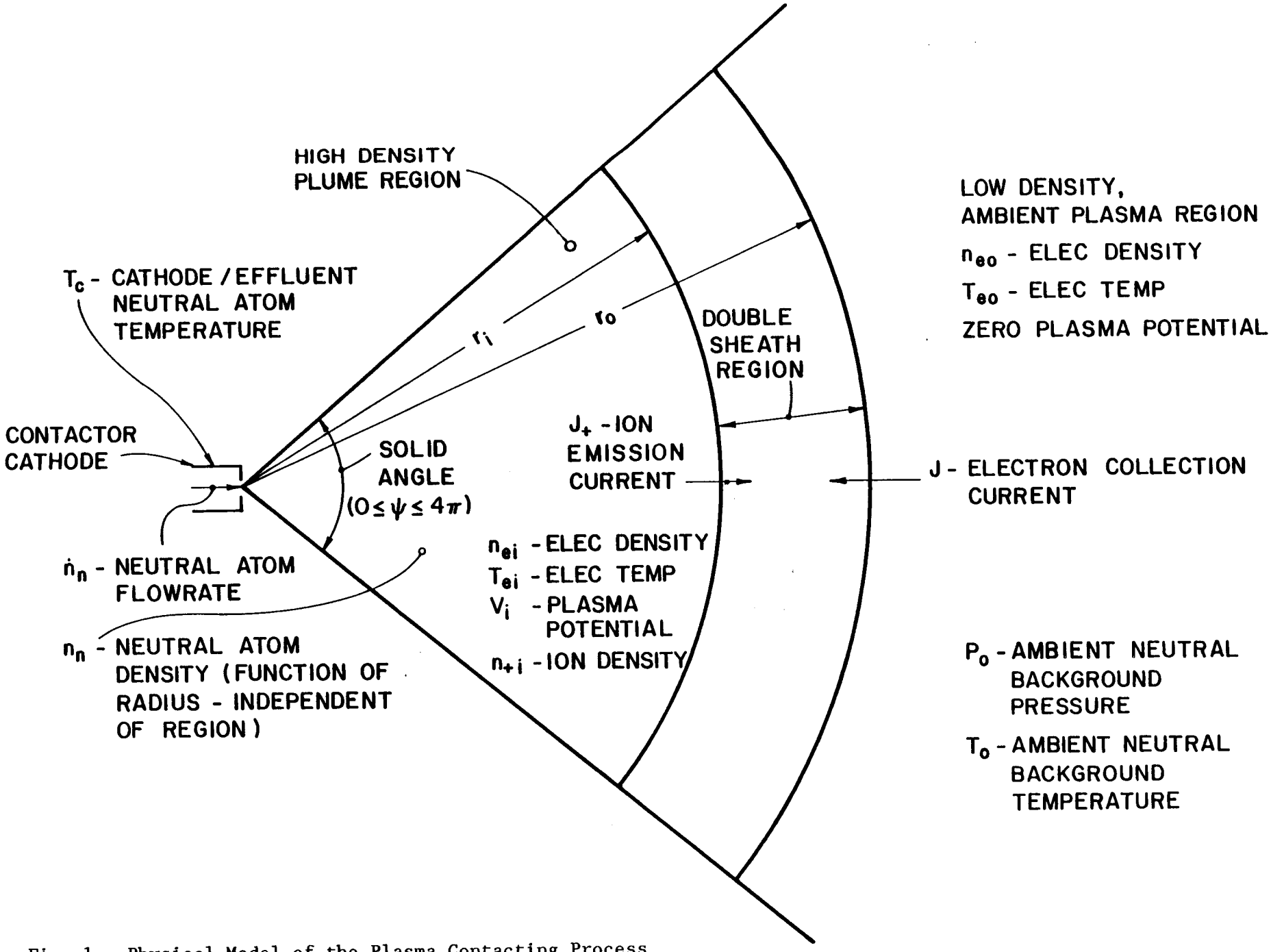

Fig. 1. Physical Model of the Plasma Contacting Process

paper in Appendix B contains a summary of key elements of the model and some details of the experimental techniques and equipment used in conducting the tests.

The simple model of the electron collection process represented in Fig. 1 involves electron flow from the ambient plasma region to the more positive high density plume region through a spherical segment characterized by a solid angle ψ. It is assumed that the electron current flowing from the ambient plasma is equal to the random electron current density in the ambient plasma times the surface area of the double-sheath boundary exposed to the ambient plasma. This fact is expressed mathematically by the equation

$$J = \frac{1}{4} e\, n_{eo} \psi\, r_o^2 \sqrt{\frac{8\, k\, T_{eo}}{\pi\, m_e}} \quad . \tag{1}$$

In Eq. 1, e, m_e and k are the electronic charge and mass and Boltzmann constant, respectively; n_{eo} and T_{eo} are the ambient plasma electron density and temperature, respectively; and $\psi\ r_o^2$ is the area of the double-sheath outer boundary which is exposed to the ambient plasma. Given values for the ambient plasma electron density n_{eo} and temperature T_{eo} and the electron current J which is being collected, Eq. 1 can also be used to solve for the outer boundary radius of the double-sheath r_o for assumed values of ψ. Note that the total current flowing in the system is actually the sum of the ion current leaving the high density plume and the electron current leaving the ambient plasma, but because the ion current is very small compared to the electron current it is reasonable to assume that the total current flowing in the system is equal to the electron current. An important consequence of Eq. 1 is the

fact that the radius of the outer boundary for a contactor collecting a fixed current depends on the ambient plasma conditions only. This radius is independent of the contactor and its operating conditions provided the extent of the ambient plasma is sufficiently great so contactor operation does not perturb ambient plasma conditions significantly. One would expect this condition to be met in the space environment even though it is frequently not satisfied in the laboratory where changes in contactor operating conditions can influence the ambient plasma density and temperature.

The ion emission current shown flowing to the inner boundary of the double-sheath from the high density plume region in Fig. 1 can be found by realizing that the ions will approach the sheath from this region at the Bohm velocity[5] in order for a stable sheath to exist. Using this assumption the ion current is given by

$$J_+ = \gamma\, e\, n_{+i} \psi\, r_i^2 \sqrt{\frac{k\, T_{ei}}{m_+}} \quad . \tag{2}$$

In Eq. 2, n_{+i} and T_{ei} are the ion density and electron temperature of the high density plume, respectively; m_+ is the ion mass; r_i is the radial location of the double-sheath inner boundary; and γ is a pre-sheath correction factor which can vary from 0.1 to 1 depending upon the plasma conditions within the high density plume.[2,6,7] As mentioned in the introduction, increases in the ion emission current described by Eq. 2 induce an increase in the radius of the inner sheath boundary r_i. For a contactor operating at a fixed electron collection current in a space plasma environment, the outer sheath boundary radius remains fixed so this means the sheath thickness decreases and as a consequence the

potential difference required between the contactor and the ambient space plasma to induce the desired electron collection current decreases.[9] Because the ions flowing through the double-sheath play an important role in controlling this sheath potential drop it is important to understand the ion production and loss mechanisms that are important in the high density plume region.

Ion production can occur when contactor discharge electrons experience inelastic collisions with neutral atoms near the orifice of the hollow cathode. Because these ions are formed in the high density plume region (Fig. 1) near the cathode and anode of the contactor, many recombine on these surfaces and do not escape through the double-sheath. Ions can also be produced in the high density plume by electrons streaming from the ambient plasma which experience inelastic collisions with neutral atoms before they are collected at the contactor anode or some other surface. It is believed that the streaming electrons produce ions closer to the inner boundary of the double-sheath (further downstream of the contactor) than do the discharge electrons and it is suggested therefore that ions produced by streaming electrons are more likely to escape from the high density plume region through the double-sheath. It is noted that the production of ions at a significant rate by the streaming electrons is accompanied by the development of luminosity within the high density plume and as a result operation in this condition has been termed the "ignited mode"[8] of plasma contactor operation. One would expect this luminosity because of the contactor expellant gas excitation/de-excitation processes that accompany ionization.

Substantial ion production induced by the streaming electrons occurs when 1) streaming electrons acquire sufficient energy as they

pass through the double-sheath to induce ionization and excitation and 2) the density of expellant atoms in the high density plume is relatively high so the probability that these collisions will occur is significant. The expression developed in Appendix A which gives the ion production rate due to streaming electrons is

$$J_{+p} = J \frac{\sigma_+}{\sigma_{in}} \left[1 - \exp\left\{ -\sigma_{in} \left\{ \frac{\dot{n}_n}{\psi v_n} \left(\frac{1}{\delta} - \frac{1}{r_i} \right) + \frac{P_o}{k T_o} (r_i - \delta) \right\} \right\} \right] \qquad (3)$$

Where σ_+ and σ_{in} are, respectively, the ionization and inelastic collision cross-sections evaluated at the streaming electron energy (i.e. the sheath potential drop); $\dot{n}_n$ and v_n are the neutral atom flowrate and thermal velocity of the neutral atoms, respectively; P_o and T_o are the neutral atom pressure and temperature of the ambient background gas, respectively; and δ is a small distance downstream of the contactor within which ions that are produced fall toward and recombine on cathode or anode surfaces rather than being drawn toward the double-sheath. This distance would be expected to be of the order of the Debye length associated with the plasma in this region, but for the present it will be left as an unspecified small distance.

The neutral density variation through the high density plume which has been prescribed in order to develop Eq. 3 is represented as a point-source of neutral atoms expanding freely from the cathode orifice through the solid angle ψ into a neutral background gas at a flowrate $\dot{n}_n$. The neutral atom density profile n_n that develops as a function of radius r within the high density plasma and double-sheath regions shown in Fig. 1 as a consequence of this neutral atom flow is described mathematically by the equation

$$n_n = \frac{\dot{n}_n}{\psi v_n r^2} + \frac{P_o}{k T_o} \quad . \tag{4}$$

The neutral atom thermal velocity v_n in this equation is assumed to be determined by the hollow cathode temperature T_c (Fig. 1) on the basis that neutral atoms flowing through the hollow cathode will probably come into thermal equilibrium with it because of their low flowrate (i.e.

$$v_n = \sqrt{\frac{8 k T_c}{\pi m_n}} \quad .$$

The first term on the right-hand side of Eq. 4 describes the variation in density due to the neutral atom flowrate and the second term imposes the ambient background neutral atom density associated with the ambient neutral gas pressure (P_o) and temperature (T_o).

The double-sheath region separating the high density plume and ambient plasma regions shown in Fig. 1 has been modeled using a general solution to the spherical, space-charge limited double-sheath problem.[9] In order to obtain a description of the phenomena involved without introducing unnecessary complexity into this preliminary model, several simplifying assumptions have been made. Specifically, for the case of the electron collection mode of operation being considered here, these assumptions are that 1) there is an infinite supply of zero velocity electrons with mass m_e at the outer boundary of the sheath (i.e. at the surface with radius r_o), 2) there is an infinite supply of zero velocity ions with mass m_+ at the inner sheath boundary (i.e. at r_i), 3) no collisions occur as these two groups of particles counterflow through

the double-sheath region and 4) the electric fields at both the inner and outer sheath boundaries are zero (i.e. the space-charge condition limits current flow on one particle group at each boundary). It is noted with regard to the first two assumptions that the condition of an infinite supply (density) of charged particles having zero velocity at a boundary represents an approximation that facilitates analysis. If complete analysis of pre-sheath regions had been undertaken rather than making these assumptions, the problem would have been more complicated than can be justified for this preliminary, first-order analysis.

The principal result of Ref. 9 developed on the basis of the four assumptions listed in the preceeding paragraph are Eqs. 5 and 6. Equation 5 describes the electron collection current J drawn through the sheath as a function of the sheath potential drop V_i and Eq. 5 describes the ion emission current J_+ which will counterflow at the doubly space-charge limited condition in terms of the electron current J.

$$J = \psi \epsilon_o V_i^{3/2} \left[\frac{2e}{m_e}\right]^{1/2} j_o \tag{5}$$

$$J_+ = J \left[\frac{m_e}{m_+}\right]^{1/2} (\alpha)^{-1} \tag{6}$$

The parameters j_o and α in Eqs. 5 and 6, which depend only upon the radius ratio r_i/r_o, have been determined numerically in Ref. 9 and plots of both j_o and α versus radius ratio reproduced from Ref. 9 are contained in Appendix A. A plot of j_o versus radius ratio which has been expanded to include values of j_o very close to radius ratios of unity, is also given in Fig. 2. This plot was made so that plasma

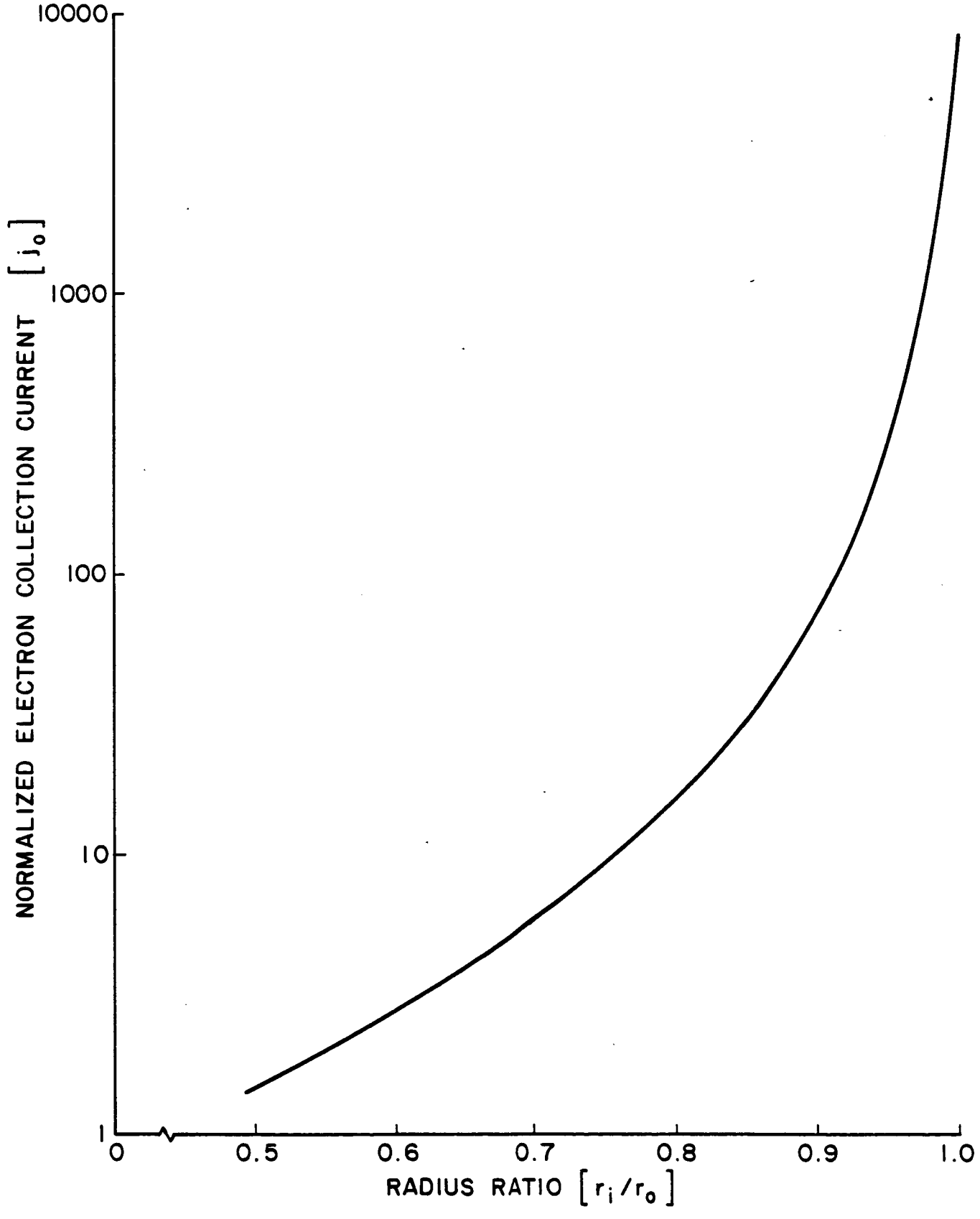

Fig. 2. Expanded Plot of Normalized Electron Collection Current vs. Radius Ratio (from Ref. 9)

contactors operating at relatively high electron collection currents and low sheath potential drops (a mode of operation which theoretically should display radius ratios approaching unity) could be studied using the model.

In this report the magnitudes and ratios of radii associated with inner and outer boundaries of double-sheaths measured over a wide range of operating conditions in a laboratory environment will be compared to corresponding magnitudes and ratios of radii computed at these operating conditions using the theoretical model outlined in the preceeding paragraphs. The degree of agreement between measured and calculated magnitudes of inner sheath boundary radii will be used as the criterion to evaluate the portion of the model that describes ion losses to this boundary at the Bohm velocity. Similarly the degree of agreement between the magnitudes of outer sheath boundary radii and the ratio of the radii will be used to argue respectively about the validity of the collection of electrons travelling at thermal velocities in the ambient plasma and the doubly space-charge limited ion and electron flow under the influence of the sheath potential drop. Evidence of shortcomings associated with the model will also be sought. These will include deficiencies related to the simplified geometry that has been used in developing it as well as basic conceptual deficiencies.

APPARATUS AND PROCEDURE

In order to test hollow cathode-based plasma contactors the apparatus shown in Figs. 3, 4, and 5 was constructed. The test apparatus shown schematically in Fig. 3 consists of two hollow cathode devices, one used to generate a dilute ambient plasma (shown on the right and labelled "simulator") and the other used to couple to the

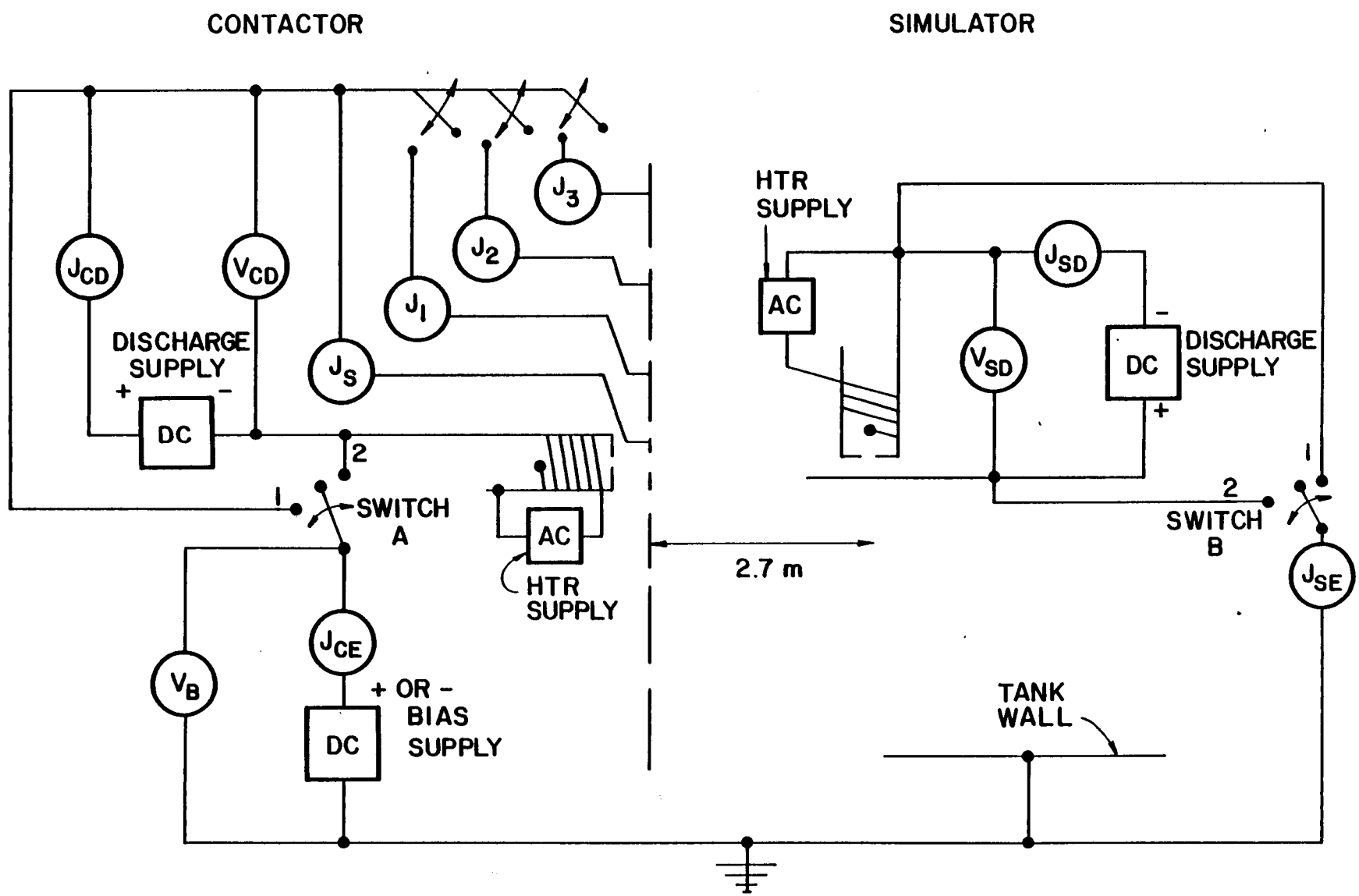

Fig. 3. Electrical Schematic Diagram

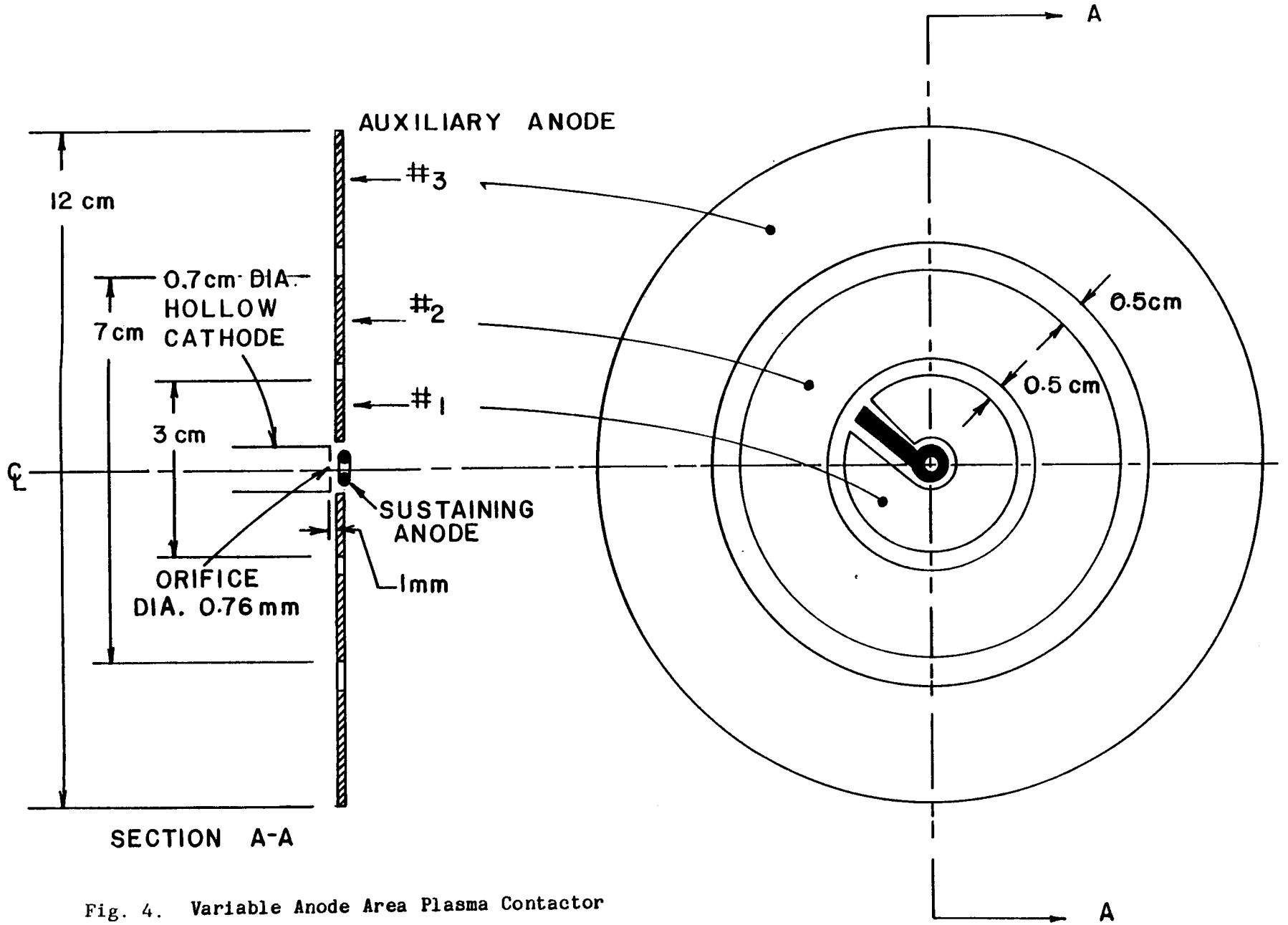

Fig. 4. Variable Anode Area Plasma Contactor

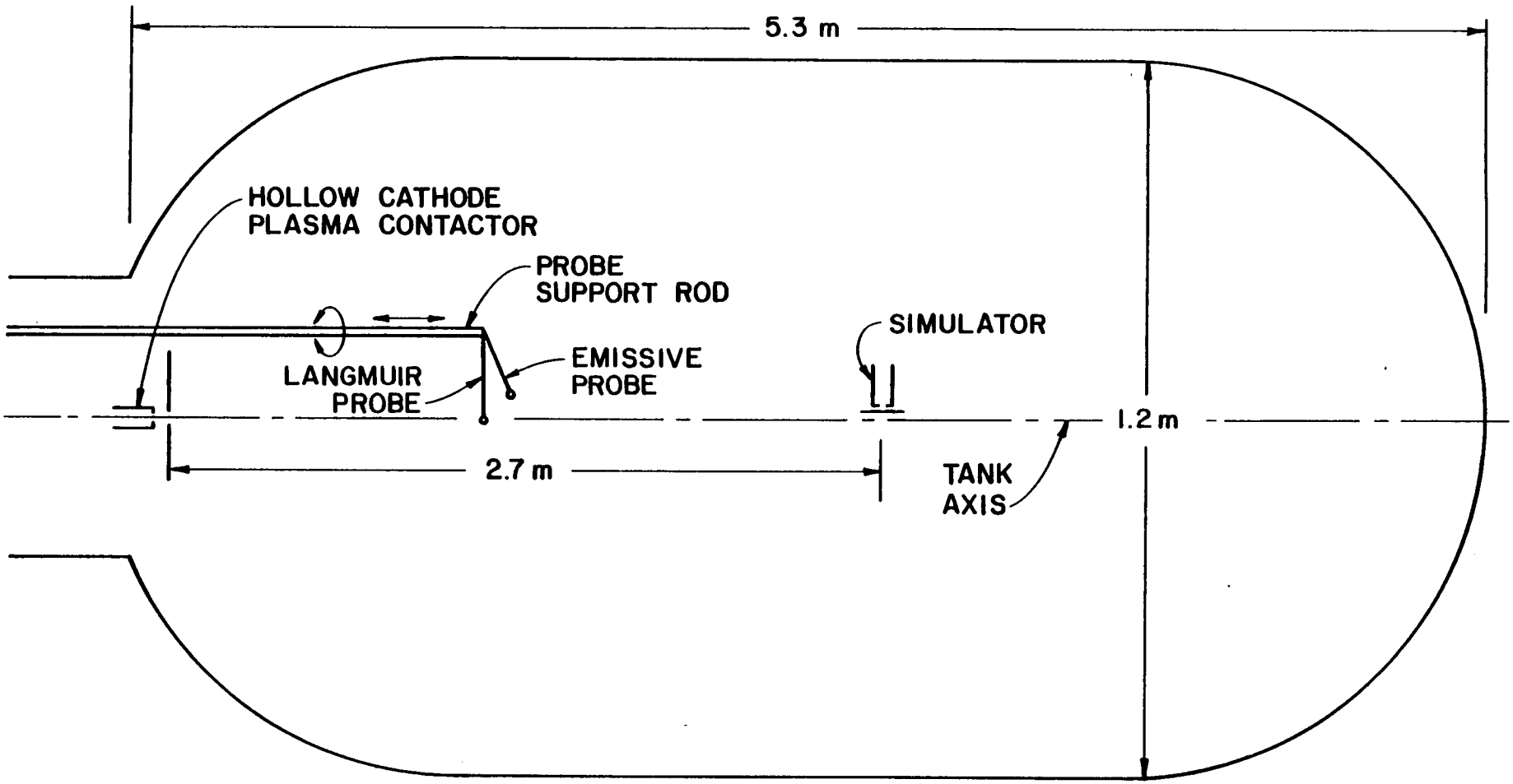

Fig. 5. Mechanical Schematic Diagram

dilute ambient plasma (shown at left and labelled "contactor"). The space plasma simulator hollow cathode consists of a 6.4 mm diameter tantalum tube equipped with an orifice plate which has a 0.38 mm dia orifice orifice hole drilled through its center. The anode of the simulator is a 30 mm dia flat plate made of tantalum oriented parallel to and ~2 mm downstream of the cathode orifice plate. The simulator hollow cathode utilizes a heater to maintain the temperature of its insert (made of rolled tantalum foil treated with Chemical R-500) and a discharge power supply to sustain an electrical discharge between the anode and the insert which is connected electrically to the hollow cathode body and orifice plate.

The plasma contactor hollow cathode, which is similar to the space plasma simulator hollow cathode, consists of a 6.4 mm tantalum tube equipped with an orifice plate which has a 0.76 mm diameter orifice hole drilled through its center. The contactor anode differs from the one on the simulator in that it is segmented into four separate anodes (see Fig. 4) which can be individually held at anode potential or allowed to float by using the anode switches shown in Fig. 3. This anode design was chosen so the effects of changing the anode area on the plasma contacting process could be studied. The bias power supply shown directly below the contactor in Fig. 3 is used to bias the contactor with respect to the simulated space plasma, simulator, and the vacuum tank wall in order to force a current to be conducted between the contactor and simulated plasma. The squares shown in Fig. 3 represent the various power supplies required to perform experiments and the circles represent electrical meters used to measure the various currents and voltages of interest in the tests.

The two switches labelled A and B in Fig. 3 are used to connect the contactor anode to the bias supply output and the simulator cathode to the tank wall (position 1) when the contactor is operating in the electron collection mode (bias supply output positive) and the contactor cathode to the bias supply output and the simulator anode to the tank wall (position 2) when the contactor is operating in the electron emission mode (bias supply output negative). By positioning these switches in the manner just described one avoids the imposition of limitations on the contactor and simulator emission currents (J_{CE} and J_{SE}) when the contactor and simulator discharge currents (J_{CD} and J_{SD}) are being controlled.[3,10]

Emissive and Langmuir probes, which are used to measure the plasma properties in the region between the contactor and the simulator, are shown in Fig. 5. The probe support rod which is shown was designed to position the probes along the tank centerline from a location within ~1 cm of the contactor anode plane to one within ~10 cm of the simulator anode. The probe support rod can also be rotated thereby allowing the probes to be positioned within the region extending to radial locations up to ~30 cm from the tank centerline over the same axial range. The emissive probe was used to measure plasma potential and was designed and operated in the manner described by Aston.[11] The emissive probe output (probe floating potential) was sensed by the Y-axis of an X-Y recorder at the same time the axial probe position was detected by a potentiometer and transmitted to the X-axis of the recorder. By using this apparatus, continuous plasma potential versus distance traces were obtained. By positioning the emissive probe at various radial locations, plasma potential contour maps of the region surrounding the contactor could also be obtained.

The Langmuir probe circuitry used for these tests is the same as that described by Laupa,[12] but the experimental procedure used to collect the data differed from the procedure he used. In the present case the plasma potential was first recorded with the emissive probe. Next, a 0.32 cm dia spherical Langmuir probe was rotated into the position where the plasma potential had been measured and a retarding region Langmuir current/voltage trace was obtained by biasing the probe below this plasma potential and inputting the resulting probe current/voltage data to an X-Y recorder. This procedure is preferred because analysis of the Langmuir trace is simplified considerably when the plasma potential (known from the emissive probe measurement) can be used to analyze the Langmuir probe data. This is especially true in low density plasmas where thick electron collection sheaths grow around the probe at positive probe biases making plasma potential determination from the Langmuir trace difficult.

The experimental procedure used to test plasma contactors in ground-based laboratories was initiated by first starting both the contactor and simulator hollow cathode devices. Typically, the simulator operating conditions were held constant with a flowrate $\dot{m}_s$ of 1.9 standard cubic centimeters per minute (sccm) of Xenon (Xe) and a discharge current J_{SD} of 0.3 A. These conditions together with a cathode heater power of ~55 W resulted in a simulator discharge voltage in the range between ~10 and 20 V. On the other hand, the contactor operating conditions, which were varied parametrically during typical experiments, were set at the first test point conditions of flowrate ($\dot{m}_c$) and discharge current (J_{CD}). Next, the bias supply was used to hold the contactor at a given potential (within the range ±150 V with respect to the vacuum tank ground) while the electron emission current

indicated by the meter labelled J_{CE} in Fig. 3 was recorded. At this operating condition a plasma potential profile within the region between the contactor and simulator was generally recorded using the emissive probe. Finally, Langmuir probe traces were obtained at several locations between the contactor and simulator. Once all the data at this operating condition had been recorded, the bias potential was changed and the procedure was repeated. After the contactor had been completely characterized over the bias potential range of interest at the given flowrate, discharge current, and anode area, the contactor operating conditions and/or anode area were changed and the procedure was repeated.

In addition to the above experiments, the manner in which the expellant flowing from the contactor hollow cathode expands was investigated using the following procedure which was carried out when the contactor and simulator discharges were extinguished. A nude Phelps/Schultz pressure gauge, mounted on the probe support rod in place of the emissive and Langmuir probes shown in Fig. 5, was used to measure the pressure. The pressure indicated by the Phelps/Schultz gauge along with corresponding probe position data were fed to an X-Y recorder so continuous traces of pressure as a function of axial position could be obtained. The process of collecting axial pressure profiles was repeated at several radial locations so an axisymmetric pressure map could be generated. This pressure map was then converted to a neutral atom density map by assuming the neutral atoms that passed through the cathode left it at the cathode temperature (~1300 K) and that the total neutral atom density consisted of this high temperature component superimposed on a uniform ambient component. The ambient component was computed using the ambient pressure assuming the ambient neutral atoms

were in equilibrium with the vacuum tank walls at a temperature of ~300 K.

RESULTS

Background

The performance of a contactor can be judged by how efficiently (i.e. at what potential drop) it exchanges current with a relatively diffuse ambient plasma. In general, the contactor performance as an electron emitter is displayed by plotting the electron current it emits as a function of its potential. In the experiments to be described, the contactor electron emission current J_{CE} will be plotted on the y-axis and the contactor potential measured with respect to the ambient plasma potential will be plotted on the x-axis. This contactor potential is defined as the bias power supply output (V_B in Fig. 3) minus the plasma potential (V_P) measured in the region downstream of the double-sheath relative to tank ground. Note that an ideal contactor would display a current/voltage characteristic curve which is close to a vertical line at zero potential on this type of plot. By convention electron current emitted and ion current collected by the contactor will be designated as positive current and electron current collected and ion current emitted by the contactor will be designated as negative current.

The typical current/voltage characteristic curve shown in Fig. 6 was obtained using a contactor operating at a discharge current J_{CD} and voltage V_{CD} of 0.3 A and 12 to 20 V, respectively, when the contactor flowrate $\dot{m}_c$ was 4.1 sccm (Xe) and the corresponding ambient tank pressure P_o was 5×10^{-6} Torr. For this test the anode diameter was 12 cm (i.e. all of the anodes shown in the contactor diagram of Fig. 4 were held at anode potential). Figure 6 shows that this contactor exhibits a characteristic curve that is close to the ideal one in the electron

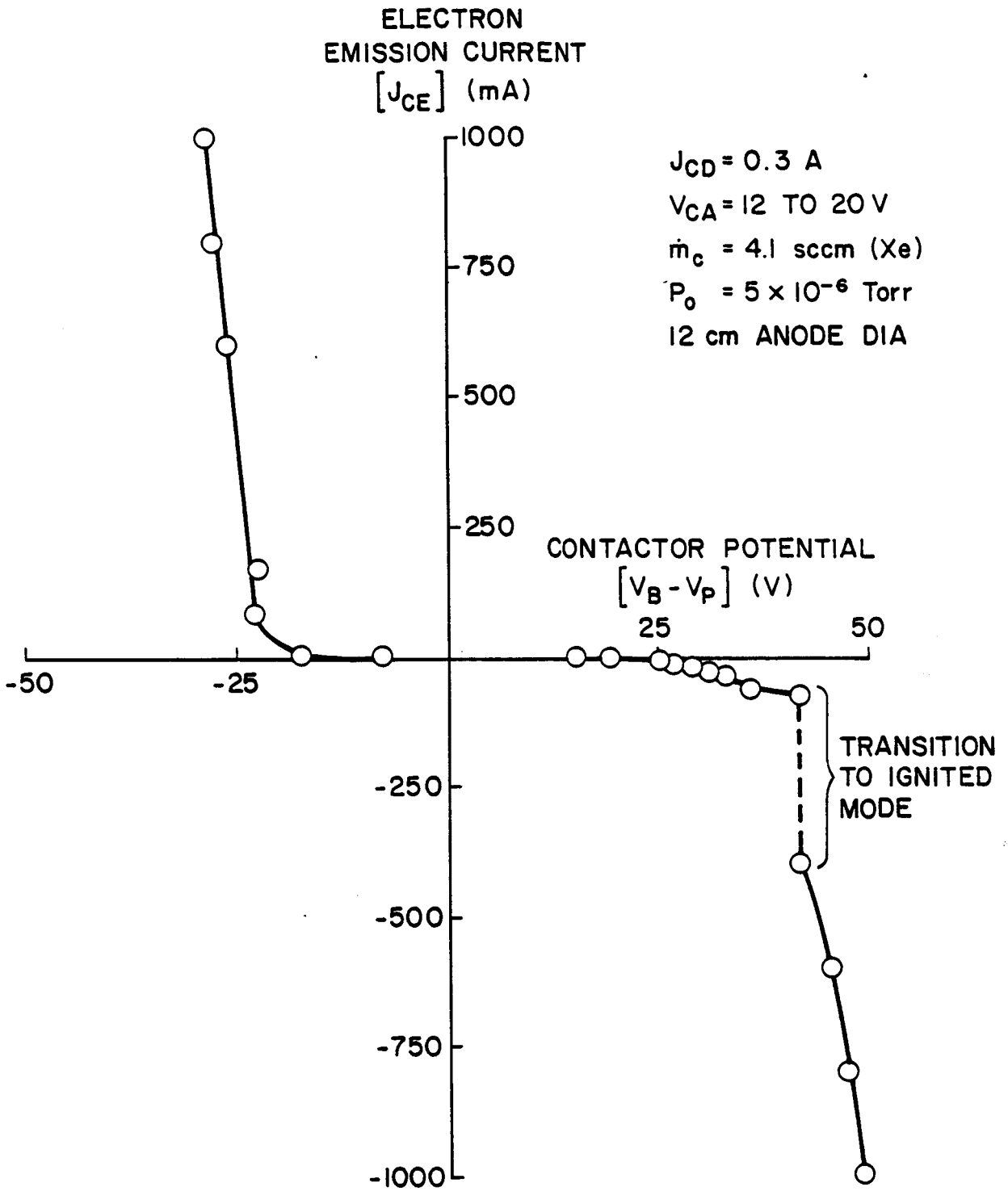

Fig. 6. Typical Plasma Contactor Performance Curve

emission mode (i.e. in the upper, left-hand quadrant) once the voltage difference between the contactor and ambient plasma is below ~-25 V. On the other hand, the curve shown in the lower, right-hand quadrant of Fig. 6 for the electron collection mode of operation shows a somewhat different structure. At contactor potentials (V_B - V_P) less than ~40 V the electron collection current is shown to first increase with increasing potentials and then to flatten out. Suddenly, at a contactor potential slightly greater than 40 V, the current is shown to increase from ~70 to ~400 mA. This transition from a relatively low electron collection current to a high current is labelled the "transition to ignited mode". The transition is accompanied by the appearance of a bright luminous glow which surrounds the contactor that could not be seen at the lower current operating conditions. It is suggested that neutral atom excitation which induces the luminosity and, presumably, ionization is occurring in the ignited mode of electron collection. Once the contactor is operating in the ignited mode small increases in contactor potential induce substantial increases in the electron current collected. At each operating point indicated by the circular symbols in Fig. 6, plasma property measurements were typically made within the region between the contactor and simulator.

A typical plasma potential profile measured along the tank centerline in the region near the contactor when it was operating in the electron collection mode is shown in Fig. 7. It was obtained at a contactor discharge current and voltage of 0.3 A and 15 V, respectively, and a contactor flowrate of 4.1 sccm (Xe). The ambient background pressure during the test was 3.2×10^{-6} Torr and the contactor was collecting 600 mA of electron current from the ambient plasma (J_{CE} = -600 mA). As shown in Fig. 7 the plasma potential in the region

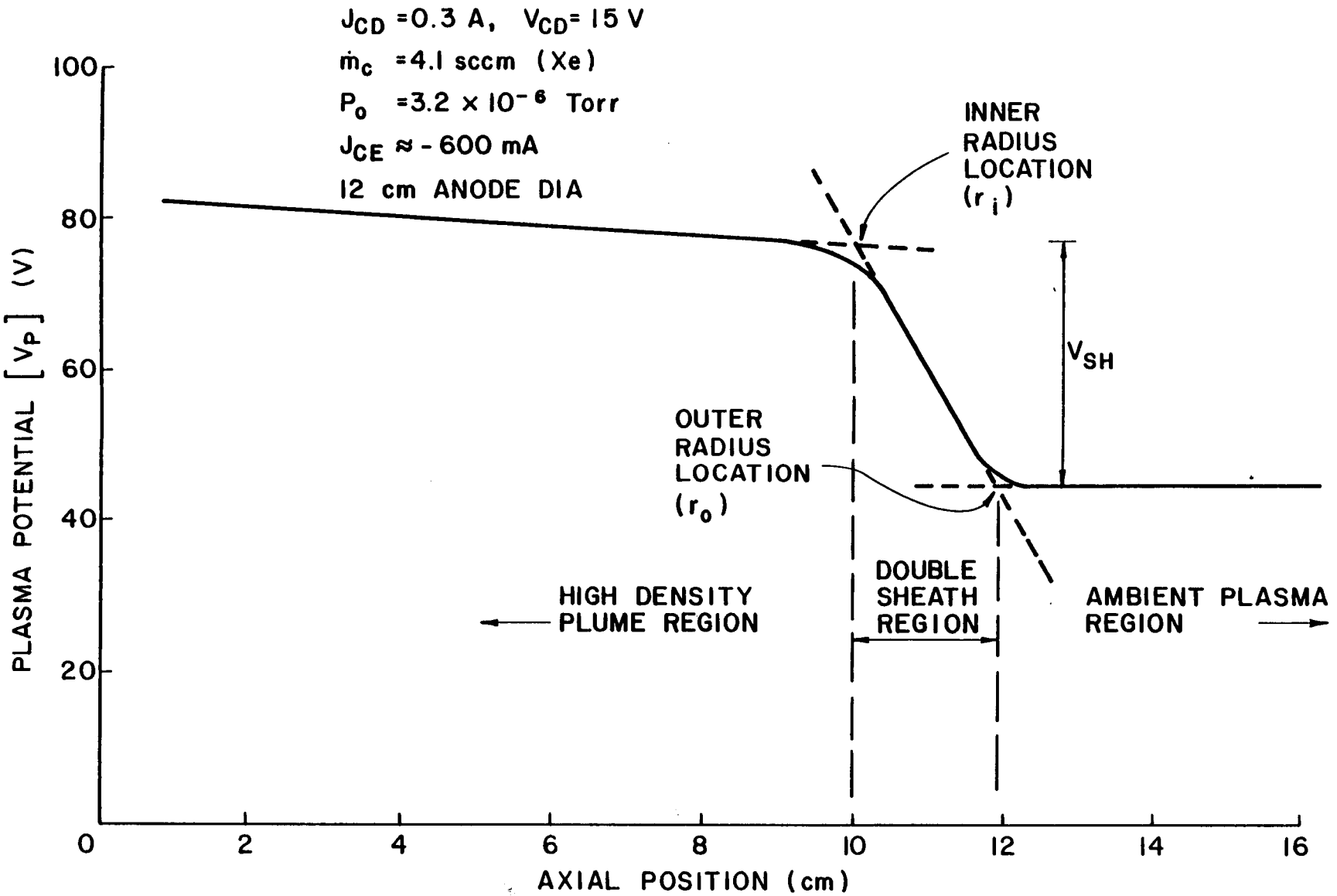

Fig. 7. Typical Plasma Potential Profile-Electron Collection Mode

immediately downstream of the contactor is relatively constant at ~80 V positive of the vacuum tank reference potential. This relatively flat potential region is labelled the "high density plume" and is shown to extend to a location ~10 cm downstream of the contactor anode plane. Far downstream of the contactor the plasma potential profile again becomes quite flat. This region is termed the "ambient plasma" and is shown to be separated from the high density plume region by a region which displays a large voltage drop. Because this region is thin (~2 cm) and the neutral density in this region is low, it is unlikely that this potential drop is caused by momentum transfer collisions. The only other possibility for this large of a potential drop to be sustained within a plasma is the development of a plasma sheath. In this case both ions and electrons are counterflowing through the sheath region and since both positive and negative space-charge plasma sheaths are observed to form at the respective boundaries, the term "double-sheath"[13] is used to describe the region. The interface between the high density plume and the double-sheath is termed the "inner radius location r_i". The term radius is used here to suggest that the contactor is coupling to the ambient plasma through a spherical segment as suggested by Fig. 1. The interface between the double-sheath and the ambient plasma is termed the "outer radius location r_o" and is shown to be located at ~12 cm. The sheath potential drop V_{SH} for the particular plasma potential profile shown in Fig. 7 is ~40 V.

The properties of the plasmas corresponding to the high density plume and the ambient plasma for many different operating conditions have been measured using a Langmuir probe. Figure 8 shows examples of Langmuir probe traces taken in each of these two regions when the contactor was operating at a discharge current and voltage of 0.5 and 19 V,

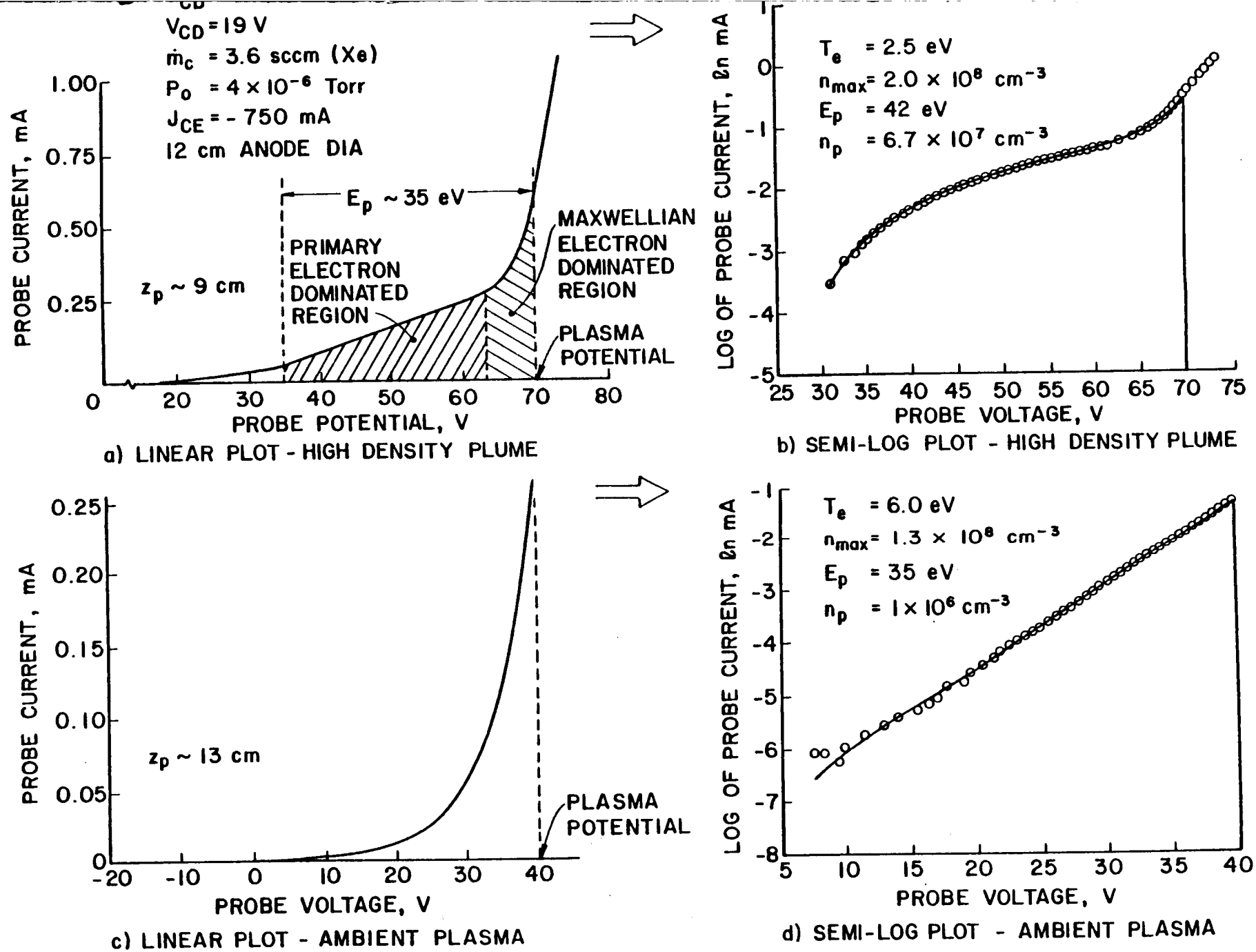

Fig. 8. Typical Linear and Semi-log Langmuir Probe Data Plots

respectively, and when the expellant flowrate was 3.6 sccm (Xe). The ambient neutral background pressure during this test was $4x10^{-6}$ Torr and the contactor was collecting 750 mA of electrons. Figure 8a, a plot of Langmuir probe current versus voltage obtained within the high density plume, shows very distinct primary (or mono-energetic--characterized by a linear probe current/voltage relationship) electron and Maxwellian (characterized by an exponential probe current/voltage relationship) electron dominated regions typical of traces obtained in the high density plume. A semi-log plot of the high density plume Langmuir probe data of Fig. 8a is shown in Fig. 8b. This figure shows (solid line) the extent to which an assumed primary-plus-Maxwellian electron distribution function model can be used to fit the data (open circles) and the plasma properties that correspond to this particular fit. Note that the value of the primary electron energy estimated directly from the data of Fig. 8a (35 eV) does not agree exactly with the energy determined by the curve fit result (42 eV). In contrast to Fig. 8a where many primary electrons were present, Fig. 8c (recorded within the ambient plasma region) shows that a straight line can be made to fit the data when it is plotted on a semi-log scale (Fig. 8d). This straight line behavior on a semi-log plot is indicative of a relatively pure Maxwellian plasma.

Analysis of Langmuir traces similar to the ones shown in Fig. 8 at many different locations along the tank centerline yields Maxwellian electron and primary electron properties that can be plotted as a function of axial position in the manner shown in Fig. 9. Figure 9a shows a plasma potential profile measured along the tank centerline for the operating conditions listed in the legend. Figures 9b and 9c show the Maxwellian electron and primary electron properties as functions of axial position. They suggest the Maxwellian temperature and density and

primary energy and density all remain constant at about 6 eV, $4x10^7 cm^{-3}$, 40 eV and $3x10^6$ cm^{-3}, respectively, in the region downstream of the double-sheath for this case where ~370 mA of electrons are being collected. It is noted that the primary electron energy in the ambient plasma is approximately equal to the ambient plasma potential. This suggests that these electrons are the ones that have been accelerated into the ambient plasma from the simulator hollow cathode at a potential near tank reference potential and have not experienced a substantial energy degradation as a result of collisions. It should be noted that the ratio of primary-to-Maxwellian electrons in the ambient plasma is small (usually less than 10% as in the case of the data of Fig. 8b). The data in Fig. 9b show the density of the Maxwellian electrons upstream of the double sheath drops rapidly with axial position. The ceiling symbol drawn on Fig. 9b near the double-sheath location indicates that the Maxwellian density and temperature were not measurable at this location because the primary electron signal overwhelms the Maxwellian signal (just as the primary signal dominates the Maxwellian signal in Fig. 8a). The data of Fig. 9c show the primary density is relatively constant both upstream and downstream of the sheath and that the upstream density is more than an order of magnitude greater than the downstream density. The primary electron density increases slightly as the radius decreases (in the region upstream of the double-sheath) probably because these electrons, after having been accelerated across the double-sheath from the ambient plasma, are concentrated as they stream radially inward toward the cathode. The energy of the primary electrons measured upstream of the double-sheath is shown to lie between 35 and 45 eV and this is roughly equal to the sheath potential drop shown in Fig. 9a. This result suggests that the

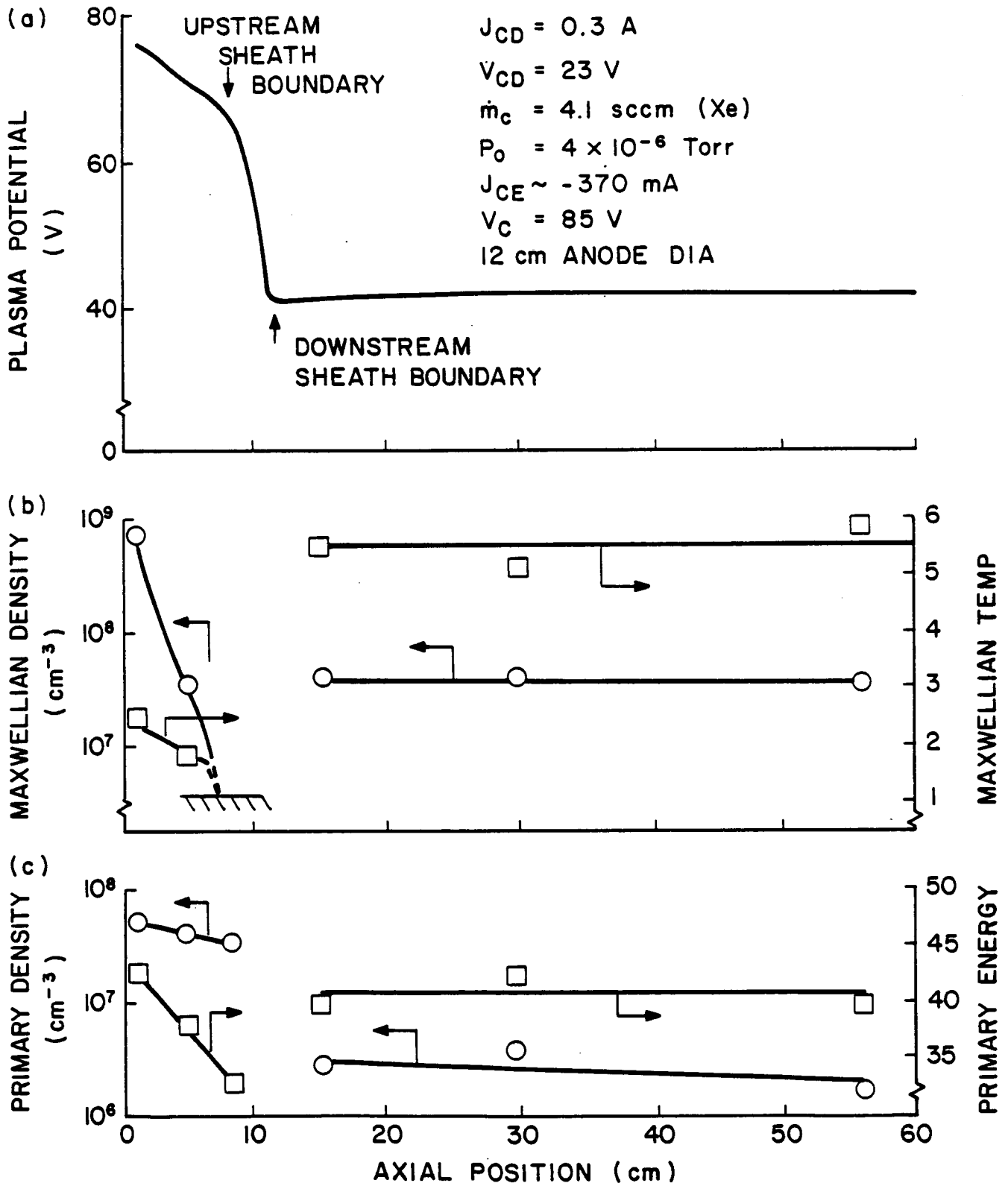

Fig. 9. Typical Plasma Property Profiles -Electron Collection Mode

primary electrons found in the high density plume region are indeed those that have been accelerated across the sheath from the relatively low temperature Maxwellian electron group in the ambient plasma. This provides additional evidence that the basic physical model that has been proposed is valid.

Data like those shown in Fig. 9 can be used to evaluate the models proposed in the theory section of this report. In Fig. 10 experimentally measured values of the outer radius of the sheath determined from potential profiles like the one in Fig. 9a are compared to theoretical predictions of this radius calculated from Eq. 1, using plasma property data and the measured electron collection current together with the assumption that the electrons are collected through a solid angle of 4π steradians. The results of Fig. 10 were obtained over the wide range of operating conditions which are listed in the legend. The proximity of the data points to the solid 45° line drawn on Fig. 10 indicates the degree to which experiment and theory agree. Similar to how Fig. 10 compares theoretical-to-experimental outer sheath radii, Fig. 11 compares theoretical-to-experimental inner sheath radii. The inner radius can be calculated by combining Eq. 2, which expresses the constraint on the ion current condition that must be satisfied in order to assure a stable inner sheath (i.e. the Bohm criterion), with Eq. 6 to obtain

$$r_i = \left[\frac{J}{e\, n_{+i}\, \psi\, \gamma\alpha} \sqrt{\frac{m_e}{k\, T_{ei}}}\right]^{1/2} . \qquad (7)$$

In order to investigate the validity of this equation, electron collection currents J and the sheath voltage drops were measured at

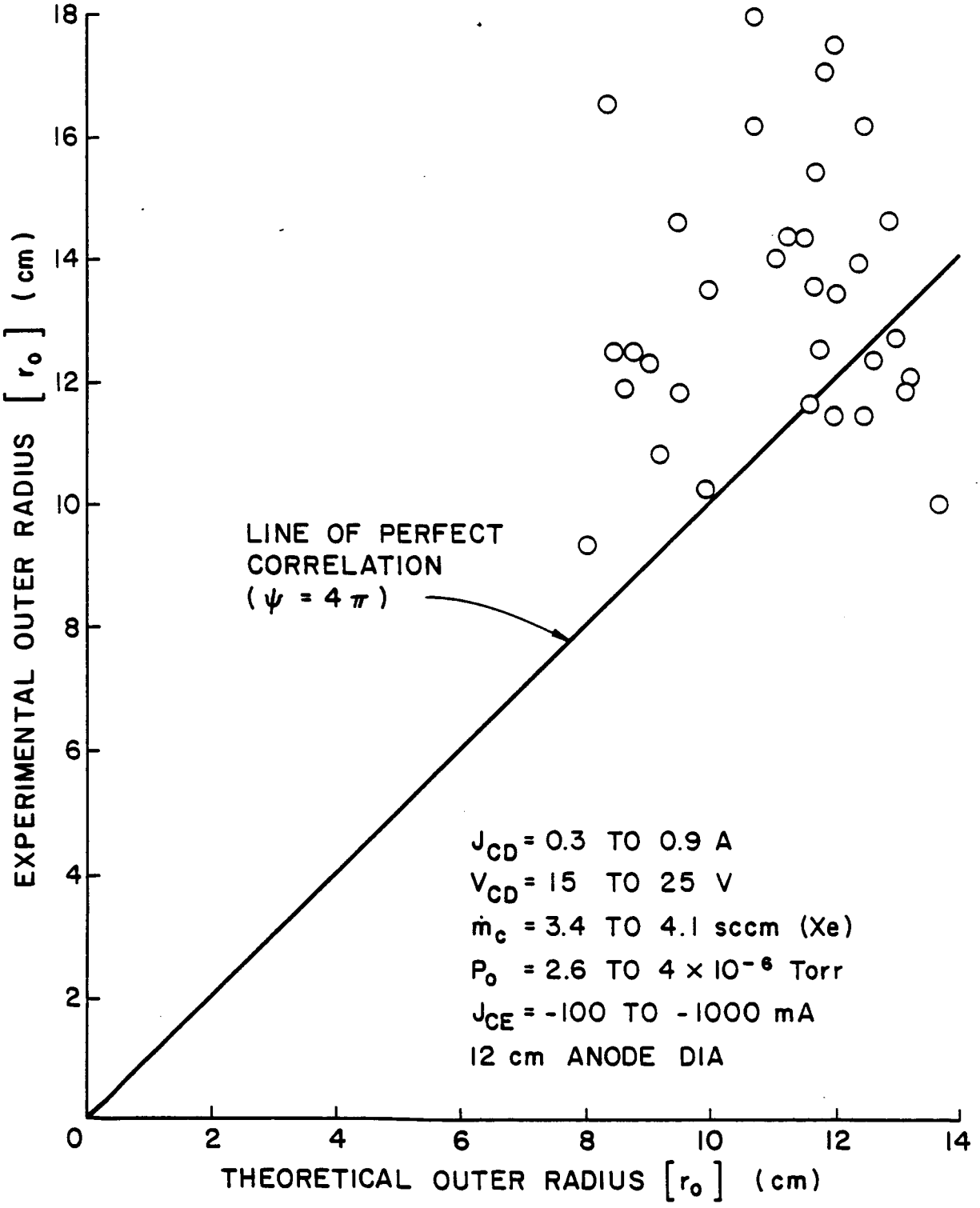

Fig. 10. Correlation of Computed and Measured Outer Sheath Radii

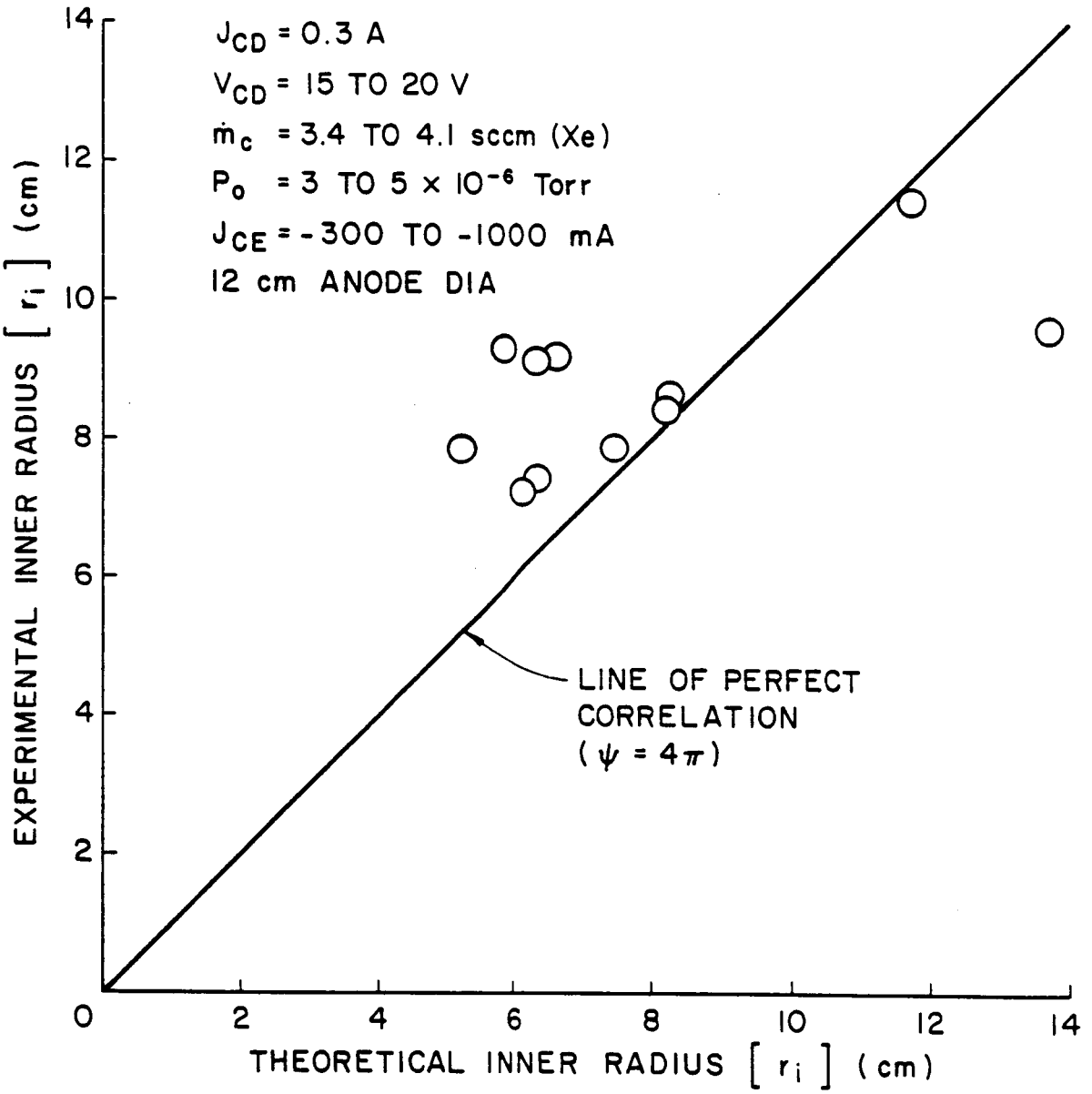

Fig. 11. Correlation of Computed and Measured Inner Sheath Radii

typical operating conditions and the parameter α was then determined using the double-sheath model described in Ref. 9. At these same operating conditions the plasma density n_{+i} and electron temperature T_{ei} in the inner sheath region were also measured. In addition, a value for the pre-sheath correction factor γ was assumed (0.3). While this value is considered reasonable, it still needs to be determined on a rigorous theoretical basis. All of these data were then used in Eq. 7 to compute values for the theoretical inner sheath radii associated with each of the operating conditions. Typical inner sheath radius values computed using Eq. 7 (theoretical) are compared to corresponding ones determined from emissive probe measurements (experimental) in Fig. 11. The proximity of the data points to the perfect fit line in Fig. 11 suggests that the model describes the experimental results to within ~30%. On the basis of this degree of agreement it is proposed that incorporation of the Bohm criterion for a stable inner sheath as the physical basis for defining the location of the inner sheath boundary is justified. A more detailed discussion of Figs. 10 and 11 along with other comparisons of experiment to theory are included in Appendices A and B.

Effects of Flowrate on Plasma Contactor Performance

It has been shown that contactor performance improves with increasing contactor cathode flowrate.[2,8,10] This effect of flowrate is especially dramatic in the electron collection mode of operation as the characteristic curves of Fig. 12 show. These curves show that the point of transition into the ignited mode of electron collection (i.e. the point at which the curves drop off abruptly) occurs at progressively lower contactor potentials as flowrate is increased and as a result contactor potentials are reduced at all emission current levels. This decrease in contactor potential with flowrate can be explained with the

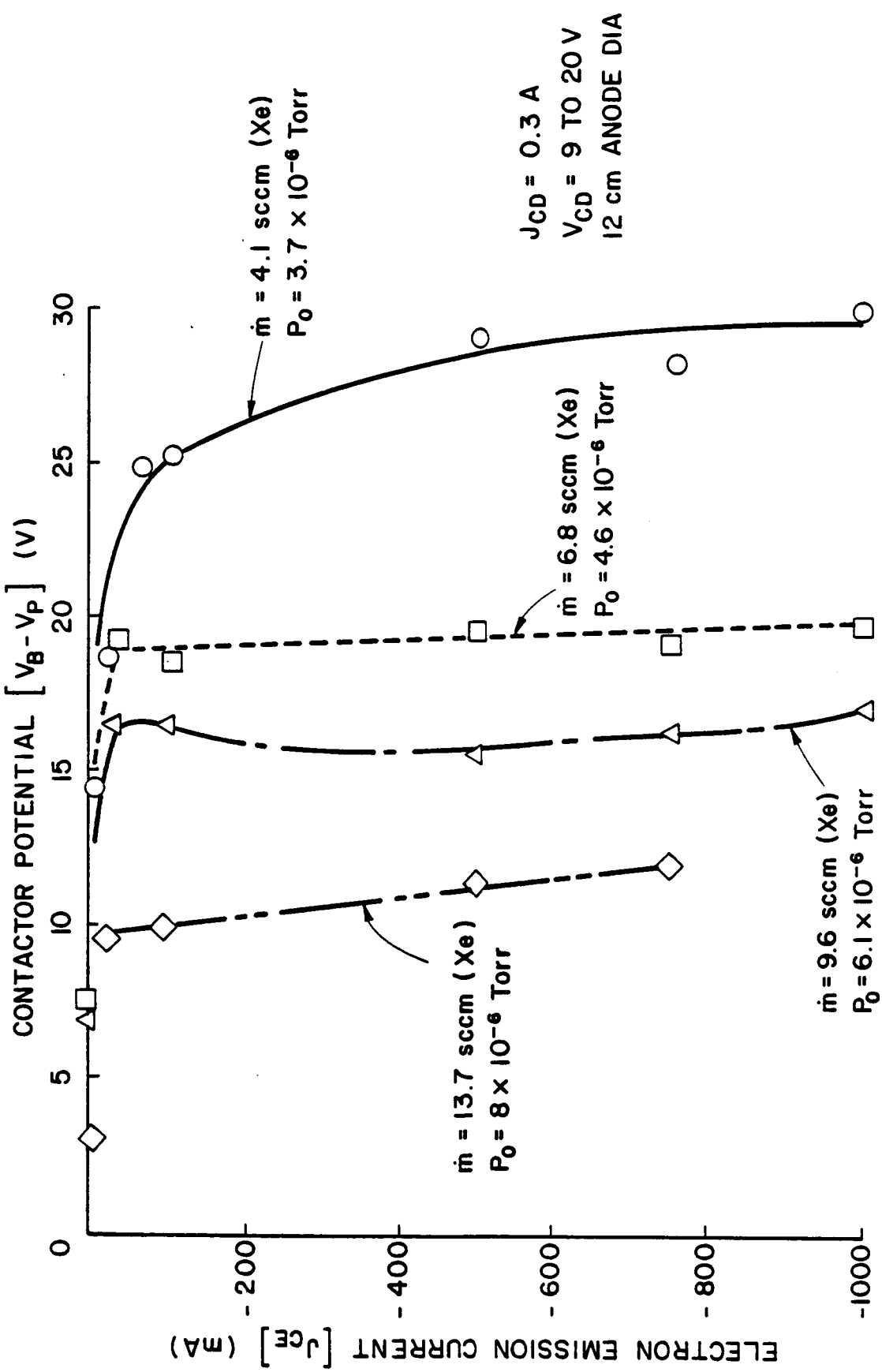

Fig. 12. Effects of Contactor Flowrate on Electron Collection Current/ Voltage Characteristic Curves

help of the spherical double-sheath model which has been outlined in the theory section of this report. The model indicates that an increase in the contactor cathode flowrate results in increased ion production in the high density plume region and this increased ion production causes the high density plume (and hence the inner boundary of the sheath) to expand. On the other hand, the outer boundary of the double-sheath, which depends only on the electron current being collected and the ambient plasma conditions, remains fixed. Consequently, the radius ratio increases and this causes the sheath potential drop to decrease at a given electron collection current condition.

When an experiment is conducted to demonstrate the details of the phenomena described in the preceeding paragraph, ambient plasma conditions existing in the vacuum tank are unfortunately observed to change. This occurs because ambient plasma conditions cannot be controlled independent of the contactor operating conditions, so some anomalies induced by changes in ambient plasma conditions are frequently observed. Still the effect of contactor cathode flowrate on sheath potential drop can be observed in plasma potential profiles like those measured at an electron collection current of 1 A which are shown in Fig. 13. As suggested in the above paragraph, the inner sheath boundary r_i moves downstream and the sheath potential drop decreases as flowrate is increased. Along with this dramatic increase in the high density plume volume with increasing flowrate, Fig. 13 also shows that the downstream sheath boundary moves further downstream with increasing flowrate. It is this downstream sheath movement that is believed to be caused by contactor-induced changes in the ambient plasma conditions in the vacuum facility.

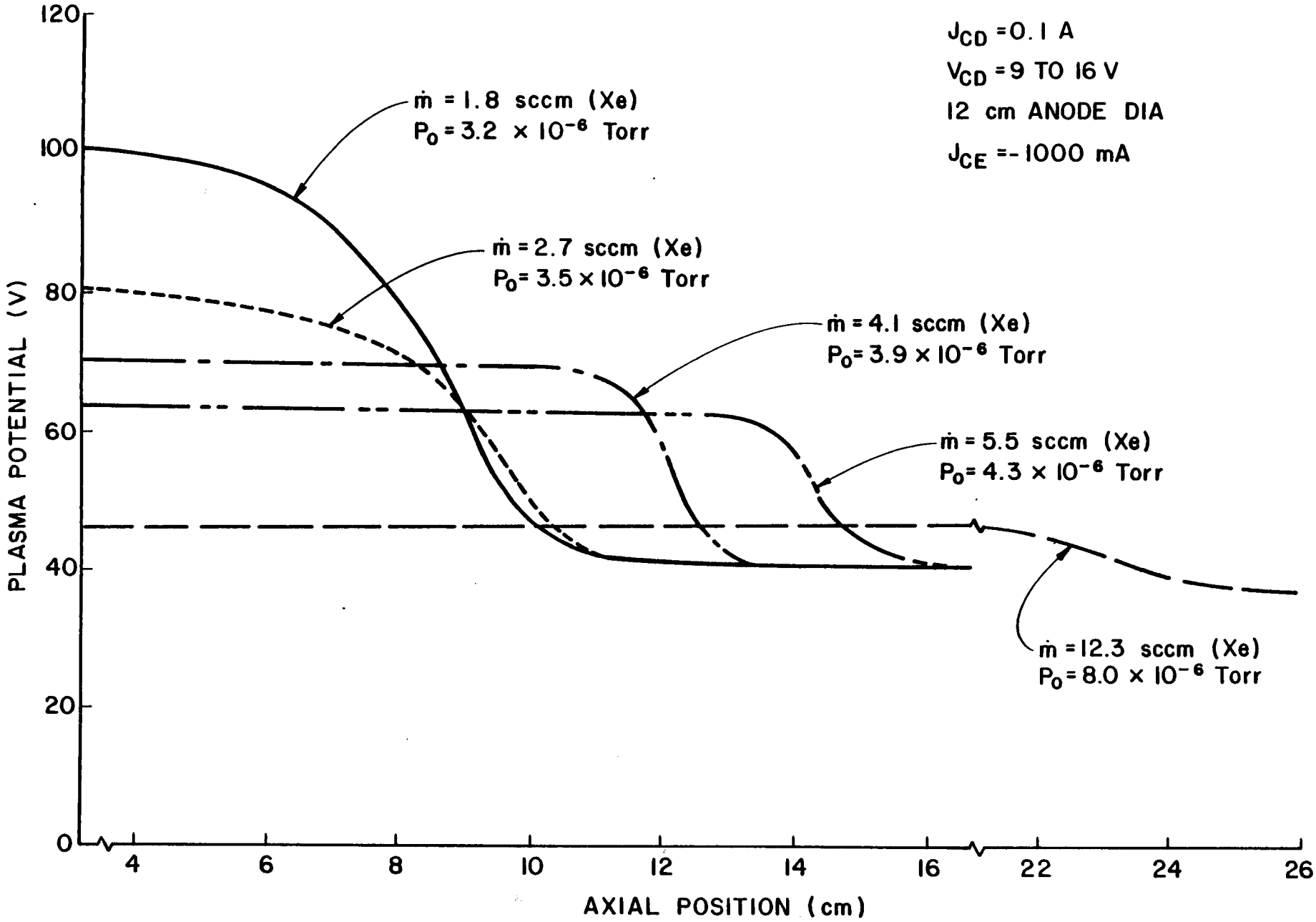

Fig. 13. Effects of Flowrate on Plasma Potential Profiles

In developing Eqs. 3 and 4 in the Theory Section of this report neutral atoms supplied through the contactor at a rate $\dot{n}_n$ were assumed to expand as though they were coming from a point-source and passing into a free-molecular flow environment. Pressure measurements were made to study the validity of this assumption. A typical neutral density versus axial position plot as computed from pressure measurements made using a Shultz/Phelps ionization gauge (and by assuming that the neutrals flowing from the contactor are at the hollow cathode temperature T_c) is shown in Fig. 14. The line drawn through the data points represents a least-squares curve fit to the data using the equation

$$n_n = c \frac{1}{z^2} + b \quad . \tag{8}$$

The closeness of the fit of the data points by the line suggests that the assumed $1/z^2$ dependence is valid and that there is spherical symmetry associated with the expansion so that $r \simeq z$ is implied. If the development based on free-molecular flow from a point-source through a solid angle ψ that led to Eq. 8 is to be valid, the curve-fit parameters "c" and "b" in Eq. 8 would then by comparison with Eq. 4 be given by

$$c = \frac{\dot{n}_n}{\psi \, v_n} \tag{8a}$$

and

$$b = \frac{P_o}{k \, T_o} \quad . \tag{8b}$$

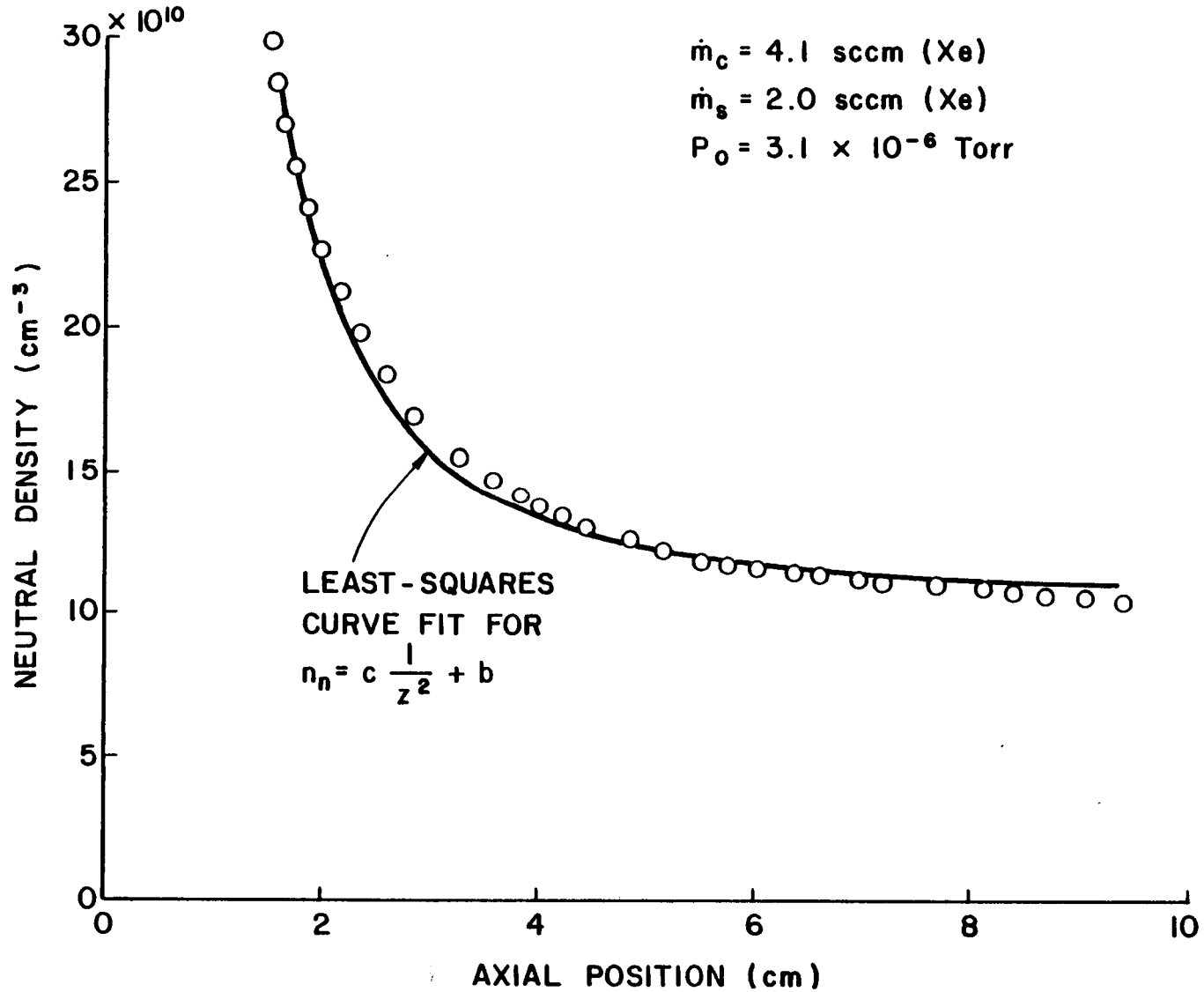

Fig. 14. Typical Neutral Density Profile along Contactor Centerline

By plotting the curve-fit parameter "c" found experimentally from curves similar to the one shown in Fig. 14 against neutral atom flowrate $\dot{n}_n$ in the manner illustrated in Fig. 15, one can determine the degree to which the one-dimensional model represented by Eq. 4 fits all of the data collected using the pressure probe. As Fig. 15 shows, most of the data fall near the $\psi = 4\pi$ line suggesting that the neutral atoms flowing from the cathode expand through a full sphere to the ambient neutral background pressure. In reality, the neutral atoms probably expand in a more complex three-dimensional pattern, but it will be assumed that the neutral density can be modeled with adequate accuracy by Eq. 4 and that the flow expands through a solid angle of 4π steradians.

The plots of Fig. 16 show the actual axial and radial variation in neutral atom density which was measured at a typical contactor flow and ambient pressure operating condition. The data of Fig. 16 suggest that the neutral atom expansion induced by the contactor flow probably does not develop through a full 4π steradians and expansion is therefore not completely consistent with Eq. 4. Previous results[2,3] have shown that the 4π steradian solid angle fits the ion and electron flow situation best so the same angle will be used to describe neutral atom flow. This should ensure that all aspects of the theory can be applied consistently, thereby making the problem tractable in the context of this preliminary study.

It is noted that the neutral atom density remains relatively uniform (Fig. 16) at distances beyond about 5-6 cm downstream of the contactor orifice for the flowrate conditions listed in the legend. In order to perturb the ambient neutral density at distances greater than 6 cm, one would need to increase the neutral atom flowrate $\dot{n}_n$ or decrease the background pressure substantially. Further, calculation of

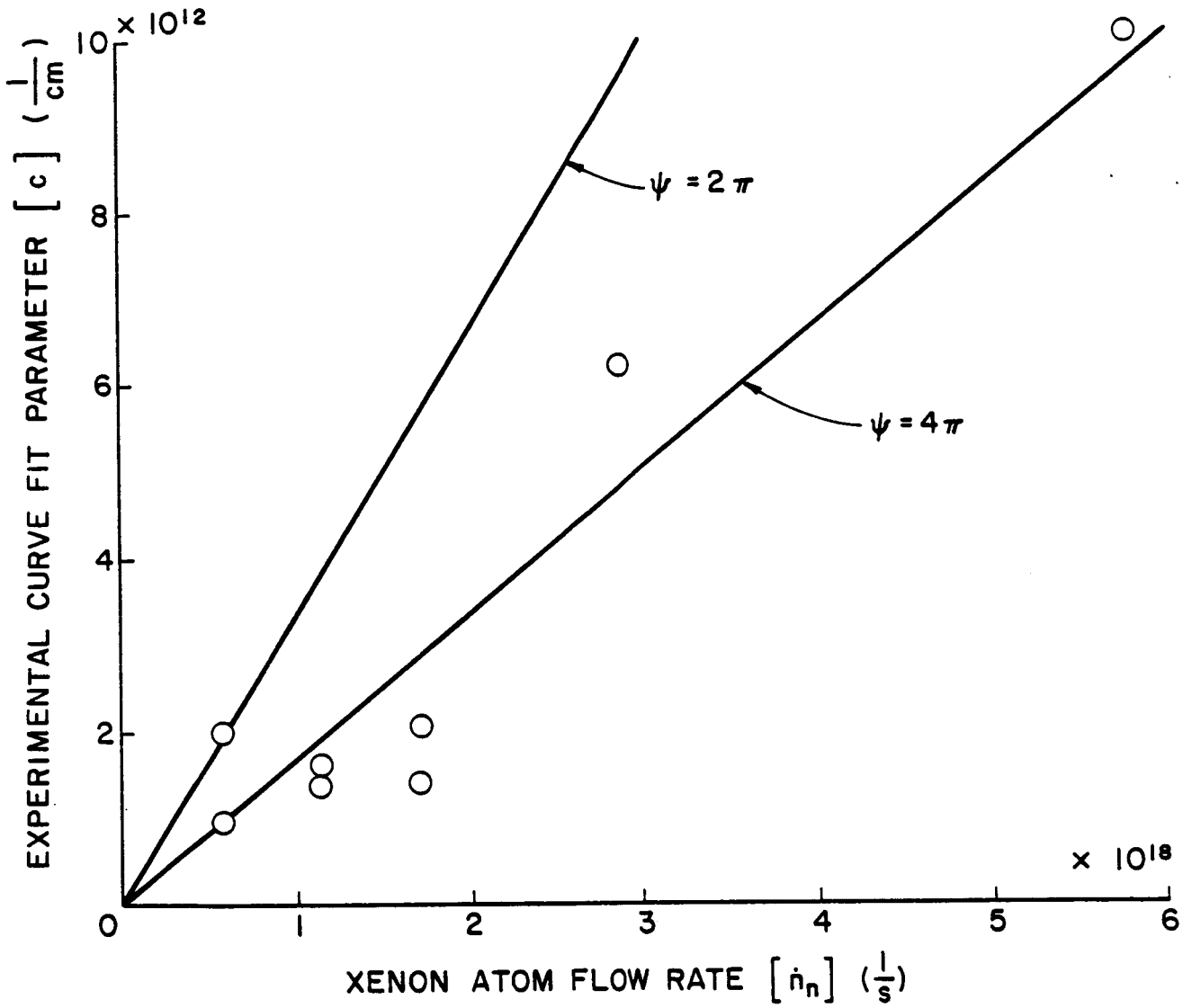

Fig. 15. Correlation of Neutral Density Expansion Parameter with Point-source, Free-expansion Model

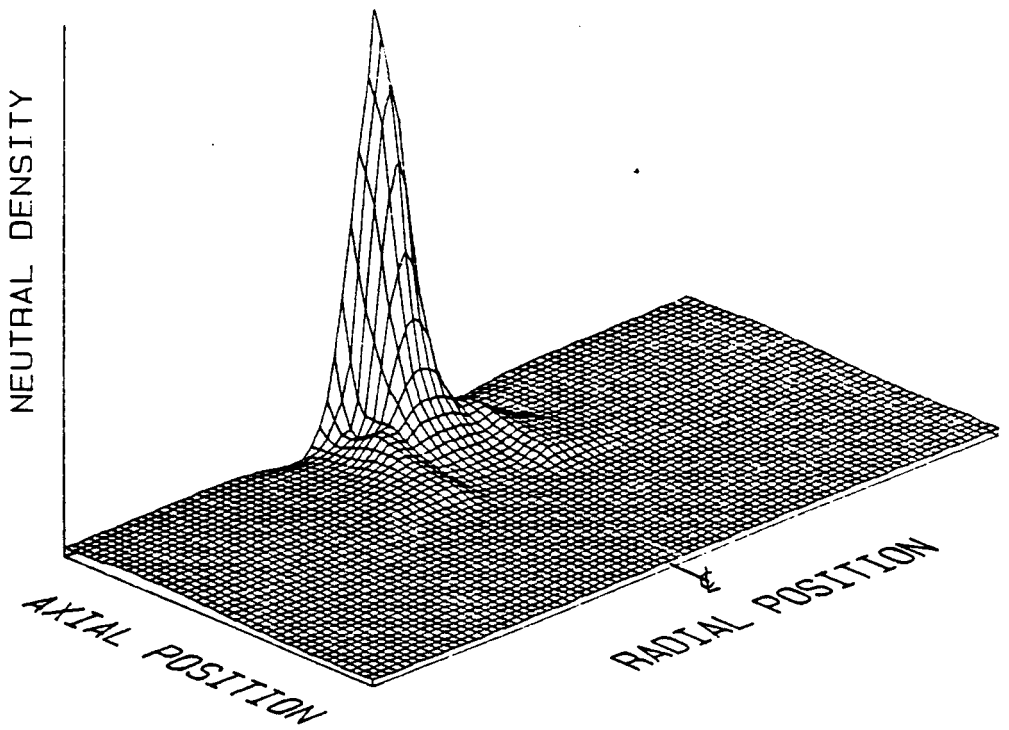

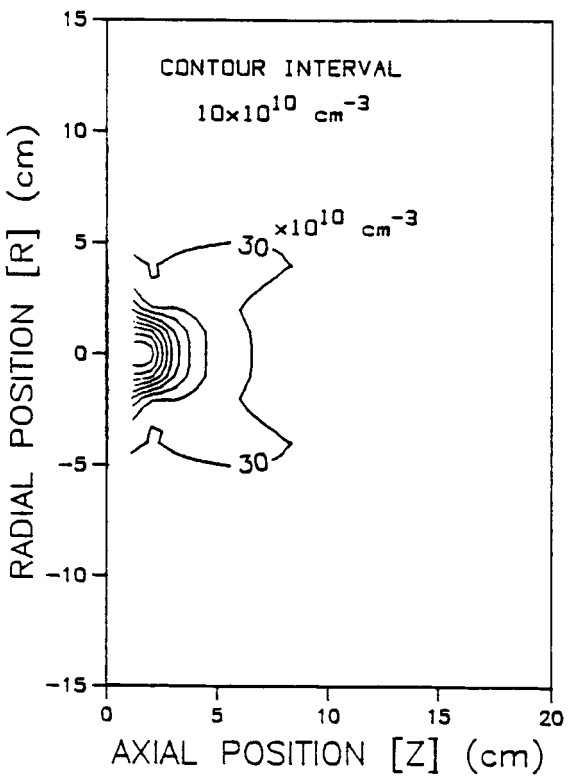

$\dot{m}_c$= 13.7 sccm (Xe)
$\dot{m}_s$= 2 sccm (Xe)
T_c= 1300 K

T_a= 300 K
P_a= 8×10^{-6} Torr

Fig. 16. Neutral Atom Density Map

inelastic collision mean free paths for typical streaming electrons has shown that most of these collisions occur close to the cathode where the atom density is highest. This suggests in turn that the detailed structure of the neutral atom expansion may be less important than the magnitude of the neutral atom density close to the cathode (i.e. within a few centimeters of it). Because the double-sheath is typically of order 10 cm from the cathode it is argued that it is the magnitude of the neutral atom density close to the cathode rather than the detailed structure of the neutral density plume that affects the shape and position of the double-sheath most.

It is interesting to compute the radial location (in the sense of the spherical model embodied in Fig. 1) at which the streaming electron current has produced sufficient ion current to satisfy the space-charge limited double-sheath condition as described in the Theory section of this report. This can be accomplished by first calculating the ion emission current required at the space-charge limited condition using Eq. 6. The radius δ at which the streaming electrons coming from the sheath edge r_i will have produced this ion current can then be determined using Eq. 3. The ion current produced by the streaming electrons within the region extending from the inner boundary of the sheath to the radius δ is referred to as the ion production rate expressed as a current integrated from the inner radius of the sheath to the radius δ. Figure 17 shows plots of this integrated ion production rate as a function of radius computed at the electron current and sheath voltage drops measured at the two different flowrate and background pressure conditions indicated on the figure. Note that the assumption of spherical symmetry together with a definition of the solid angle ψ through which electrons, atoms and ions counterflow (4π in this case)

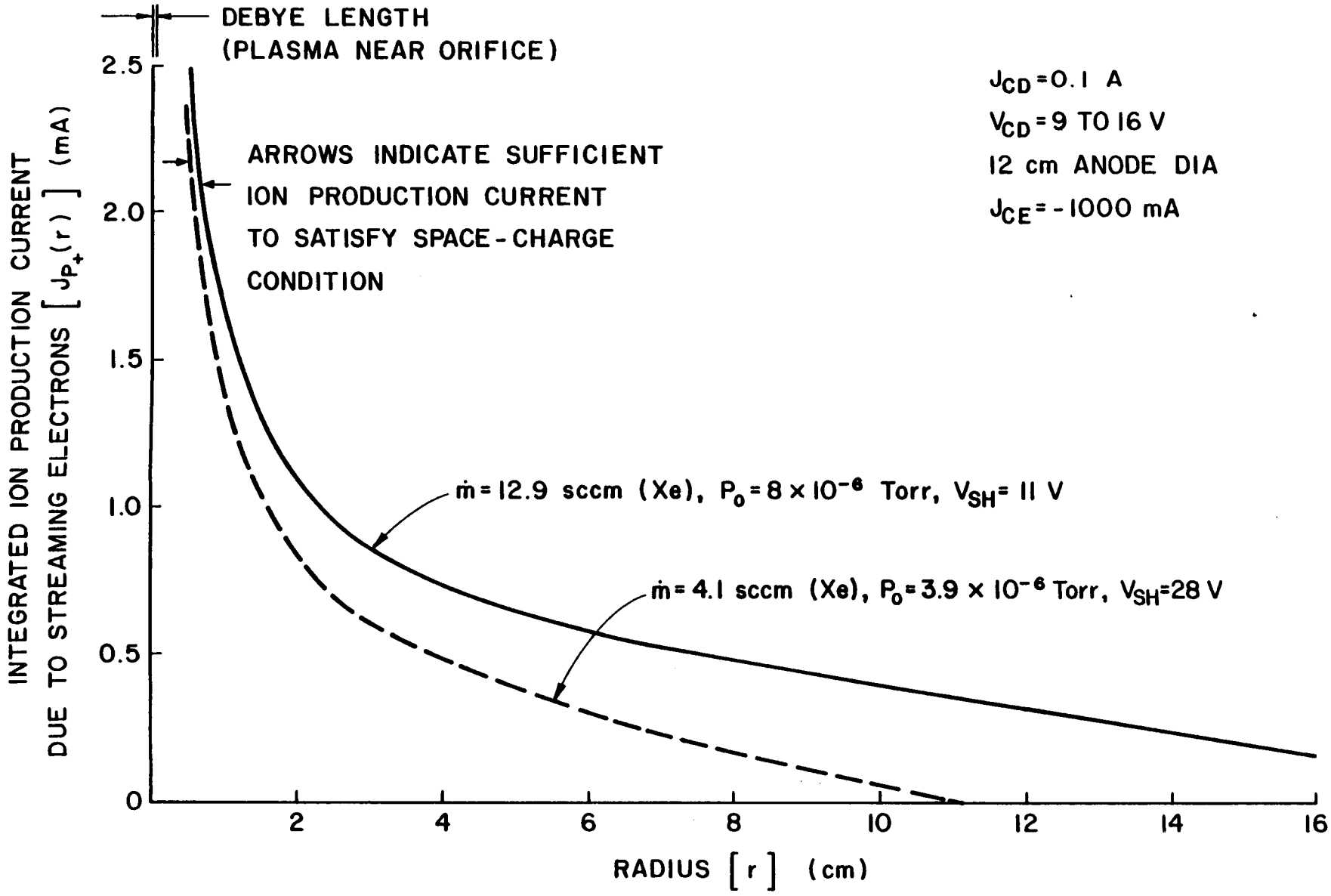

Fig. 17. Effect of Flowrate on Ion Production by Streaming Electrons

must be made before Eq. 3 can be solved for the integrated ion current to a particular radius. In accordance with Eq. 3, Fig. 17 shows the ion production current increases as the integration is carried to smaller radii for both curves. The location of the arrows on each curve (at about 1 cm) indicate the radial positions where the ion production is sufficient to satisfy the space-charge limited condition for the electron current being collected (J_{CE} = -1.0 A). It should be noted that the integration could theoretically be carried to a radius of about one Debye length (<1 mm at typical cathode plasma conditions) so this result suggests that many ions produced by the streaming electrons very close to the cathode orifice may be lost to anode and cathode surfaces where they recombine.

Comparison of the curves of Fig. 17 suggests that a substantial number of ions are being produced by the streaming electrons further away from the contactor cathode and anode surfaces in the higher flowrate case than are being produced in the lower flowrate case. One would expect that ions produced too close to the cathode (certainly those within about one Debye length of the orifice) would fall back into the cathode rather than escaping out to the region of the double-sheath where they could be extracted from the high density plume. On the other hand, ions produced further from the the cathode and anode surfaces would have a higher probability of escaping through the double-sheath region thereby causing the inner sheath boundary and radius ratio to increase and the sheath potential drop to decrease. This trend (i.e. increased neutral flowrates inducing higher ion production rates and hence higher ion currents across the double-sheath which in turn lead to increased inner sheath boundary radii and smaller sheath voltage drops) is consistent with the data presented in Fig. 13.

Effects of Anode Area

Just as increasing the contactor flowrate has been shown to facilitate transition into the ignited mode of electron collection and to thereby cause the contactor to operate more efficiently, increasing the contactor anode diameter has also been shown to improve contactor performance.[3,10,14] The effect of changing anode diameter on contactor performance is displayed quite dramatically in Fig. 18, a plot which shows contactor characteristic curves corresponding to anode diameters of 1, 3, 7, and 12 cm (i.e. 1, 3, 7, and 12 cm contactors). During the conduct of the tests that produced the data of Fig. 18, the contactor discharge current J_{CD} was controlled at 0.3 A and the discharge voltage varied between 14 and 22 V. The contactor flowrate $\dot{m}_c$ was set at 4.1 sccm (Xe) and the ambient background pressure was 4.3×10^{-6} Torr. It is noted that the 1 and 3 cm contactor characteristic curves do not extend to electron collection currents that are as high as those for the 7 and 12 cm contactors because of power supply limitations.

In order to understand the mechanism by which changes in anode diameter induced changes in characteristic contactor performance curves, plasma potential profiles were collected at an electron collection current of 250 mA using different contactor anode diameters. Typical profiles, obtained using contactors with anode diameters of 3, 7, and 12 cm, are shown in Fig. 19. From this figure one can see that the ratio of the inner sheath to outer sheath radii for the 3 cm contactor is smaller than corresponding ratios for the 7 and 12 cm contactor plasma potential profiles. Viewing this observation in light of the contactor model represented by Eq. 5 and Fig. 2, the sheath potential drop for the 3 cm contactor would be expected to be higher than the potential drops corresponding to the 7 and 12 cm dia anode contactor

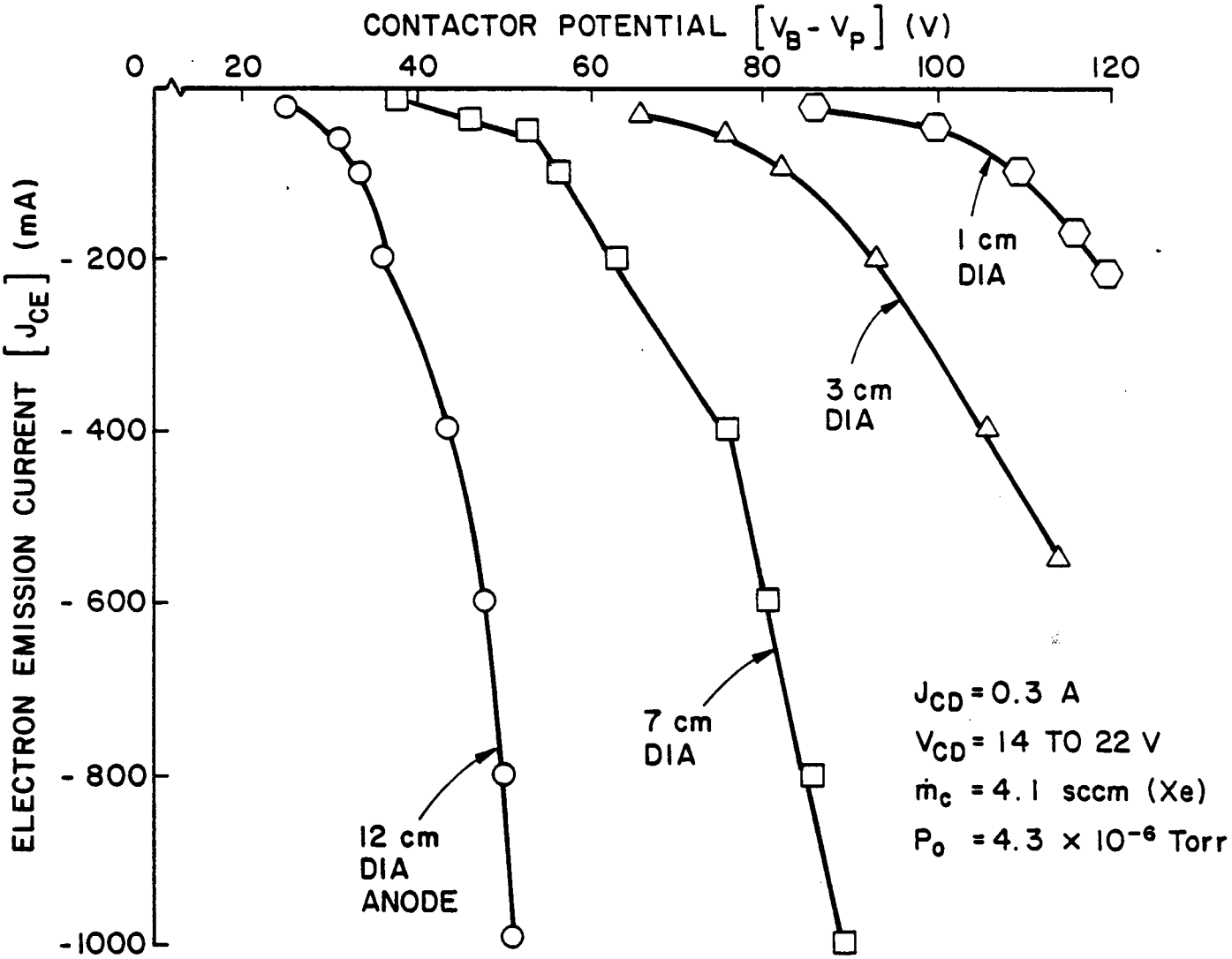

Fig. 18. Effect of Anode Diameter on Current/Voltage Characteristic Curve

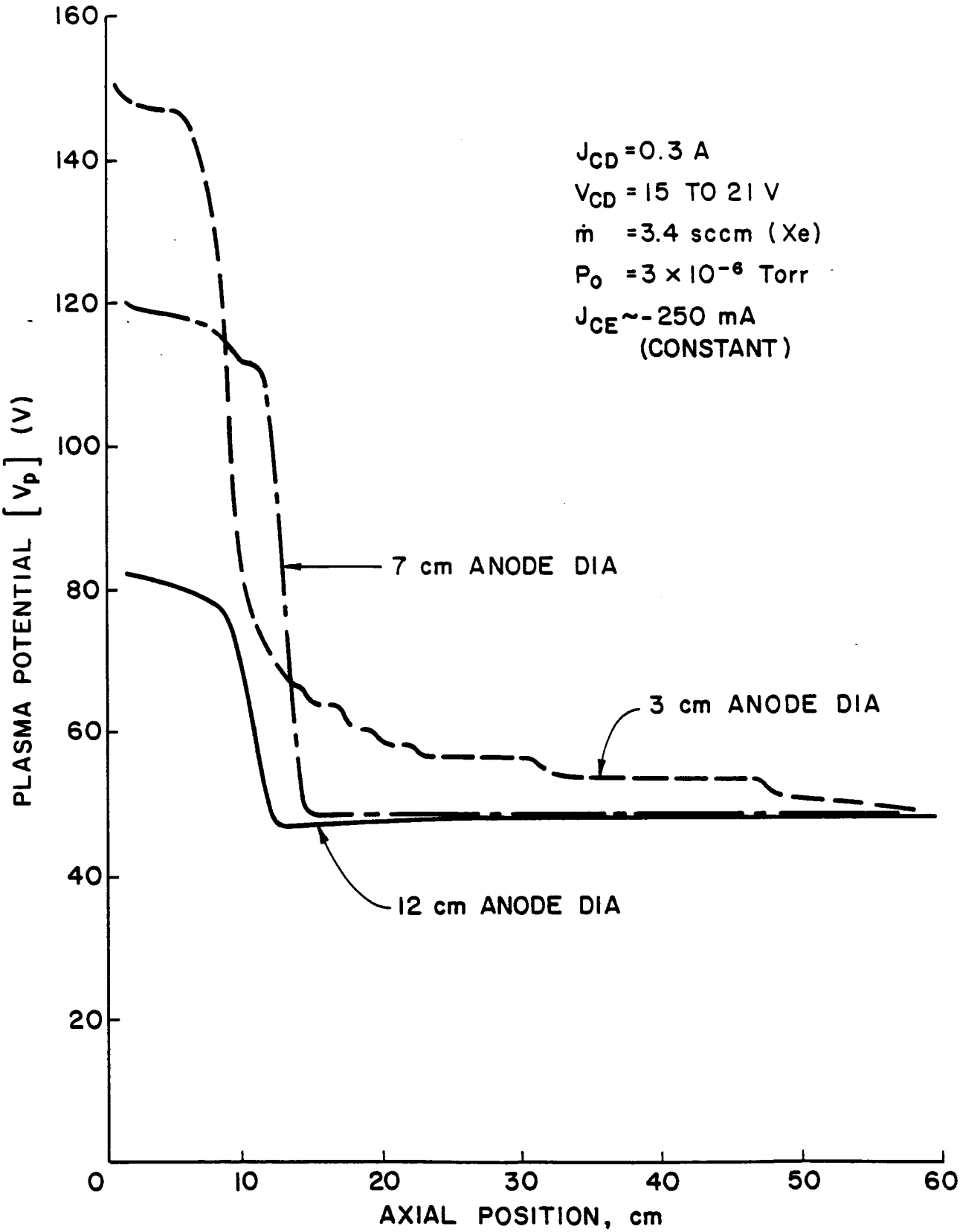

Fig. 19. Plasma Potential Profiles for 3,7 and 12 cm diameter Anode Contactors

profiles and this is indeed what the figure shows. The 7 and 12 cm contactor profiles are smoother, and they show less structure within the high density plume region than the 3 cm contactor profile. From Fig. 19 one can also see that the radius ratios for the 7 and 12 cm contactors are comparable and one would expect therefore that voltage drops would also be comparable. The fact that they are not is a reflection of the great sensitivity of the sheath voltage drop to the radius ratio particularly when the radius ratios are near unity as they are in this case. It should be noted, however, that in general the potential drop across the sheath does decrease monotonically with increases in anode diameter (see for example Fig. 18). It is also noted that changes in anode diameter might be expected to influence the solid angle ψ through which the contactor couples to the ambient plasma and Eq. 5 indicates this would also influence the sheath voltage drop.

Typically, the largest factor that would cause sheath potential drops to change with contactor anode diameter is the sheath radius ratio. This point, along with a demonstration of the applicability of the simple, double-sheath model, can be best made by plotting radius ratios measured over a wide range of operating conditions against corresponding theoretically predicted ones. This has been done in Fig. 20. The fact that the model[9] predicts the radius ratios with reasonable accuracy over this rather large range of operating conditions is demonstrated by the extent to which the data points in the figure fall about the perfect fit line and generally within the ±25% error boundary lines. Note that the 12 cm contactor (circular data points) fall above ~0.7 radius ratio values while the smaller diameter anode data extend to values in the region below ~0.7 that decrease with decreasing anode diameter. Consequently, Fig. 20 shows that the larger

J_{CD} = 0.1 TO 0.9 A
V_{CD} = 10 TO 25 V
$\dot{m}_c$ = 1.4 TO 4.1 sccm (Xe)
P_o = 2.6 TO 4 × 10^{-6} Torr
J_{CE} = -10 TO -1000 mA

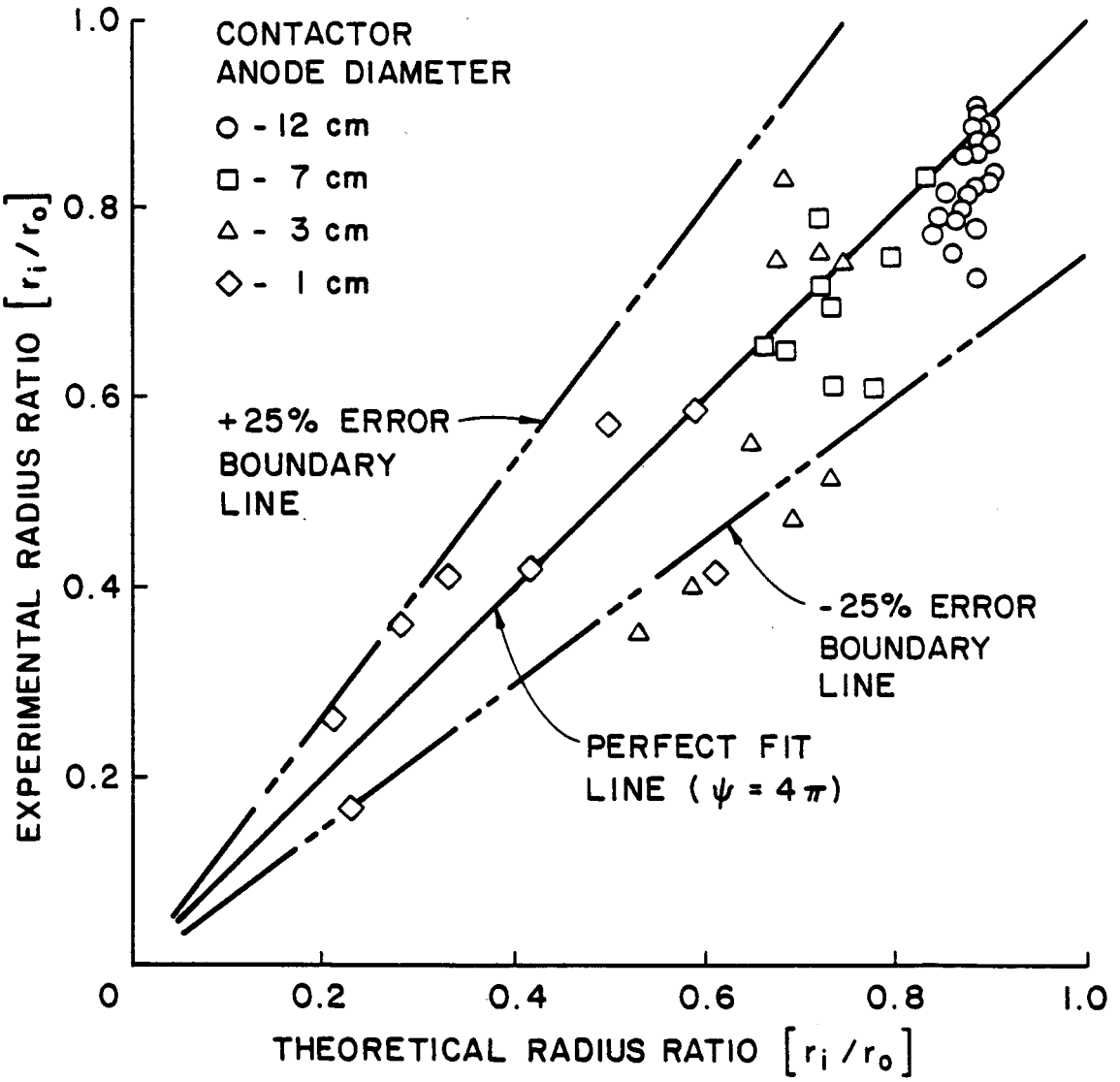

Fig. 20. Comparison of Theoretical-to-Experimental Sheath Radius Ratios Showing Anode Diameter Effects

anode diameter contactors should perform better than smaller anode diameter contactors due to the larger radius ratios observed with the larger anode diameters. This trend has been observed over a wide range of operating conditions as the data in the legend indicate.

Test Facility Effects

After the 12 cm anode diameter contactor had been tested in the Colorado State University (CSU) vacuum tank, it was tested in the 4.6 m diameter by 19.2 m long vacuum tank at the NASA Lewis Research Center (LeRC).[14] For these tests the contactor-to-simulator separation distance was 8.6 m (more than three times the separation distance used in the CSU experiments). Not only was the tank size larger, but the ambient background pressure at comparable contactor and simulator flowrates was about one fourth the pressure in the CSU facility. The LeRC simulator was a hollow cathode device which was operated at a discharge current J_{SD} of 3.5 A, a flowrate $\dot{m}_s$ of 6.8 sccm (Xe) and a discharge voltage V_{SD} of ~16 to 20 V. Unlike the CSU simulator, the LeRC simulator was operated at a sufficiently high discharge current so no external heater power was needed to sustain the insert temperature.

A comparison of typical current/voltage characteristic curves obtained at both facilities with the contactor operating at the same flow and discharge conditions in the electron collection mode is shown in Fig. 21. The figure shows the contactor performing nearly ideally in the CSU facility with the contactor potential nearly constant at -11 V over the range of currents investigated at this relatively high flowrate and a high ambient tank pressure condition. This performance is shown to be considerably poorer in the LeRC facility (~4 to 8 times higher contactor potentials were required at similar current levels). In addition, the contactor potential begins to increase as electron

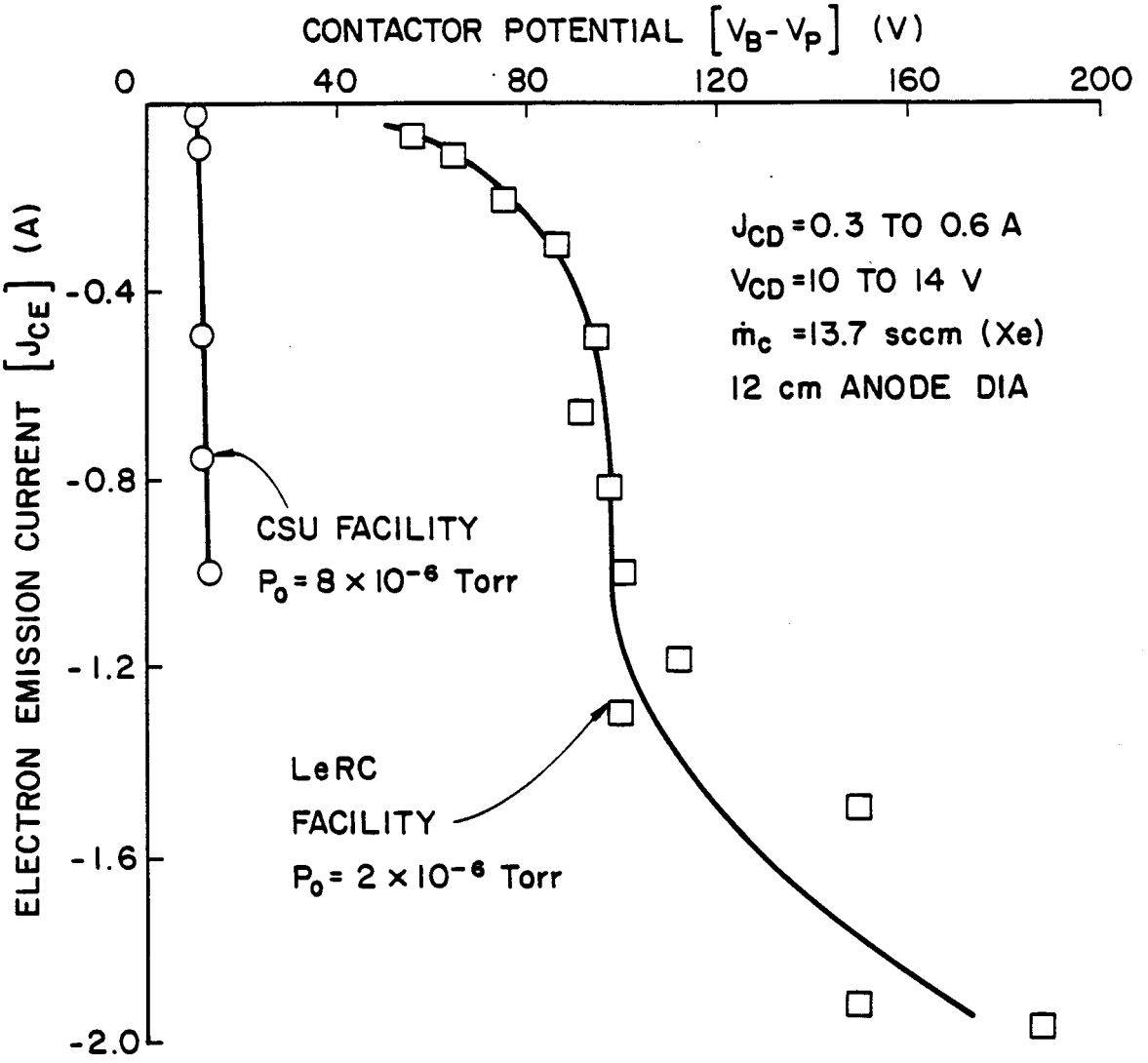

Fig. 21. Effects of Test Facility on Current/Voltage Characteristic Curves

collection currents are increased above about ~1.2 A. No data were taken above 1 A of electron collection for the experiments performed at the CSU facility.

Typical plasma potential profiles taken on the tank centerline in the LeRC facility are shown in Fig. 22. The data of Fig. 22a correspond to operation at a relatively low electron collection current condition (J_{CE} = -100 mA). This profile displays what appear to be sheaths at two locations, one within the region near the contactor which does not exhibit a large voltage drop, and a second, sheath having a larger potential drop located ~25 to 45 cm downstream of the contactor. Figure 22b shows a potential profile measured at an electron collection current of 1.2 A. At this higher current a well defined double-sheath region located between ~25 and 40 cm is apparent, however, a non-uniform potential variation similar to the small sheath structure shown in Fig. 22a still seems to exist within the high density plume region. By comparing Figs. 22 and 13 or 19, it is apparent that the magnitudes of the outer sheath radii are about three times those measured in the CSU facility at comparable electron collection currents. The outer sheath radii measured in the LeRC facility are probably larger than those measured at CSU because the ambient plasma density is lower in the LeRC facility. The actual plasma properties were not measured during these tests, however, so this statement cannot be made conclusively.

A comparison of experimentally measured radius ratios made against values computed using the model inherent in Eq. 5 and Fig. 2 using data taken at both facilities is shown in Fig. 23. This figure shows that experimentally measured radius ratios are typically less than computed ratios when tests are conducted in the LeRC test facility (near the -25% error line) while these ratios as measured and then computed from data

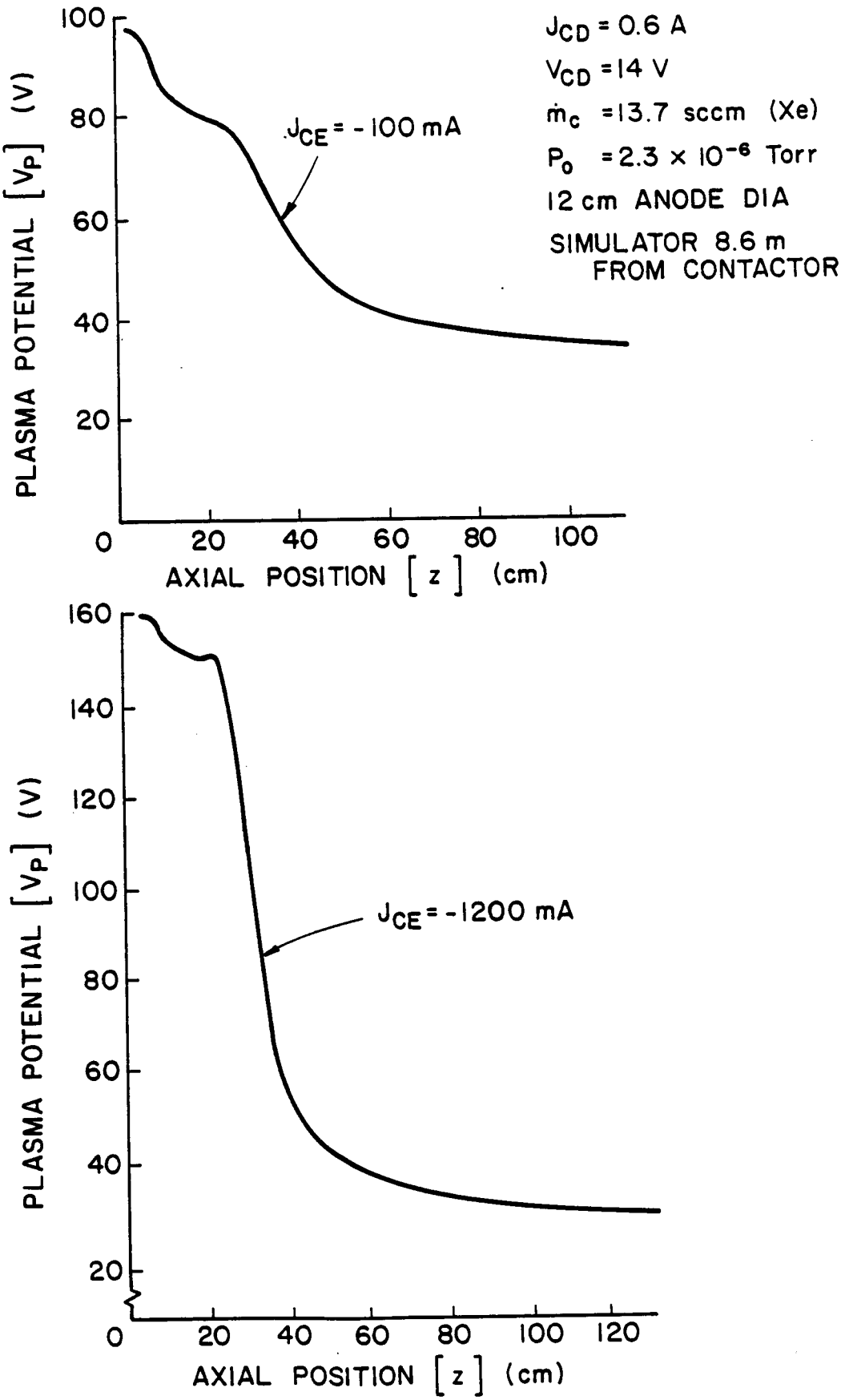

Fig. 22. Examples of Contactor Centerline Plasma Potential Profiles Measured at LeRC-/Electron Collection Mode

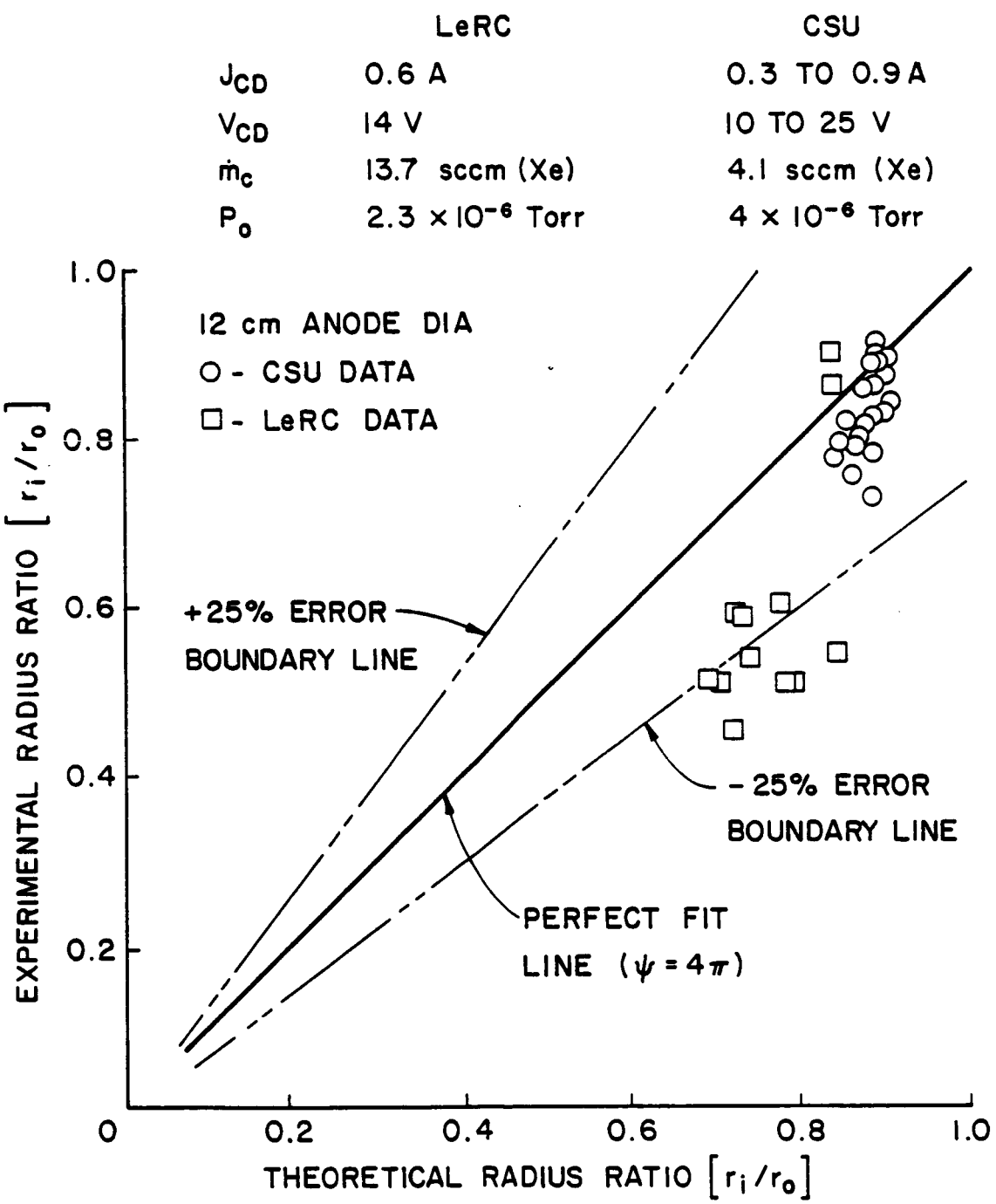

Fig. 23. Comparison of Theoretical-to-Experimental Sheath Radius Ratios Showing Facility Effects

collected in the CSU facility are in better agreement. This result suggests that a shortcoming in the double-sheath model which was not apparent in the more restrictive test environment at CSU may have been uncovered in the LeRC tests. Specifically, the results suggest the either the assumption that the double-sheath is spherical in shape or the assumption that no collisions occur within the double-sheath may be breaking down. In evaluating these possibilities it is noted that the likelihood of a significant collision rate within the double-sheath is smaller in the lower pressure environment associated with the LeRC tests than it is in the CSU test environment and that calculations suggest it should be negligible in both cases. On the other hand, the luminous plume observed when the contactor was operating in the ignited mode, which appeared spherical during the CSU tests had an ellipsoidal shape when it was observed during the LeRC tests. This ellipsoid was aligned with its major axis along the contactor cathode axis and it is considered that this geometrical configuration could have been induced by either a non-spherical neutral atom expansion or the lower plasma and neutral atom density conditions that existed in the LeRC facility. Finally, it is noted that an ellipsoidally-shaped double-sheath, in which the radius ratio was determined from measurements made along the major axis and the theoretical radius ratio was computed assuming a spherically-shaped sheath, would be expected to cause the downward shift in the LeRC data shown in Fig. 23. The fact that sheath potential drops observed in the LeRC tests (Fig. 21) were higher than those in the CSU tests is consistent with the fact that inner-to-outer sheath radius ratios measured at LeRC were lower than those measured with similar operating conditions at CSU.

Although experimental results obtained at the two facilities do not indicate the same performance for the 12 cm contactor, several similarities between the two sets of experimental results can be listed. First, the double-sheath is observed to develop between the contactor and the simulated plasma in both facilities, and the majority of the voltage drop between the contactor and simulated space plasma is shown to occur across this sheath. First-order approximations of the double-sheath radius ratio computed using a simple spherical space-charge limited double-sheath model agree to within about 30% with experimentally measured radius ratios. Second, the plasma potential directly adjacent to the contactor anode (i.e. ~2 cm downstream) was found to be close to the output of the bias power supply (i.e. the potential of the plasma near the contactor was always close to the contactor anode potential). Finally, the transition to the ignited mode of electron collection was observed in both facilities when sufficient flowrate and bias voltage were applied.

CONCLUSIONS

A simple, first-order model of the plasma contacting process based on the assumption of spherical symmetry has been developed. The essential elements of the model reflect the fact that a double-sheath develops between the plasma produced by the contactor and the ambient plasma when a contactor is collecting electrons. The inner boundary of this sheath is located at a position where ion losses through the sheath will satisfy both the Bohm stability criterion and the space-charge limit on ion extraction. The outer boundary of the double-sheath is located such that its surface area is sufficient to collect the electron current being demanded from the random current density in the ambient

determined by the fact that both the ion and electron currents that counterflow through the sheath do so at their space-charge limited values. The bulk of the experiments that have been conducted to date indicate that the model represents the essential physical elements of the plasma contacting process when electrons are being collected.

From the experimental results presented, contactor performance as reflected in the sheath voltage drop is shown to improve when anode diameter and/or contactor flowrate are increased. By considering the model these improvements in performance induced by increasing the contactor anode diameter have been correlated with an increase in the inner-to-outer sheath radius ratio at a given collection current operating condition. It is not known with confidence why increasing the anode diameter causes the radius ratio to increase, but it is believed that the high density plume expands under the influence of larger anodes and that this causes a more nearly spherical high density plume to develop when the tests are conducted at the ambient plasma density conditions realized in the CSU facility. The performance improvement induced by increasing the flowrate can be explained by recognizing that ion production by streaming electrons is induced progressively closer to the sheath where their likelihood of migrating to the sheath is higher as the flowrate is increased. This increase in ion flow causes the high density plume to expand and this in turn increases the sheath radius ratio and causes the sheath potential drop to decrease. It is noted that increasing either the anode diameter or flowrate causes an increased ion emission current which in turn reduces the sheath potential drop experienced at a given electron collection current. The model suggests that it is the ion current emitted from the high density plume which controls the performance of the plasma contactor even though

this current is a small fraction of the total current which is being conducted. The ion current is important because it mitigates the space-charge limit imposed on the electron current flow.

Separate tests carried out using the same plasma contactor operating at the same flowrate and discharge power conditions in two different test facilities both suggest that it is the double-sheath that forms between the contactor and simulated space plasmas that induces the bulk of voltage drop associated with the contacting process. These tests show, however, that the double-sheath model describes the sheath radius ratios measured in tests conducted at CSU much better than it does in tests conducted at LeRC. The reason for this is considered to be due to the fact that the model is based on spherical symmetry and the sheath appeared to be near-spherical in the CSU tests while it was more ellipsoidal in the LeRC tests.

REFERENCES

1. Hastings, D.E., N.A. Gatsonis and D.A. Rivas, "A Two-Dimensional Theory of Plasma Contactor Clouds Used in the Ionosphere with an Electrodynamic Tether," submitted to J. Spacecraft and Rockets, preview copy dated Sept. 1987.
2. Williams, J.D., P.J. Wilbur, and J.M. Monheiser, "Experimental Validation of a Phenomenological Model of the Plasma Contacting Process," PSN/NASA/ESA Second International Conference on Tethers in Space, Venice, Italy, Oct. 4-8, 1987.
3. Wilbur, P.J., and J.D. Williams, "An Experimental Investigation of the Plasma Contacting Process," AIAA Paper No. 87-0571, 12-15 Jan. 1987.
4. Kerslake, W.R. and L.R. Ignaczak, "SERT II 1980 Extended Flight Thruster Experiments," AIAA Paper No. 81-1539, 21-23 April 1981.
5. Bohm, D., "Minimum Ionic Kinetic Energy For A Stable Sheath," The Characteristics of Electrical Discharges in Magnetic Fields, A. Guthrie and R.K. Wakerling, eds., McGraw-Hill, New York, 1949, pp. 77-86.
6. Self, S.A., "Exact Solution of the Collisionless Plasma-Sheath Equation", Physics of Fluids, V.6, No.12, Dec. 1963, p.p. 1762-1768.
7. Waymouth, J.F., "Perturbation of a Plasma by a Probe," Physics of Fluids, V.7, No.11, Nov. 1964, pp. 1843-1854.
8. Patterson, M.J., and P.J. Wilbur, "Plasma Contactors for the Electrodynamic Tether," Aerospace America, V.25, No.2, Feb. 1987, pp. 32-34.
9. Wei, R., and P.J. Wilbur, "Space-Charge-Limited Current Flow in a Spherical Double-Sheath," J. Appl. Phys., V.60, Oct. 1, 1986, pp. 2280-2289.

10. Williams, J., "Electrodynamic Tether Plasma Contactor Research," appears in "Advanced Electric Propulsion and Space Plasma Contactor Research," P.J. Wilbur, ed., NASA CR-180862, Jan. 1987, pp. 1-78.

11. Aston, G., "Ion Extraction From a Plasma," NASA CR-1159849, June 1980, pp. 12-19.

12. Laupa, T., "Electrodynamic Tether Research," appears in "Advanced Electric Propulsion and Space Plasma Contactor Research," P.J. Wilbur, ed., NASA CR-175119, Jan. 1986, pp. 128-139.

13. Langmuir, I., Collected Works of Irving Langmuir, G. Suits, Ed., V. 5, Pergamon Press, Oxford, 1961, pp. 140-175.

14. Patterson, M.J., and R.S. Aadland, "Ground-based Plasma Contactor Characterization," PSN/NASA/ESA Second International Conference on Tethers in Space, Venice, Italy, Oct. 4-8, 1987.

APPENDICES

Appendix A - Experimental Validation of a Phenomenological Model of the Plasma Contacting Process

Appendix B - An Experimental Investigation of the Plasma Contacting Process

Appendix A

Experimental Validation of a Phenomenological Model of the Plasma Contacting Process*

John D. Williams+, Paul J. Wilbur++ and Jeff M. Monheiser+
Colorado State University
Ft. Collins, Colorado

Abstract

A simple model of the near-field electron collection process induced by a hollow cathode-based plasma contactor biased positive of an ambient plasma is presented. It considers three regions associated with the process, namely, a high density plasma plume adjacent to the contactor, an ambient plasma from which electrons are collected, and an intermediate double-sheath region in which the bulk of the voltage drop associated with the process develops. Spherical symmetry is suggested by the experimental results and is used as the basis of the model. Experimental validation of the model is suggested on the basis that measured radii associated with the boundaries between regions and radii computed using the model generally agree within ~25%. This degree of agreement between the radii is used to infer that 1) the surface area at the ambient plasma boundary is equal to the electron current being collected divided by the ambient plasma random electron current density, 2) the surface area of the high density plume boundary is equal to the ion current being emitted from the plume divided by the ion current density required to sustain a stable sheath and 3) the voltage drop across the double-sheath is determined based on space-charge limited ion and electron current flow between these two boundaries.

Introduction

The development of a theoretical model of the plasma coupling process is essential if results obtained in the laboratory are to be used to predict what will occur in space-based experiments, and to understand the phenomena inherent in the plasma coupling process. The purpose of this paper is to present a preliminary model describing the phenomena observed in ground-based experiments using a hollow cathode plasma contactor to collect electrons from a dilute ambient plasma under conditions where magnetic field effects can be neglected. In the electron collection mode electrons not only flow from the dilute ambient plasma to the contactor, but ions produced in the region adjacent to the contactor flow away from it. Recent experimental results suggest that the plume region, in which ions are produced, has a relatively high plasma density and that the dominant voltage drop associated with electron collection by a plasma contactor occurs across a double-sheath that separates the high density plasma plume from the ambient plasma.[1] These same experiments also suggest that the sheath which develops in the electron collection mode is spherical. Furthermore, if it is assumed that both the ion and electron currents flow through the sheath at their space-charge limited values, experimentally measured dimensions of such sheaths have been shown to be consistent with theoretically predicted dimensions found using a simple model of the spherical double-sheath.[1,2]

A simple model which can be used to estimate the locations of the double-sheath region boundaries will be presented and correlated with experimental results. This model will focus on current density constraints at these boundaries, but it will also address ion production mechanisms in the plasma plume caused by discharge electrons from the contactor cathode and by electrons streaming into the plasma plume through the double-sheath from the ambient plasma. Substantial volume ionization induced in the contactor plasma plume by these streaming electrons is believed to be accompanied by the atomic excitation reactions that cause the plume to be luminous and have led to the use of the term "ignited electron collection" to describe operation in this luminous condition.[3]

Experimental Apparatus and Procedure

In order to investigate the process of electron collection from a dilute ambient plasma by a hollow cathode-based plasma contactor the apparatus shown schematically in Fig. 1 was built. The essential elements of the apparatus are the simulator, used to generate a dilute, simulated space plasma; the plasma contactor to be tested; and the power supply used to bias the contactor relative to the simulator. Both the simulator and contactor are contained within a 1.2 m diameter by 5.3 m long stainless steel vacuum tank. The contactor is located at one end of the tank and the simulator is located ~2.7 m downstream near the center of the tank. As illustrated in Fig. 1, both the simulator and contactor are hollow cathode devices equipped with heater power supplies to facilitate startup, and discharge power supplies required to sustain discharges and, consequently, produce plasmas. The bias power supply shown directly below the contactor system was used to bias the contactor anode positive relative to the simulator, simulator plasma and the vacuum tank so the phenomenon of electron collection could be studied.

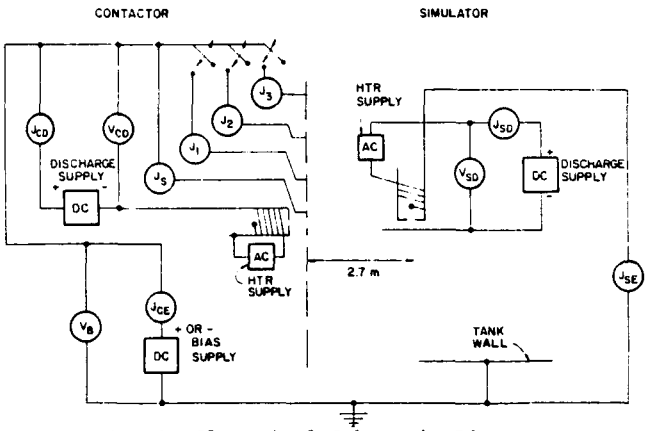

Fig. 1 Electrical Schematic Diagram

*Work supported by NASA Research Grants NAG-9-120 and NAG3-776

+Research Assistant, Dept. of Mech. Engr.
++Professor, Dept. of Mech. Engr., Member AIAA

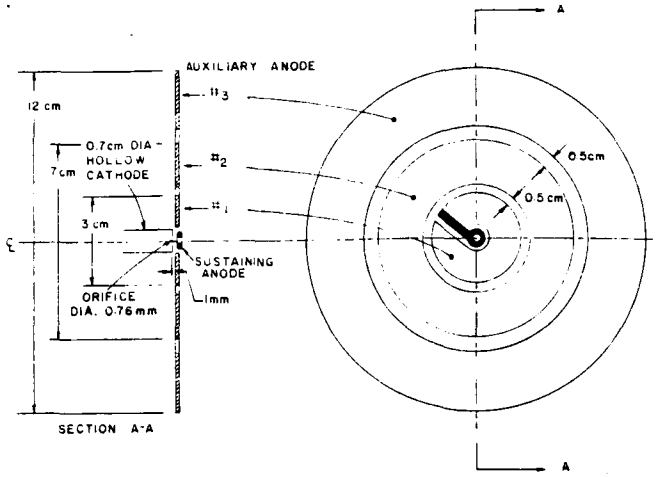

Fig. 2 Plasma Contactor Apparatus

The contactor anodes shown in Fig. 1 are shown in more detail in Fig. 2 along with the essential details of the hollow cathode device. The hollow cathode is a 7 mm diameter tantalum tube electron beam welded to a thoriated tungsten orifice plate with a 0.76 mm diameter hole drilled through its center. The low work function emissive surface within the cathode tube is made of thin (0.008 mm) rolled tantalum foil treated with chemical R-500 (a triple carbonate mixture used to lower the work function of the tantalum foil). The anodes, which are located in a plane parallel to and 1 mm downstream of the orifice plate plane, are segmented in the manner suggested in Fig. 2. The sustaining anode has a ~0.5 cm inside diameter and ~1 cm outside diameter. The various auxiliary anodes can be floated or switched to anode potential independently (see Fig. 1). Therefore, the effect of increasing the anode diameter from 1 cm to 3 cm, 7 cm and 12 cm can be studied. The ammeters labelled J_s, J_1, J_2 and J_3 in Fig. 1 allow the currents flowing to the various anodes to be measured. The bias supply output was connected directly to the contactor anodes so that a limitation on the contactor discharge current J_{CD} would not impose a limit on the contactor emission current J_{CE}.[1] Similarly, the cathode of the simulator was connected to the negative terminal of the bias supply and to the tank so its electron emission current J_{SE} would not be limited by its discharge current setting J_{SD}. It is noted that because only the electron collection process is being studied in this paper, the contactor emission current, measured with the ammeter labelled J_{CE} in Fig. 1, will be defined as negative.

The simulator utilizes the same type of hollow cathode as the contactor, but its orientation and anode geometry differ. Its anode is a single, 3 cm dia flat plate made of tantalum. This anode does not have an orifice and the entire simulator assembly is oriented with its axis at right angles to the centerline joining the contactor and simulator. This simulator configuration was used because it was believed that this cathode axis and anode orientation would cause the plasma produced by the simulator to spread out into a diffuse plume.

Plasma properties were measured using emissive and Langmuir probes that could be swept through the region between the contactor and simulator. The emissive probe consists of a 0.076 mm diameter tungsten wire heated to thermionic emission temperatures by a floating battery power supply connected in the manner described in Ref. 4. This probe, along with the Langmuir probe, could be moved along the centerline joining the contactor and simulator and along paths parallel to this centerline at radii varying from 0 to 30 cm. At each operating condition the contactor discharge voltage and current, V_{CD} and J_{CD}; the bias voltage, V_B; the contactor emission current, J_{CE}; the simulator discharge voltage and current, V_{SD} and J_{SD}; and the simulator emission current, J_{SE}, were measured using the meters shown schematically in Fig. 1. For all tests to be described here the simulator was operated with a 1.9 standard cubic centimeter per minute (sccm) Xenon flowrate and a discharge current J_{SD} of 0.3 A.

Structural Basis of Model

A typical potential profile measured along the tank centerline using the emissive probe when the contactor was operating in the electron collection mode is shown in Fig. 3. For this profile the contactor discharge current and voltage were 0.3 A and 15 V, respectively, and the contactor flowrate was 4.1 sccm (Xe). The electron collection current was ~600 mA and the 12 cm anode dia was being used (i.e. all anodes shown in Fig. 2 were at anode potential) and the bias potential V_B was ~85 V. During the test the ambient pressure P_o within the vacuum tank was 3.2×10^{-6} Torr. The figure shows a large potential drop sheath structure near the contactor after which the potential profile becomes flat (>12 cm). This flat (constant potential) region between 12 and 80 cm is followed by another sheath that extends between 80 and 150 cm. Beyond 150 cm the plasma potential becomes flat again and remains this way until the position of the simulator is reached at ~270 cm. It should be noted that the emissive probe was not positioned closer than ~10 cm from the simulator. Consequently, the detailed structure of the potential variation immediately surrounding the simulator has been assumed in Fig. 3. This was done to show the complete potential field that an electron emitted from the simulator cathode and collected on the contactor anode moves through. The potentials of the simulator and contactor electrodes are also identified by the anode and cathode sketches shown on Fig. 3.

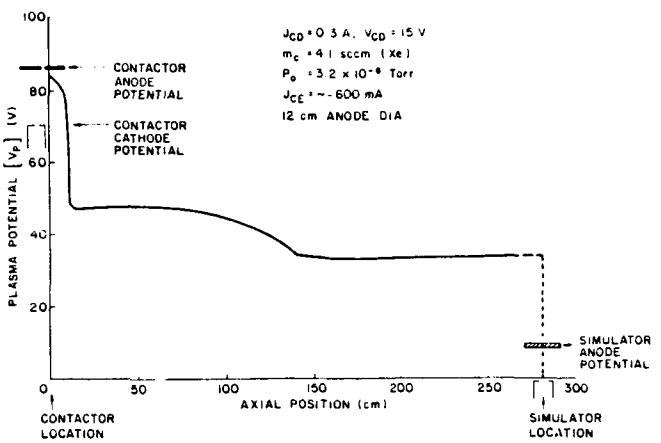

Fig. 3 Typical Centerline Plasma Potential Profile

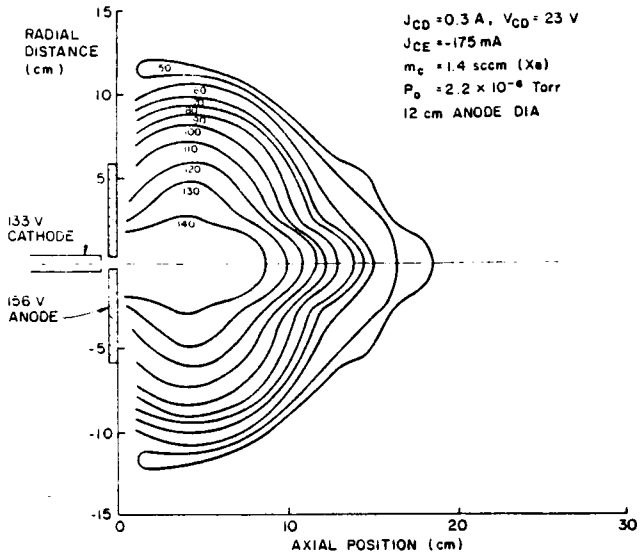

Fig. 4 Typical Equipotential Contour Plot

When several potential profile sweeps are made at various radii from the centerline of the contactor, a potential contour map, like the one shown in Fig. 4, of the region directly downstream of the contactor can be constructed. The particular data in this figure were obtained with the 12 cm anode dia configuration and a contactor discharge current and voltage of 0.3 A and 23 V, respectively. The contactor flowrate was 1.4 sccm (Xe) which, along with the simulator flowrate of 1.9 sccm (Xe), induced an ambient tank pressure of $2x10^{-6}$ Torr. At these operating conditions an electron collection current of 175 mA was observed when the contactor was biased 156 V above the tank reference potential. The contours shown in Fig. 4 suggest that the potential is relatively uniform in the vicinity of the high density plume region and that it drops relatively rapidly from about 140 V to 50 V. At a location near 17 cm downstream of the contactor a potential well is shown to exist by the 50 V potential contour after which the potential rises to a value that remains between 50 and 60 V throughout the ambient plasma region. The fact that the contour lines take on a spherical or hemispherical shape suggests that electrons are flowing nearly radially inward from the ambient plasma and ions are flowing nearly radially outward from the high density plasma plume located within the 140 V contour. While the particular potentials observed on contour maps change as the operating conditions change the relatively spherical shape shown in Fig. 4 is typical so it is considered appropriate to assume this shape in models of the electron collection plasma contacting process.

Figure 5 shows a potential profile, similar to the one discussed in Fig. 3, immediately downstream of the contactor on an expanded scale. This profile, typical of essentially all electron collection plasma potential profiles collected to date, shows the three distinct plasma regions that have been observed. These regions are: 1) a high density plasma plume region adjacent to the contactor and sustained by the contactor discharge electrons and the electrons drawn from the ambient plasma, 2) a double-sheath region across which a substantial voltage drop develops and 3) an ambient plasma region in which the plasma is Maxwellian and its properties are quite uniform. In the case of Fig. 5 the high density plume region is shown to extend from the contactor anode to a location ~10 cm downstream. This region is typically characterized by a slight plasma potential gradient where the plasma potential near the contactor is usually near the bias supply output voltage and drops to a value several volts below this at the high density plume/double-sheath interface location (i.e. the inner sheath radius r_i). It is assumed that the electrons from the ambient simulated space plasma and the ions from the high density plume region counterflow through the sheath at the space-charge limited current condition. The axial location of the interface between the double-sheath and the ambient plasma region is labelled the outer radius location r_o. It should be noted that the inner and outer radii of the sheath are defined as the intersections of lines drawn along the potential profiles associated with each of the three regions in the manner suggested in Fig. 5. These locations are essentially the same as those at which the second derivatives of the plasma potential with respect to distance are a minimum and a maximum. The magnitude of the sheath potential drop V_{SH} and the sheath thickness $r_o - r_i$ correspond to an electric field strength of 2000 V/m at an axial position near 11 cm for the case of Fig. 5. Downstream of the double-sheath region is the ambient plasma region, which is typically characterized by a very flat potential profile and constant plasma state variables up to ~80 cm downstream when the contactor is operating in the ignited electron collection mode.

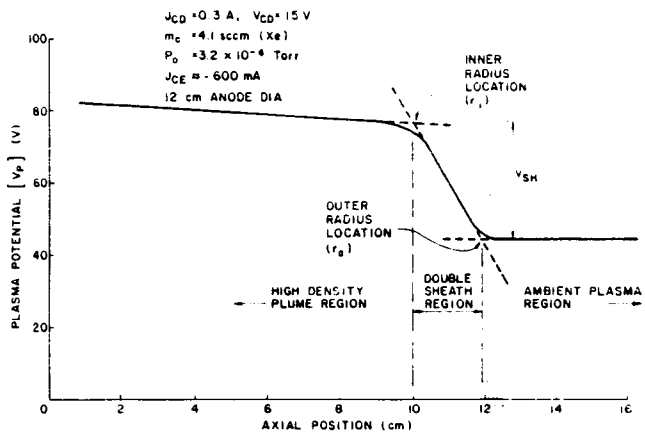

Fig. 5 Typical Centerline Plasma Potential Profile on Expanded Axial Scale

Theoretical and Physical Elements of the Model

The approach to the problem of developing a theoretical model, which describes electron collection from an ambient neutral plasma was to write basic charge conservation equations for ions and electrons flowing through the high density plume and double-sheath regions. This model was developed on the basis that the current being drawn through the circuit is conducted almost entirely by electrons and that the current flows through each region via a spherical segment of solid angle ($0 < \psi < 4\pi$) in the manner suggested in Fig. 6. The ambient plasma region in Fig. 6 is characterized by an electron (and ion) density n_{eo} and an electron temperature T_{eo}. The neutral atom pressure and temperature reach ambient values P_o and T_o far from the contactor in the ambient plasma region. The neutral atom density n_n varies from a minimum, corresponding to the ambient pressure and temperature,

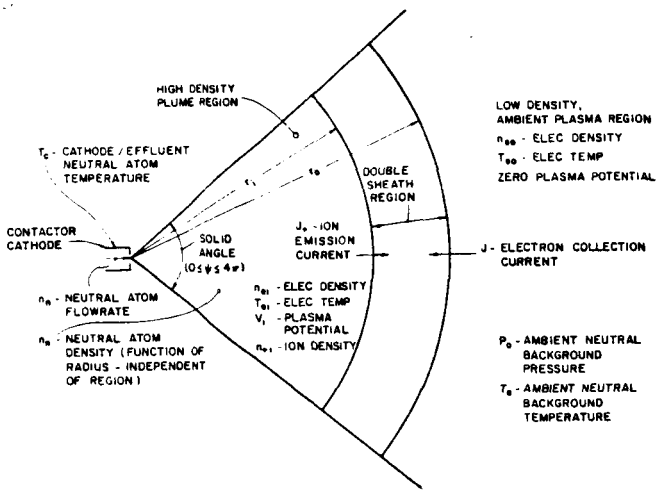

Fig. 6 Physical Model of Electron Collection

to a maximum at the contactor where neutral atoms of temperature T_C are being supplied from a point source at a rate of $\dot{n}_n$.

While the total current flowing through the double-sheath region is equal to the sum of the electron collection current J and the ion emission current J_+, the ratio of the magnitudes of these currents varies as the square root of the ion-to-electron mass ratio; therefore, the electron current dominates. The electron current flowing from the ambient plasma region into the high density plume region is assumed to be equal to the random ambient electron current incident on the outer boundary of the double-sheath region located at r_o and is given by:

$$J = \frac{e\, n_{eo}\, \psi\, r_o^2}{4} \sqrt{\frac{8\, K\, T_{eo}}{\pi\, m_e}} \qquad (1)$$

Both the ion and electron currents, shown counterflowing through the double-sheath region in Fig. 6, are assumed to be space-charge limited on the basis that it is the space-charge phenomenon that causes the double-sheath to form. The assumptions made to obtain the solution of the sheath problem[2] together with the pertinent equations and figures are included here for completeness. The basis of the development is that an inner spherical surface of radius r_i and potential V_i is supplying an ion current from an infinite supply of zero velocity ions of mass m_+ on the inner surface (the high density plume region boundary). At the same time electrons of mass m_e and zero velocity are drawn from the outer spherical surface of radius r_o (the ambient plasma region boundary). In order to simplify the analysis, it is assumed there are no collisions (elastic or inelastic) within the double-sheath region. When equations describing conservation of energy and conservation of charge are used in conjunction with Maxwell's formulation of Gauss' Law, equations describing the maximum flow of ions from the inner sphere (J_+) and electrons from the outer sphere (J) can be obtained in terms of the applied potential difference and the radius ratio of the two spherical segment surfaces. These limiting maximum currents, which are achieved when the potential gradients at the edges of both spherical surfaces are zero, are given in Ref. 2 by

$$J = \psi\, \epsilon_o\, V_i^{3/2} \sqrt{\frac{2e}{m_e}}\, j_o \qquad (2)$$

and

$$J_+ = J \sqrt{\frac{m_e}{m_+}}\, (\alpha)^{-1}; \qquad (3)$$

where ϵ_o is the permittivity of free space and α and j_o are parameters that depend only on the radius ratio r_i/r_o. It is interesting to note that the currents flowing from the inner and outer spherical surfaces are dependent only on the radius ratio and not on the absolute magnitude of these radii. The variation of the parameters α and j_o with radius ratio have been determined numerically[2] and these relationships are shown in Figs. 7 and 8.

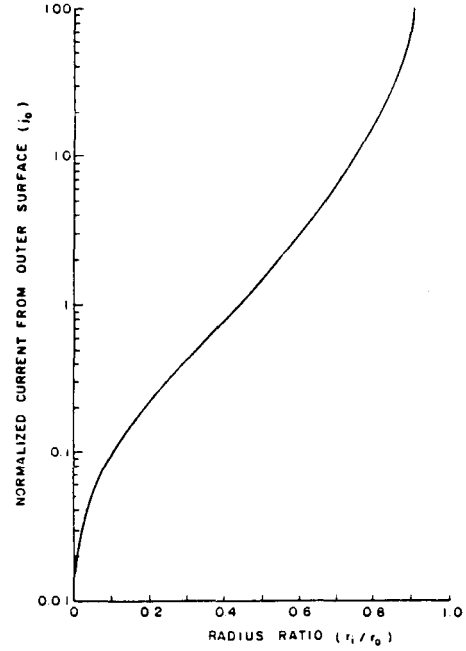

Fig. 7 Normalized Electron Collection Current Versus Sheath Radius Ratio (from Ref. 2)

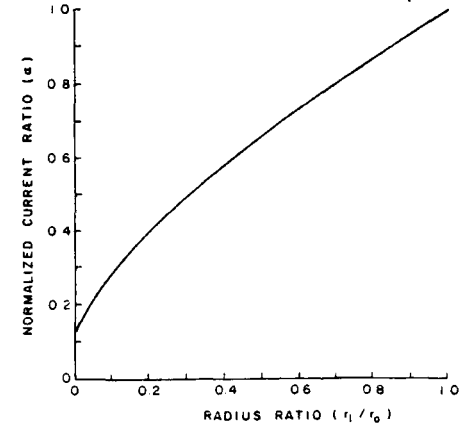

Fig. 8 Normalized Ion-to-Electron Current Ratio Versus Sheath Radius Ratio (from Ref. 2)

The model presumes the double-sheath develops between the radii r_i and r_o and at radii less than r_i the plasma properties are constant at an electron density and temperature of n_{ei} and T_{ei} and a plasma potential V_i (measured relative to the ambient plasma potential). The ion density n_{+i}, which is equal to the electron density in this region, is sufficiently high so ions can be extracted through the double-sheath at a current J_+. This ion current can be written in terms of the plasma density in the high density plume region if it is recognized that the ion loss rate is controlled by the Bohm criterion for a stable sheath[5] defined by the equation

$$J_+ = e\, n_{+i}\, \psi\, r_i^2 \sqrt{\frac{K\, T_{ei}}{m_+}}\ \gamma \qquad (4)$$

where γ is a correction factor that accounts for the effects of pre-sheath acceleration of ions from the high density plume region toward the double-sheath.[6] The factor γ may take on values ranging from 0.1 to 1 depending upon the plasma environment existing in the high density plume region. For the present work a value of 0.3 has been used for γ so Eq. (4) can be used to compare predictions of the model with experimental results. More work needs to be done to determine if this assumed value for γ can be justified theoretically.

The final portion of the proposed electron collection model describes the balance between ion production and loss rates within the high density plume region. It is this balance which determines the ion density n_{+i} in the plume region that can be used in Eq. (4). In addition to the ion loss rate from the high density plume described by Eq. (4), the following additional phenomena could be acting to induce significant ion losses:

1) Ion collection on solid surfaces at a rate J_{+s} determined by the area of the surfaces exposed to the high density plasma plume and the Bohm criterion[5] that must be satisfied in order for a stable sheath to exist at a surface collecting ions,

2) Radiative recombination[7] at a rate J_{+r} and

3) Three body recombination[7] at a rate J_{+b}.

On the other hand, ions are produced within the high density plume region through the following mechanisms:

1) Discharge induced ionization near the contactor at a rate J_{+d} by electrons supplied from the contactor cathode, and

2) Ionization within the high density plume region at a rate J_{+p} by electrons directed at the contactor cathode that have been accelerated to high energies as they pass through the double-sheath. Conservation of ion current considering these ion production and loss rates yields the requirement

$$J_+ + J_{+s} + J_{+r} + J_{+b} = J_{+d} + J_{+p} \ . \qquad (5)$$

The ion loss rate through the double-sheath J_+ is described in Eq. (4) and the ion loss rate to solid surfaces J_{+s} can be estimated using a similar equation; namely,

$$J_{+s} = e\, n_{ei}\, A_s \sqrt{\frac{K\, T_{ei}}{m_+}}\ \gamma \qquad (6)$$

where A_s is the area of the ion collecting surface exposed to the high density plasma (generally a cathode potential surface).

The radiative recombination loss mechanism can be described using a rate factor given by Mitchner and Kruger[7] and may be computed using

$$J_{+r} = e\, n_{ei}\, n_{+i}\, (2.7 \times 10^{-13})\, T_{ei}^{-3/4}\, \frac{\psi\, r_i^3}{3} \ . \qquad (7)$$

It is apparent from this equation that this process is favored by low electron temperatures and high plasma densities. Using values of plume plasma density $n_{ei} = n_{+i} = 10^8$ cm^{-3}, temperature $T_{ei} = 3$ eV and inner radius $r_i = 10$ cm measured under typical ground-based experimental conditions like those associated with Figs. 3, 4 and 5, one finds J_{+r} to be of the order 10^{-11} to 10^{-10} A. This current is much less than the milliampere level ion currents predicted using Eqs. (2) and (3) so it appears that radiative recombination losses can be neglected.

The rate at which ions are lost to three body recombination J_{+b} can be estimated using another rate factor given by Mitchner and Kruger[6]

$$J_{+b} = e\, n_{ei}^2\, n_{+i}\, (5.6 \times 10^{-27})\, T_{ei}^{-9/2}\, \frac{\psi\, r_i^3}{3} \qquad (8)$$

This equation, which considers electrons to be the most likely third body participants, shows that the reaction is even more heavily favored by low electron temperatures and high plasma densities than the radiative recombination process represented by Eq. (7). Substitution of the typical experimentally measured properties cited in the previous paragraph yields values of J_{+b} on the order of 10^{-18} to 10^{-17} A, so this process should also contribute negligibly as an ion loss mechanism.

The two ion production processes identified in Eq. (5) involve the ionization of neutrals coming from the contactor by the contactor discharge electrons and by electrons being collected from the ambient plasma. The rate of production by contactor discharge electrons can be determined experimentally by biasing the contactor positive of the vacuum tank wall, with the simulator shown in Fig. 1 off, so electrons from the contactor discharge are reflected from the tank wall and the ion production current J_{+d} going to the tank wall can be measured directly. Under typical operating conditions current levels on the order of a few

milliamperes are measured. The second ion production mechanism, which involves electrons drawn from the ambient plasma, has not been measured directly, but can be computed using a simple model describing the process.

In order to determine the rate at which ions are produced by high energy electrons that pass through the double-sheath and bombard neutral atoms within the inner plume region, it is first necessary to determine the neutral atom density profile through which these electrons pass. One might do this using a neutral gas plume model like the one suggested by McCoy [8], but in this analysis a simple point source model was used instead. This point source model was used because it is both sufficiently accurate and consistent with other assumptions of this analysis. For a hollow cathode expelling neutral atoms at a rate $\dot{n}_n$ from a point source into an ambient neutral background at pressure P_o and temperature T_o through a solid angle ψ, the radial variation in neutral density may be described using the expression

$$n_n = \frac{\dot{n}_n}{\psi\, r^2\, v_n} + \frac{P_o}{K\, T_o} \quad , \qquad (9)$$

where r is the radius at which the atom density is sought. The neutral atom velocity v_n is given by

$$v_n = \sqrt{\frac{8\, K\, T_c}{\pi\, m_+}} \quad ; \qquad (10)$$

where T_c is the hollow cathode wall temperature. It has been assumed that the neutral atoms flowing out of the contactor come into equilibrium with cathode surfaces at this temperature and that the atom and ion masses are equal.

As the electrons being collected from the ambient plasma pass along radial trajectories through the double-sheath and then through the high density plume they can have inelastic collisions with neutral atoms having a density given by Eq. (9) at any radial location. It is, however, the ionizing collisions occurring within the high density plume region that contribute to the plume ion production rate. It will be assumed that electrons flowing through the double- sheath region which experience any type of inelastic collision (ionizing or exciting) lose sufficient energy so they will produce no further ions in the high density plume. At the conditions where experiments have been run, analysis has shown the rate at which these collisions occur in the sheath is small compared to both the ion and electron currents so the effect of these collisions on the double-sheath problem presented earlier has been neglected. Streaming (high energy) electrons that reach the radius r_i shown in Fig. 6 without experiencing an inelastic collision have the energy associated with the sheath voltage drop V_i and they can experience ionizing collisions as they move radially from r_i to a radius that is one Debye length (λ) from the cathode orifice. It is assumed that any ionizing collisions which occur within one Debye length of the cathode will result in the ions produced being collected by the cathode. In order to make the analysis tractable it has been assumed that electrons which experience any inelastic collision within the high density plume region have their energy degraded sufficiently so they will not produce additional ions. Any energy retained by streaming electrons that have produced ions is assumed to be dissipated in exciting neutral atoms and heating background electrons within the high density plume region.

The rate (expressed as a current) at which high energy streaming electrons are lost as potential ion producers as a result of inelastic collisions in the double-sheath region is given by

$$eR_\ell = \int_{r_i}^{r_o} e\, n_n\, n_e\, \sigma_{in}\, v_e\, \psi\, r^2\, dr \quad , \qquad (11)$$

where n_e is the electron density, and σ_{in} and v_e are the inelastic collision cross section and electron velocity, respectively, corresponding to the electron energy at a radial location r. If one assumes the rate of electron loss given by Eq. (11) is small compared to the current flowing ($e\, R_\ell \ll J$) then current continuity can be applied to obtain

$$J \approx e\, n_e\, v_e\, \psi\, r^2 \qquad (12)$$

Substitution of Eqs. (9) and (12) into Eq. (11) yields

$$e\, R_\ell = \int_{r_i}^{r_o} \left(\frac{\dot{n}_n}{\psi\, r^2\, v_n} + \frac{P_o}{K\, T_o} \right) J\, \sigma_{in}\, dr \qquad (13)$$

This can be integrated numerically if the variation in cross section with electron energy and the variation in electron energy with radial position are known. The needed cross section data are given for Xenon in Refs. 9 and 10 and the exact variation in electron energy with radius can be computed using the model of Ref. 2. In the present analysis, however, it has been assumed that the potential variation through the double-sheath is linear with radial position. Substitution of typical experimental data measured in ground-based experiments conducted to date into Eq. (13) yields values of this rate ($e\, R_\ell$) that are less than 5 % of the ion current flowing from the high density plume region through the double-sheath. Consequently, the current of electrons that have been accelerated through the double-sheath and have not had inelastic collisions in the double-sheath region may be assumed to be equal to the electron current being collected J.

The gradient of the streaming electron current J' that develops in the high density plume region as a result of inelastic collisions occurring there is given by

$$\frac{dJ'}{dr} = e\, n'_e\, n_n\, \sigma_{in}\, v'_e\, \psi\, r^2 \quad , \qquad (14)$$

where the inelastic cross section σ_{in} and streaming electron velocity v'_e are evaluated at an energy corresponding to the sheath potential drop. Conservation of the streaming electron current J' in the high density plume region requires

$$J' = e\, n'_e\, v'_e\, \psi\, r^2 \qquad (15)$$

Combining Eqs. (9), (14), and (15) and integrating one obtains

$$\int_{J}^{J'_f} \frac{dJ'}{J'} = \int_{r_i}^{\lambda} \sigma_{in} \left[\frac{\dot{n}_n}{\psi\, r^2\, v_n} + \frac{P_o}{K\, T_o} \right] dr \qquad (16)$$

where J'_f designates the current carried by streaming electrons that have not had an inelastic collision when they reach a radius that is one Debye length (λ) from the cathode orifice. The ionization rate induced by the electrons that do have ionizing collisions in the high density plume region is then given by the difference between the primary electron currents at r_i and λ times the fraction of the collisions that induce ionization, namely

$$J_{+p} = (J - J'_f) \frac{\sigma_+}{\sigma_{in}} \qquad . \quad (17)$$

In this equation, both the inelastic and the ionization cross sections σ_{in} and σ_+, respectively, are evaluated at the sheath potential drop V_i.

Integration of Eq. (16) and substitution of the result into Eq. (17) yields

$$J_{+p} = J \frac{\sigma_+}{\sigma_{in}} \left[1 - \exp\left(-\sigma_{in} \left\{ \frac{\dot{n}_n}{\psi\, v_n} \left(\frac{1}{\lambda} - \frac{1}{r_i} \right) + \frac{P_o}{K\, T_o} \left(r_i - \lambda \right) \right\} \right) \right] \qquad (18)$$

where the Debye length is given by

$$\lambda = \sqrt{\frac{\epsilon_o\, K\, T_{ei}}{n_{+i}\, e^2}} \qquad . \quad (19)$$

Equations (1) through (19), when coupled with a model of the spherical double-sheath like the one embodied in Figs. 7 and 8, represent a simple, first-order model of the electron collection process in the region close to the contactor. If one prescribes the ambient plasma density and temperature and the temperature of the high density plume plasma, these equations can be solved simultaneously to yield the sheath voltage drop, ion current and inner and outer sheath radii as a function of the electron current being collected. It is anticipated that an energy balance on the high density plasma region might be applied to enable one to compute the electron temperature in this region rather than having to assume a value for it, but this has not been accomplished at this point in time.

Experimental Validation of the Model

There are some aspects of the model, presented in the preceeding section, that have been studied experimentally using the apparatus shown in Figs. 1 and 2 and described in the associated text. They are the model elements associated with 1) electron current collection at the outer sheath boundary, 2) space-charge limited ion and electron current flow through the sheath itself and 3) ion current emission across the inner sheath boundary. Experimental results that bear on each of these elements of the model will be discussed. While the model has been couched in terms of a variable solid angle ψ the value of this angle will be assumed to be 4π in all of the comparisons that follow (i.e. the processes will be assumed to be occurring within a full spherical segment). This has been done because this assumption appears to produce a model that agrees best with experimental observations. In this regard it is noted that this implies electron collection maybe occurring on both the upstream and downstream faces of the anodes shown in Fig. 2.

Electron Collection at the Outer Sheath Boundary

Equation (1) can be rearranged to give the radius of the outer sheath boundary

$$r_o = \left[\frac{4\, J}{e\, n_{eo}\, \psi} \sqrt{\frac{\pi\, m_e}{8\, K\, T_{eo}}} \right]^{1/2} \qquad . \quad (20)$$

At various operating conditions, measurements of electron collection current, ambient plasma density n_{eo} and electron temperature T_{eo} were made. The electron collection current J is obtained by recording the magnitude of the contactor emission current from the ammeter labelled J_{CE} in the electrical schematic diagram shown in Fig. 1. The plasma property measurements taken at this electron collection current condition showed that the density and temperature were quite uniform throughout the ambient plasma region so unambiguous values of the current and the ambient plasma properties could be put into Eq. (20) and an outer sheath radius based on this aspect of the theoretical model could be determined. At each operating condition the outer sheath radius could also be measured directly from a corresponding potential profile like the example shown in Fig. 5. Figure 9 presents a comparison of these directly measured experimental and theoretical outer sheath radii for cases where the contactor anode dia was 12 cm, the contactor discharge power ranged from 10 to 25 W, contactor flowrates ranged from 3.4 to 4.1 sccm (Xe), tank pressures ranged from 2.6 to 4 $\times 10^{-6}$ Torr and electron collection currents varied from 100 to 1000 mA. The straight line drawn on the figure shows where the data would fall if the experiment agreed perfectly with the model. Although the data show considerable scatter, presumably because of errors associated with plasma property measurements and/or a non-spherical sheath boundary, the data suggest the model does yield a relatively accurate value of the outer radius.

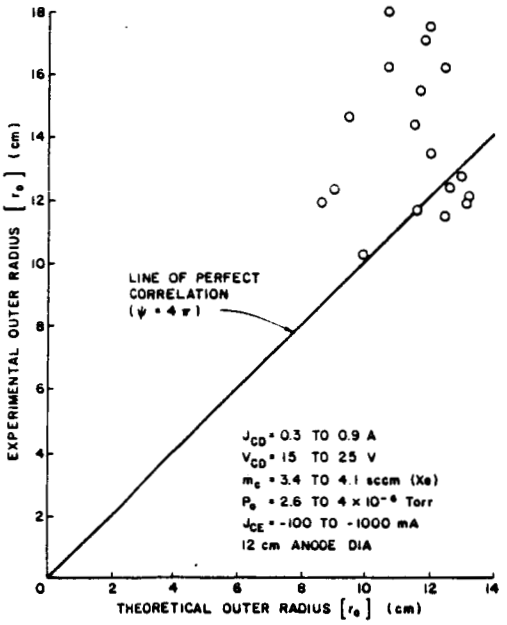

Fig. 9 Correlation of Computed and Measured Outer Sheath Radii

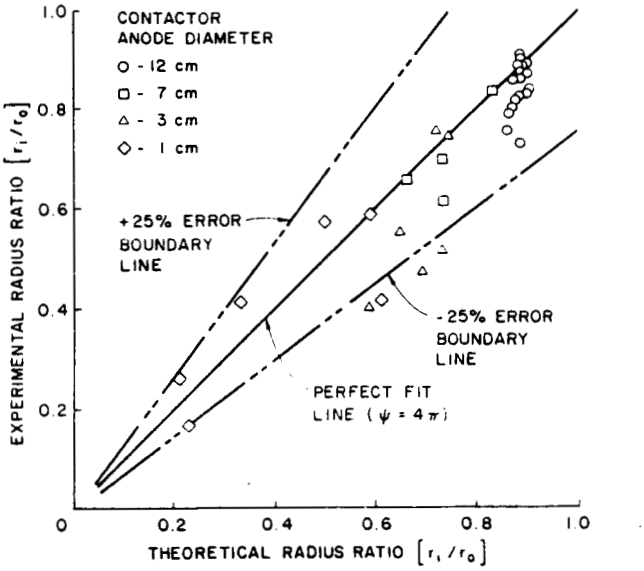

Fig. 10 Correlation of Computed and Measured Radius Ratios Based on Space-Charge Limited Double Sheath Criteria

Space-Charge Limited Current Flow Condition

The validity of the double-sheath portion of the model can be checked by comparing measured radius ratios, inner radius-to-outer radius of the sheath region, with those the model predicts should exist at the specified electron collection current and sheath potential drop conditions at which the radius ratios are being measured. The radius ratio is expressed given in terms of the normalized current parameter j_o in Fig 7. This parameter is related to the electron collection current $J = |J_{CE}|$ and the sheath potential drop $V_i = V_{SH}$ by Eq. (2) which can be rewritten

$$j_o = \frac{J}{\epsilon_o \psi V_i^{3/2}} \sqrt{\frac{m_e}{2e}} \qquad (21)$$

Using Eq. (21) together with the data of Fig. 7, measured electron collection currents and sheath voltage drops, radius ratios associated with a particular operating condition can be computed and compared to experimentally measured ratios determined from corresponding emissive probe plasma potential profiles. Figure 10 shows this comparison for data obtained over a wide range of operating and test conditions. The circular data points correspond to a contactor anode diameter of 12 cm and to the data and operating condition ranges listed in Fig. 9. The other data points which correspond to smaller anode diameters were obtained in previous tests[1] and are included on the figure for completeness. As indicated by the perfect fit and 25% error boundary lines, the model predicts radius ratios with reasonable accuracy over a rather large range of operating conditions. It is interesting to note that the 12 cm anode dia data fall above a 0.8 radius ratio while the smaller diameter anode data extend over greater ranges in the region below 0.8 with the 1 cm anode dia covering the largest radius ratio range. It is also noted that all of the circular data points were obtained when the contactor was operating in the ignited electron collection mode. In this mode large electron collection currents are observed and, for typical sheath voltage drops, this implies the radius ratios approaching unity that are observed on the figure.

Ion Current Emission at the Inner Sheath Boundary

Equation (4), which expresses the constraint on the ion current condition that must be satisfied in order to assure a stable inner sheath (i.e. the Bohm criterion), can be combined with Eq. (3) to obtain

$$r_i = \left[\frac{J}{e\, n_{+i}\, \psi\, \gamma\alpha} \sqrt{\frac{m_e}{k\, T_{ei}}}\right]^{1/2} . \qquad (22)$$

At a particular operating condition where the electron collection current and the sheath voltage drop are known, the radius ratio associated with that operating condition can be determined from Eq. (21) and Fig. 7. This radius ratio can in turn be used to enter Fig. 8 and determine the value of the parameter α which can be used in Eq. (22). If, at the same operating condition, the plasma density n_{+i} and electron temperature T_{ei} in the inner sheath region are measured, all of these data can be used in Eq. (22) to compute a theoretical inner sheath radius. In order to make this computation, the value of the pre-sheath correction factor γ was assumed to be 0.3. While this value is considered reasonable, it still needs to be determined on a rigorous theoretical basis. Figure 11 presents a comparison of this computed radius r_i with the radius measured from data like those shown in Fig. 5. The proximity of the data points to the perfect fit line suggests that the model describes the experimental results to within ~25 %, and, hence, the incorporation of the Bohm criterion for a stable inner sheath is probably justified.

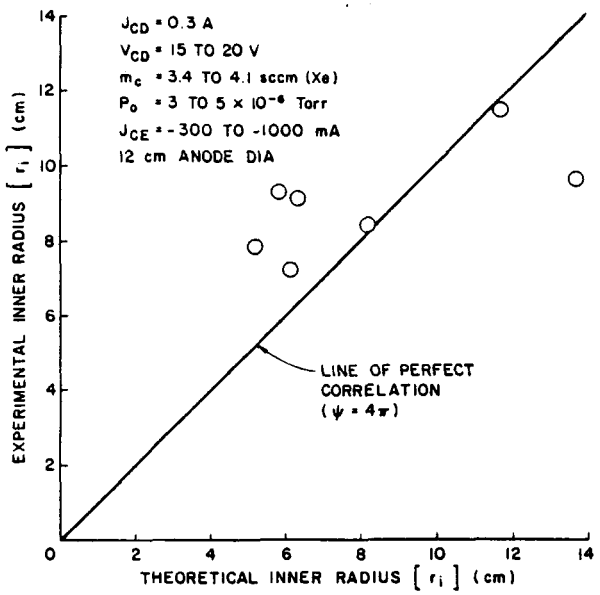

Fig. 11 Correlation of Computed and Measured Inner Radius Data Based on Bohm Constraint on Ion Currents

Ion Production and Loss Mechanisms

Additional elements of the model that are manifest in Eqs. (5) through (19) have not been investigated experimentally to any significant extent at this time. Calculations that have been performed using typical experimental data suggest that the rate of ion production due to electrons streaming through the sheath into the high density plume is on the order of a milliampere. This value is consistent with the space-charge limited ion current demanded by the solution to the spherical double-sheath problem and the discharge induced production of ions in the high density plume region since both of these ion currents are also on the order of a milliampere.

Conclusion

The simple model presented in Eqs. (1) through (5) seems to yield results that generally agree with experimentally measured ones. It suggests that the near-field plasma contacting process can be described using three distinct regions. These three regions are the high density plume region adjacent to the plasma contactor, a double-sheath region, and the ambient plasma region.

Experimental results correlate well with the predictions of the model and show that space-charge phenomena control the development of the double-sheath. This double-sheath supports the bulk of the voltage drop which occurs between the contactor and the ambient plasma at a given electron collection current. Experimental results also suggest that the electron current flowing through the sheath is equal to the random electron current density in the ambient plasma times the surface area of the outer sheath boundary. Finally, the rate at which the ions flow across the inner sheath boundary is determined by the product of the ion current density required to sustain a stable sheath at the inner sheath boundary times its surface area.

References

1. Wilbur, P.J., and J.D. Williams, "An Experimental Investigation of the Plasma Contacting Process," AIAA Paper No. 87-0571, 12-15 January 1987.

2. Wei, R. and P.J. Wilbur, "Space-Charge-Limited Current Flow in a Spherical Double Sheath," J. Appl. Phys., V 60, 1 Oct. 1986, pp. 2280-2284.

3. Patterson, M. and P.J. Wilbur,"Plasma Contactors for Electrodynamic Tether," Aerospace America, V 25, No. 2, February 1987, pp. 32-34.

4. Aston, G., "Ion Extraction from a Plasma," NASA CR-1159 849, June 1980, pp. 12-19.

5. Bohm, D., "Minimum Ionic Kinetic Energy for a Stable Sheath," The Characteristics of Electrical Discharges in Magnetic Fields, Guthrie, A., and Wakerling, R.K., Eds., McGraw-Hill, New York, 1949, pp. 77-86.

6. Waymouth, J.F., "Perturbation of a Plasma by a Probe," Physics of Fluids, V 7, No. 11, November 1964, pp. 1843-1854.

7. Mitchner, M. and C.H. Kruger, Jr., Partially Ionized Gases, John Wiley and Sons Publishing Co., 1973, pp. 35-36,440,463.

8. McCoy, J.E., "200 kW PMG Reference System for Power and Propulsion," AIAA Paper No. 87-0570, 12 - 15 January 1987.

9. Hayashi, M., "Determination of Electron-Xenon Total Excitation Cross Sections, from Threshold to 100 eV, from Experimental Values of Townsend's α," Journal of Physics D: Applied Physics, V 16, 1983, pp. 581-589.

10. Rapp, D. and Englander-Golden, P., "Total Cross Sections for Ionization and Attachment in Gases by Electron Impact. I. Positive Ionization," Journal of Chemical Physics, V 34, No. 5, 1965, pp. 1464-1479.

AN EXPERIMENTAL INVESTIGATION OF THE PLASMA CONTACTING PROCESS*

Paul J. Wilbur** and John D. Williams+
Colorado State University
Fort Collins, CO 80523

Abstract

Measurements including plasma potential profile measurements made on a simple hollow cathode plasma contactor operating in the electron collection and emission modes are described. The ignited electron collection mode of contactor operation is identified, shown to improve contactor performance and found to be facilitated by increasing the size of the contactor anode. Potential profile data are compared to the predictions of a simple theoretical model that describes space-charge-current limitations imposed by the formation of a double sheath and found to agree with each other to within about ± 25%. Because electrons, which are the dominant charge carriers, tend to be emitted from the hollow cathode in the emission mode and collected by the anode in the collection mode it is suggested that operation at high electrodynamic tether currents will probably require switching the point of tether connection to the contactor between its cathode and anode when the direction of tether current is reversed.

Introduction

Plasma contactors are intended to clamp a point on a spacecraft to local space plasma potential under conditions where significant currents might be required to flow in either direction between the space plasma and this point on the spacecraft to prevent a potential difference from developing. For electrodynamic tethered satellite applications, it is especially important that these contactors be designed to handle large currents that can flow in either direction between the ends of the tether and the low density ambient space plasma. While it is possible to collect substantial electron current from the ambient space plasma to a sufficiently large collecting surface,[1] space experiments have shown that it is difficult to supply electrons to the space plasma unless the electron source is a plasma plume produced by a contactor.[2,3] Further, at high current levels, the surface area required to collect electrons may be too large to be practical and since the surface of a plasma plume can serve both as an electron collector and emitter a dense plasma plume is proposed as the preferred space plasma coupling element for both electron collection and emission. Such a plume can be produced by a hollow cathode when the circuit between the dense plasma surface it produces and the end of the tether is completed through one of its electrodes.

In order to produce a plasma plume it is generally necessary to supply some gas from which the plasma can be produced. An efficient plasma contactor should require very little expellant gas and operating power to make a good electrical connection and should be able to handle very large currents. Recent ground-based experiments have indicated that the most restrictive limitation on effective plasma coupling is induced by space charge effects which result in the formation of sheaths across which substantial voltage drops can occur.[4] Hence achieving effective plasma contactor operation can be translated into the requirement to limit these voltage drops to acceptable levels without requiring an excessive consumption of expellant and/or operating power. These same experiments have suggested that the hollow cathode discharge device developed for electric propulsion applications can be an effective plasma contactor that meets this requirement. Both ground and space experiments have demonstrated that the hollow cathode functions effectively as an electron emitter in its original configuration;[5] however, some modification may be required to improve its electron collection capabilities. The focus of this study has been, therefore, on the electron collection mode of hollow cathode contactor operation.

Experimental results obtained will be correlated with the predictions of a simple theoretical model describing the voltage drop developed across a double sheath at a given current flow condition.[6] This model neglects the effects of collisions but considers the effects of both ions and electrons which counterflow under the influence of the applied potential difference to supply the total current demanded. While the contribution of the ions to the current that flows is small their effect is substantial because they tend to mitigate the space charge limitation imposed on the electrons thereby allowing them to conduct more current.

Apparatus and Procedure

In order to investigate the current/voltage characteristics of plasma contactors the apparatus shown schematically in Fig. 1 has been set up. The essential elements of the apparatus are the simulator used to generate a dilute, simulated space plasma and the plasma contactor to be tested. These two elements are contained within a 1.2 m diameter by 5.3 m long stainless steel vacuum tank with the contactor located near one end and the simulator located 2.7 m downstream of it near the middle of the tank. Both the simulator and the contactor are hollow cathode devices. Both are equipped with a heater power supply used to facilitate startup and an anode power supply required to sustain a discharge and thereby produce the plasma adjacent to

*Work supported by NASA Lewis Research Center and NASA Johnson Space Center under grants NGR-06-002-112 and NAG 9-120.
**Professor, Department of Mechanical Engineering.
+Research Assistant, Department of Mechanical Engineering.

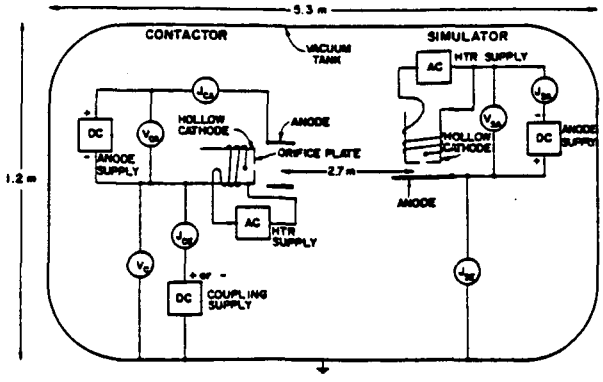

Fig. 1 Test apparatus schematic

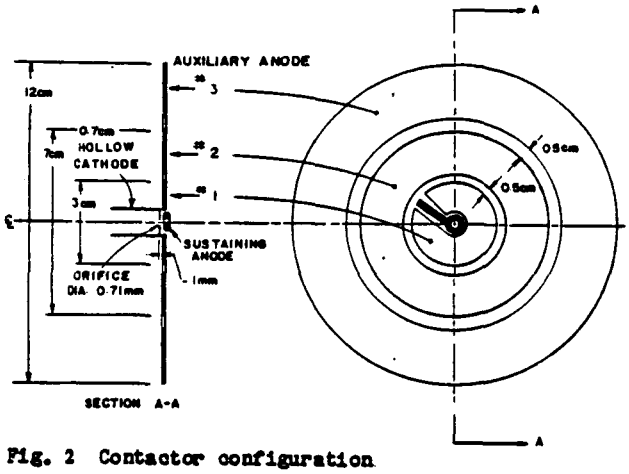

Fig. 2 Contactor configuration

the hollow cathode that can couple to the simulated space plasma. The coupling power supply shown in Fig. 1 is bimodal and can be used to bias the contactor either positive or negative of the vacuum tank. The simulator anode is connected to the vacuum tank to provide a return current path for current either supplied from or to the tank and/or dilute simulator plasma. While the simulator anode has been connected in this way to minimize the current flow between the tank wall and the simulated plasma, recent tests have shown that the simulator cathode must be connected to the tank when large electron collection currents are being demanded by the contactor under test (i.e. when the contactor emission current, J_{CE}, is greater than the simulator anode current, J_{SA}). These same tests have shown, however, that the coupling between the contactor and the simulated plasma is not affected measurably by which connection (simulator anode or cathode) is made to the tank. For the tests described here the simulator anode will be connected to the tank unless noted otherwise.

An emissive probe that can be swept through the region between the contactor and simulator to measure plasma potential as a function of position is also available although it is not shown in Fig. 1. It consists of a 0.08 mm diameter tungsten wire heated to thermionic emission temperatures by a floating battery power supply connected in the manner suggested in Ref. 7. This probe can be moved along the centerline joining the contactor and simulator and along paths parallel to this centerline at radii varying from 0 to 30 cm. At each operating condition the contactor anode voltage and current, V_{CA} and J_{CA}; the contactor coupling voltage, V_C; the contactor emission current, J_{CE}; the simulator anode voltage and current, V_{SA} and J_{SA}; and the simulator emission current, J_{SE}, are measured using the meters shown schematically in Fig. 1.

The hollow cathode contactor used for the study to be described here is shown in Fig. 2. It includes a 7 mm diameter tantalum tube electron beam welded to a thoriated tungsten orifice plate with a 0.7 mm diameter orifice in it. The low work function emissive surface within the cathode tube is made of thin (0.008 mm) rolled, tantalum foil treated with chemical R-500. The anode, which is located 1 mm downstream of the orifice plate, is segmented in the manner suggested by Fig. 2 into four sections. The sustaining anode shown is 5 mm in inside diameter and 1 cm in outside diameter. The various auxiliary anodes shown can be allowed to float or they can be switched independently to anode potential so the effect of increasing the anode diameter from 1 cm to 3 cm, 7 cm, and 12 cm can be studied. The simulator shown in Fig. 1 utilizes the same hollow cathode as the one just described but it utilized a single, flat plate, tantalum anode 2 cm in diameter positioned 1 mm downstream of the orifice plate. This anode does not have an orifice in it, and the entire simulator assembly is oriented with its axis at right angles to the centerline joining the contactor and simulator. It is believed that this orientation and anode configuration causes the plasma produced by the simulator to spread out into a diffuse plume extending through the tank rather than being concentrated at and directed through an anode orifice. For all tests to be described here, the simulator hollow cathode was sustained with a 1.4 standard cubic centimeter per minute (sccm) xenon flowrate and an anode current, J_{SA}, of 0.3 A. At this flow and anode current condition the simulator anode voltage, V_{SA}, was about 12 volts and the simulator produced a plasma having a density between 10^5 and 10^6 cm^{-3} in the region midway between the simulator and the contactor.

Results

When contactors like the one shown in Fig. 2 operating at constant anode current and constant flowrate are biased with respect to the simulator plasma and tank, an electron emission current versus contactor potential curve like the one shown in Fig. 3 is measured. Characteristic contactor performance curves similar to this one have been measured for a wide range of flowrates, anode currents, anode sizes, and contactor configurations. These curves all show that substantial electron emission currents (of order 1A) are measured when the contactor potential is less than about -30 volts. Contactor potential as used here is the potential of the contactor anode measured relative to the simulator anode and tank (i.e. $V_C + V_{CA}$). It should be noted that contactor potential is actually a potential difference and it is greater than the potential difference between the contactor anode and the simulated space plasma potential. In the second quadrant region where contactor potentials are negative, electrons are being emitted from the hollow cathode and ions are being drawn from the simulated space plasma. When the contactor is biased positive of the tank, on the other hand, it begins to collect electrons from the simulated space plasma and emit ions generated in the hollow cathode discharge. The electron collection curve associated with this process,

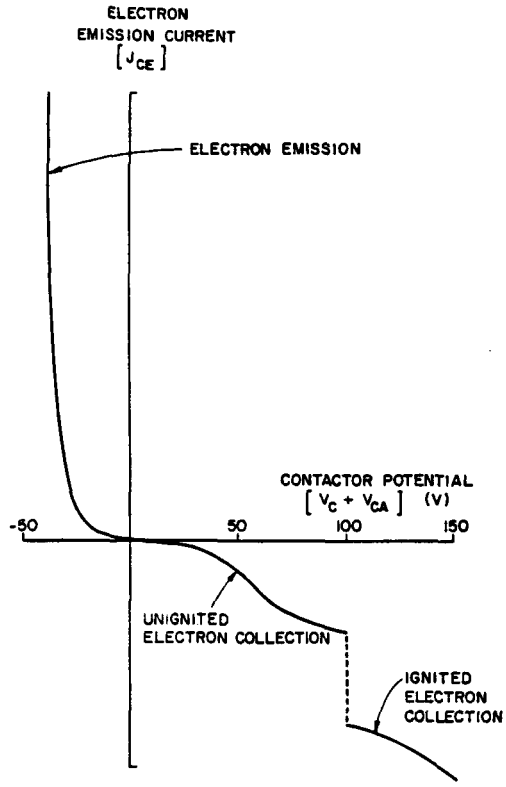

Fig. 3 Generalized hollow cathode contactor current/voltage characteristic

which is shown in generalized form in the fourth quadrant in Fig. 3, shows considerably more structure than the electron emission portion of the curve. As contactor potential is increased from low positive values the electron collection current begins to increase in both magnitude and absolute gradient until some limiting phenomenon begins to slow down the gradient of electron emission with contactor potential and the curve levels out. The point at which the slope of the electron collection curve inflects and begins to level out is determined by such factors as the contactor anode current and the contactor flow rate and it may be that the contactor voltage at which it occurs is determined by the rate at which ions are being produced in the region of the contactor discharge.

At contactor potentials of the order of 100 volts the contactor has been observed to undergo a transition from what might be termed the unignited mode to the ignited mode of electron collection. This transition, which is accompanied by the appearance of a visible plume within which expellant excitation and presumably ionization are occurring, is most likely to occur in contactors utilizing anodes having a large diameter. The visible plasma plume associated with ignited mode operation usually extends downstream of this anode a few tens of centimeters. Again the point at which transition to ignited electron collection occurs is dependant on hollow cathode operating conditions. For example this transition may occur before or after the unignited electron collection curve begins to level out.

A typical electron collection portion of a contactor characteristic curve illustrating the conditions associated with a transition to the ignited mode is shown by the solid curve in Fig. 4. In this case it is observed that contactor potential actually decreases markedly as the electron collection current increases into the few hundred milliamp range during the transition. This curve is also useful because it illustrates the perturbing effect of the vacuum tank wall which become increasingly important as contactor potential is increased. This is seen by recognizing that the solid line in Fig. 4 is the measured electron current collected by the contactor while the dotted line is the electron current emitted from the simulator. If the tank is not affecting the test these two currents should agree, and at voltages below about 80 volts these two currents are observed to be in relatively good agreement. However, above this voltage they begin to depart substantially. The departure suggests that electrons are being received by the contactor from some source other than the simulator plasma presumably the tank wall. In fact at voltages above about 100 volts arcs can be seen jumping randomly over the tank surface near the contactor. These arcs produce noise on the instrumentation and it is suggested they also serve as a source of electrons collected at the contactor from other than simulated plasma. They therefore introduce an error in the measured contactor emission current. The extent of this error is a function of the particular contactor being used; in the present case it reaches a maximum of about 50 mA which in the ignited electron collection mode implies an error of about 10%. For the data presented in this paper the contactor voltage was limited so this error did not exceed 10%.

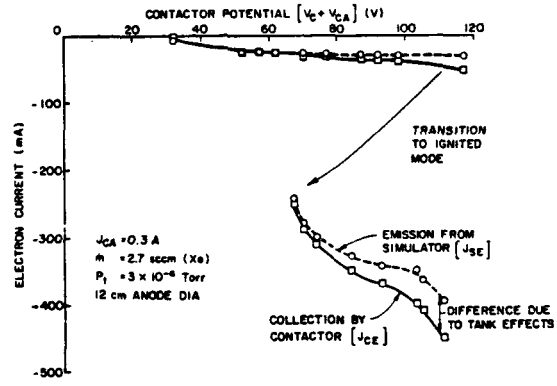

Fig. 4 Typical current balance comparison

When the contactor is operated in the electron collection mode the plasma potential profile along the centerline joining the contactor and simulator has the general shape shown in Fig. 5a. This figure shows that the plasma potential at the contactor is near contactor anode potential and that it remains at this potential as one moves downstream to the point r_u. Between the points r_u and r_d the potential drops by V_S because of the double sheath that develops at the prevailing current condition. Beyond the location r_d the potential changes very slowly until it drops rapidly to simulator anode potential through an electron extraction/ion collection sheath that develops adjacent to the simulator. The region between the double sheath and the simulator in Fig. 5 shows a small potential drop that could develop because of collisional effects or magnetically induced impedance but slight potential increases and negligible potential gradients have also been observed in this region. It is noted that

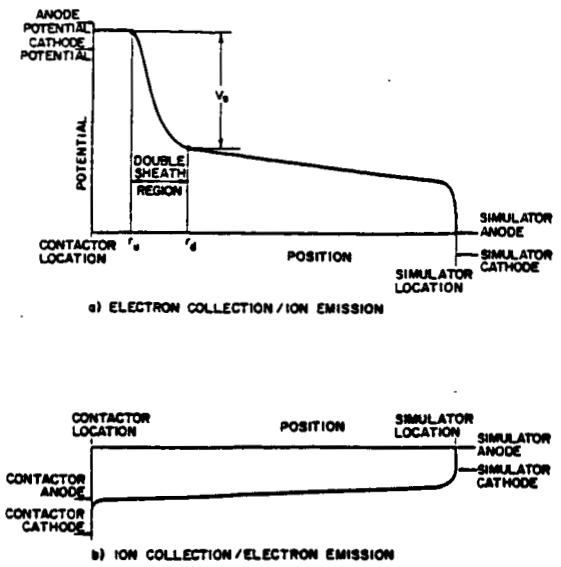

Fig. 5 Generalized plasma potential profiles

the potential profile shown in Fig. 5 cannot be measured continuously using the emissive probe because this probe can only be swept from the contactor to a point one meter downstream of it. Its shape has been constructed from potential profile data measured on a hollow cathode being operated in the electron emission and then the electron collection modes. Figure 5b shows the generalized potential profile for a contactor operating in the electron emission mode. In this case the plasma adjacent to the contactor is near anode potential and the potential changes only slightly with position until the bulk of the potential rise occurs near the simulator.

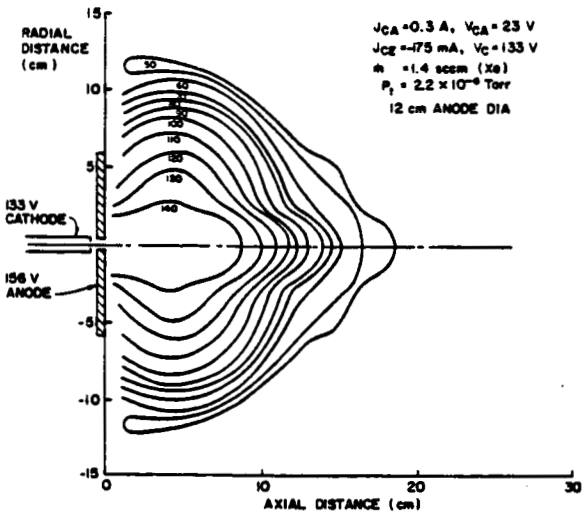

Fig. 6 Potential contour map-ignited electron collection mode

When several potential profile sweeps are made at various radii from the centerline of the contactor the potential contour map like the one shown in Fig. 6 can be constructed. These data were obtained with the 12 cm dia anode configuration at a contactor anode current of 0.3 A and a 1.4 sccm xenon flow-rate ($\dot{m}$) that induced a tank pressure (P_t) of 2×10^{-6} Torr. These operating conditions resulted in a contactor anode voltage that was 23 v above the contactor cathode potential and an electron collection current from the contactor of 175 mA when the contactor cathode was 133 v above the vacuum tank reference potential. These contours suggest that the potential is relatively uniform in the vicinity of the high density plasma associated with the contactor and that it drops relatively rapidly from about 140 v down to 50 v. At 50 v there is a well located about 17 cm downstream of the contactor anode and then the potential rises again and remains between 50 and 60 v until the limit of probe extensions is reached at the 1 m downstream location. The fact that the contours take on a spherical or hemispherical shape suggests that electrons are flowing nearly radially inward and ions are flowing nearly radially outward from the high density plasma within the 140 v contour.

The voltage/current characteristic curve for the contactor of Fig. 2 with the 12 cm dia anode coupling to the simulated plasma at the indicated operating conditions is shown in Fig. 7. The contactor anode voltage varied as the electron emission current was varied but was generally in the range of 10 to 15 v. As suggested previously this contactor exhibits high electron emission current at a relatively modest negative contactor potential around -60 v. Biasing the contactor positive about 80 v results in a modest electron collection current of a few tens of milliamperes but beyond this the transition to the ignited mode of electron collection occurs and electron currents of the order of a few hundred milliamps are collected. It should be noted that the contactor potentials plotted on the hor-

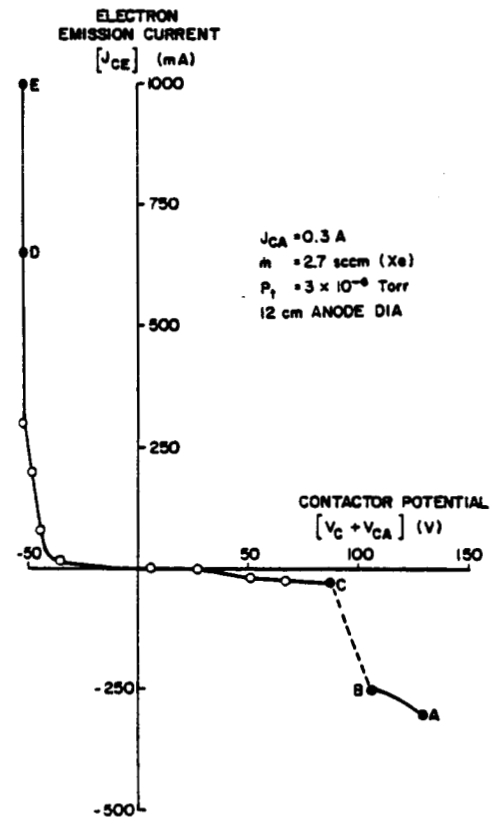

Fig. 7 Typical contactor voltage/current characteristic

izontal axis of Fig. 7 do not correspond to the potential differences that would exist between the contactor anode and a space plasma. This is the case because the contactor potential as defined in this figure involves coupling through both the contactor and the simulator so it always involves coupling through two devices, one emitting electrons and one collecting them.

At each of the solid data points identified by letter in Fig. 7 plasma potential profiles downstream of the contactor and on the centerline joining the contactor and simulator were measured using the emissive probe. These profiles are identified in Fig. 8 by the same letters. Under conditions of electron emission (curves D and E) the potential profiles are observed to be quite flat except immediately adjacent to the contactor, i.e., within about 5 cm, where a voltage drop indicative of a sheath is observed to exist. This must be a double sheath which develops as the contactor emits electrons to and draws ions from the simulated plasma, but the sheath is located close to the contactor and its detailed structure is not apparent. Under conditions of electron collection (curves A, B and C) the profiles are observed to be quite different. In general these curves show a region of relatively constant plasma potential adjacent to the contactor followed by a region of steep potential variation and a final region in which the potential is relatively constant. These curves are consistent with the contour potential map of Fig. 6 which was measured under conditions of electron collection. It is apparent from examining the curves of Fig. 8 that an emissive probe positioned 1 m downstream of the contactor is downstream of the double sheath and so one can measure the potential drop through the sheath by measuring the potential drop between the anode and the emissive probe at this location. When this is done a voltage/current characteristic curve like the one shown in Fig. 9 is obtained. This curve shows the actual potential drop between the contactor anode and the ambient plasma and it shows that these actual potential drops across the double sheath are

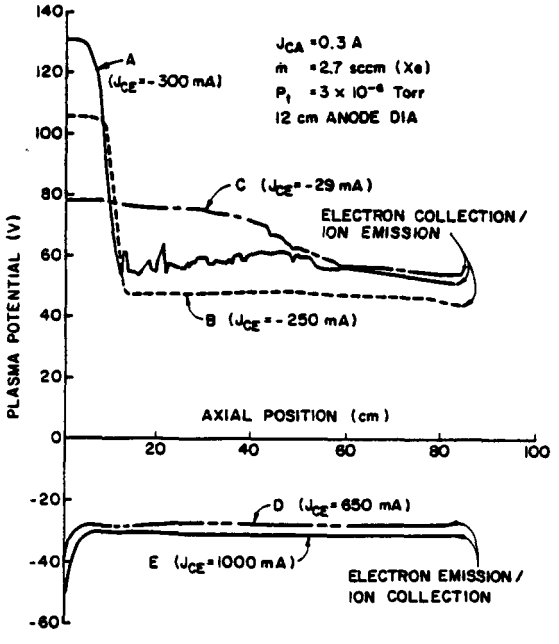

Fig. 8 Typical centerline potential profiles

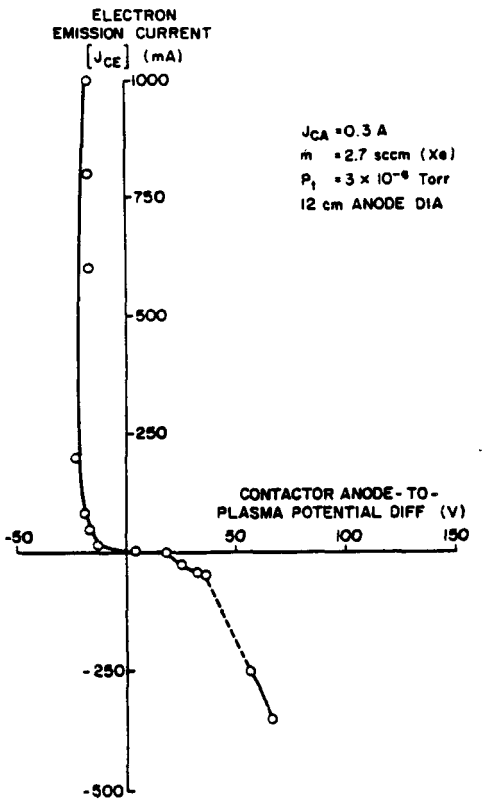

Fig. 9 Typical contactor anode-to-ambient plasma potential/current characteristic

considerably less than the contactor potentials plotted on the horizontal axis of Fig. 7. Comparison of Figs. 9 and 7 shows that the potential drop across the double sheath in the electron collection region is actually about one-third of the contactor potential and the potential drop across the double sheath in the electron collection region is two-thirds to one-half of the contactor potential. Thus the abscissa data on Fig. 9 represent the actual potential drop between the anode and the actual space plasma or the true voltage difference associated with contactor operation in the electron emission and electron collection modes. At the low-power, low-flowrate operating condition which has been used for the data presented here, Fig. 9 indicates that this contactor can operate over the range from 1 A of electron emission to few hundred milliamps of electron collection when the potential difference between it and the ambient plasma varies through a range less than 100 v.

Comparison of Theory with Experiment

Since the typical sheath contours of Fig. 6 were somewhat spherical and the potential difference across the sheaths could be measured using the emissive probe the experimentally measured data could be compared to the predictions of the simple, spherical double-sheath model developed in Ref. 6. The basis of the model is illustrated in Fig. 10 which shows an inner spherical surface of radius r_1 and potential V_1 supplying a current of particles from an infinite supply of zero velocity particles of mass m_1 on the inner surface. At the same time particles having the opposite charge of those coming from the inner surface are drawn from an infinite supply of

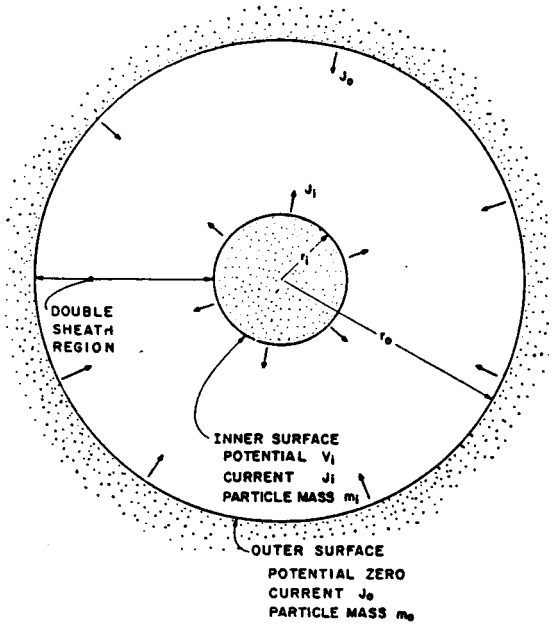

Fig. 10 Theoretical model configuration

zero velocity particles of mass m_o on the outer spherical surface of radius r_o at zero potential. When equations describing conservation of energy and conservation of charge are used in conjunction with Maxwell's formulation of Gauss' Law, equations describing the maximum flow of charged particles from the inner sphere, J_i, and from the outer sphere, J_o, in terms of the applied potential difference and the radius ratio of the two spheres can be obtained. These limiting maximum currents which are achieved when the potential gradients at the edges of both spherical surfaces are zero, are given by

$$J_o = 4\pi\varepsilon_o V_i^{3/2} \sqrt{\frac{2e}{m_o}}\, j_o(r_i/r_o) \qquad (1)$$

$$J_i = \frac{J_o}{\alpha(r_i/r_o)} \sqrt{\frac{m_o}{m_i}} \qquad (2)$$

where α and j_o are parameters that depend only on the radius ratio r_i/r_o. It is interesting to note that the currents flowing from the inner and outer spherical surfaces are dependent only on the radius ratio and not on the absolute magnitude of these radii. The variation of the parameters α and j_o with radius ratio have been determined numerically and these relationships are shown in Figs. 11 and 12 which have been reproduced from Ref. 6.

In order to determine the extent to which the model just outlined describes the physical behavior that occurs in the plasma contacting processs, a number of potential profiles like those shown in Fig. 8 for the electron collection/ ion emission mode of operation were analyzed. The method by which this analysis was carried out can be understood by reconsidering Fig. 5a. The quantities that need to be determined are the experimentally measured voltage drop across the sheath which is designated V_s in Fig. 5a, and the experimentally determined radii associated with the upstream and downstream boundaries of the double-sheath region r_u and r_d. This was accomplished by defining the upstream and downstream boundaries as the points of minimum and maximum second derivative of the potential with respect to position respectively. Using the measured potential drop, V_s, together with the measured electron emission current, J_{CE}, the normalized current from the outer surface j_o could be computed by substituting $V_i = V_s$ and $J_o = J_{CE}$ into Eq. 1.

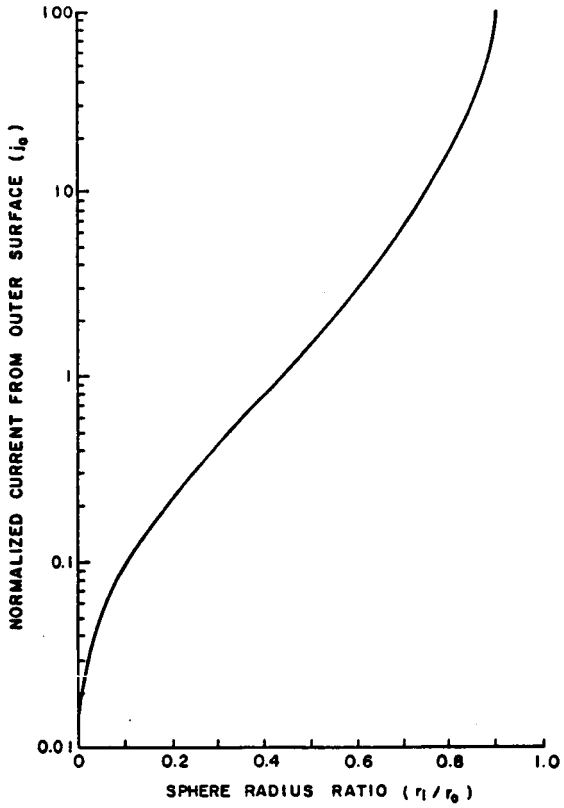

Fig. 11 Effect of radius ratio on space-charge-limited current factor

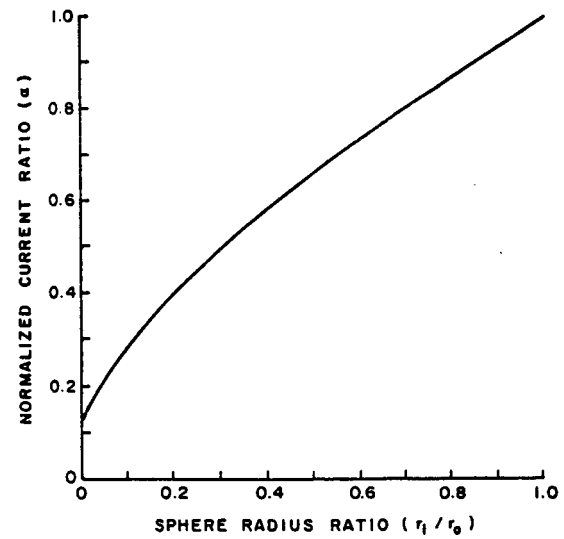

Fig. 12 Effect of radius ratio on counterflowing current ratio

This value of j_o could then be used to enter Fig. 11 and determine the theoretical sphere radius ratio r_i/r_o predicted for collection of the current J_{CE} at a sheath potential drop V_s. This theoretically based radius ratio could then be compared to the measured radius ratio r_u/r_d. A typical example of a comparison of the actual potential profiles measured and then computed using equations from Ref. 6 is shown in Fig. 13. In this case the electron current from the outer sphere, $J_{CE} = J_o$, was 250 mA, the potential drop across the double-sheath, $V_s = V_i$, was 103-48 = 55 v and the normalized electron current from the outer sphere j_o was 8.96. From Fig. 11, this value of j_o corresponds to theoretically based radius ratio (r_i/r_o) of 0.73 compared to the experimental value of $r_u/r_d = 7.8/12.8 = 0.61$ determined using the solid profile in Fig. 13.

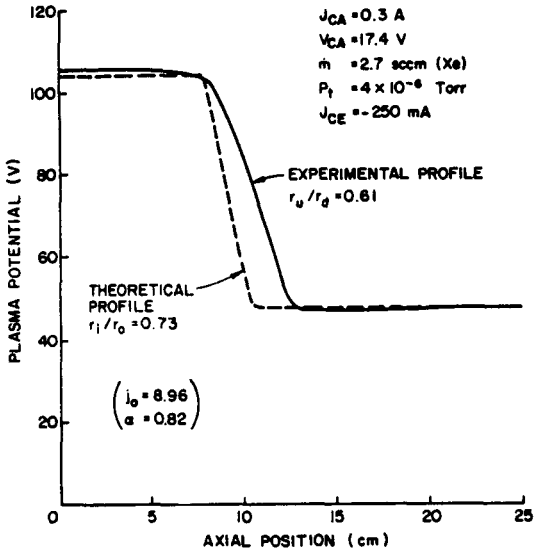

Fig. 13 Typical comparison of measured and predicted potential profiles

Hence the theory predicts a profile that is steeper than the experimentally measured one as the figure shows.

A comparison of experimental and theoretically determined radius ratios obtained in the manner just described over a wide range of operating conditions is presented in Fig. 14. To obtain these data the anode diameter was allowed to vary from 1 to 12 cm, the hollow cathode discharge power was varied from 0 to 17 watts, the xenon flowrate was varied from 1.2 to 6.8 sccm and this also resulted in tank pressure variations from 2 to 10 x 10^{-6} Torr. The extent to which the theoretical model describes the physical results is reflected in the proximity of the data points to the solid, perfect-fit line in Fig. 14. Examination of the data in this figure suggests that the predicted radius ratios agree with the measured ones to within about 25% and that the predicted ratios are systematically greater than the measured ones. It is noted that the points that fall below the -25% error boundary are ones that were obtained either under conditions where significant electron current was being drawn from the tank (~10%) or where extra expellant other than that through the hollow cathode orifice was being fed into the vacuum chamber to increase the tank back pressure. Operation of either of these conditions could be expected to cause the theoretical development to be in error because both electron emission from any point other than the outer sphere and the effects of collisions have been neglected in the theoretical model.

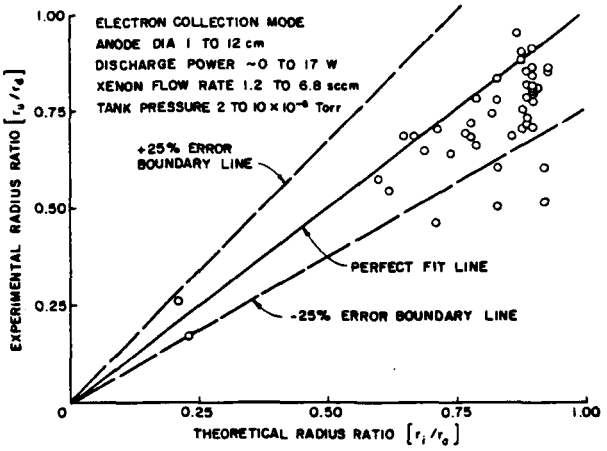

Fig. 14 Radius ratio comparison for spherical model

Reconsideration of the potential contour map of Fig. 6 suggests that it might be more appropriate to consider the current flow process to be occurring between hemispherical rather than spherical surfaces. In order to investigate this the equations developed in Ref. 6 were redeveloped and the current flowing from the outer sphere was determined to be given by

$$J_o = 2\pi\varepsilon_o V_i^{3/2} \sqrt{\frac{2e}{m_o}}\, j_o(r_i/r_o) \ . \qquad (3)$$

When this equation was applied to the same data as that used to obtain the results of Fig. 14 results presented in Fig. 15 were obtained. Since these data appear to be skewed further from the perfect fit line than results of Fig. 14 it was concluded that disagreement between the theory and experiment

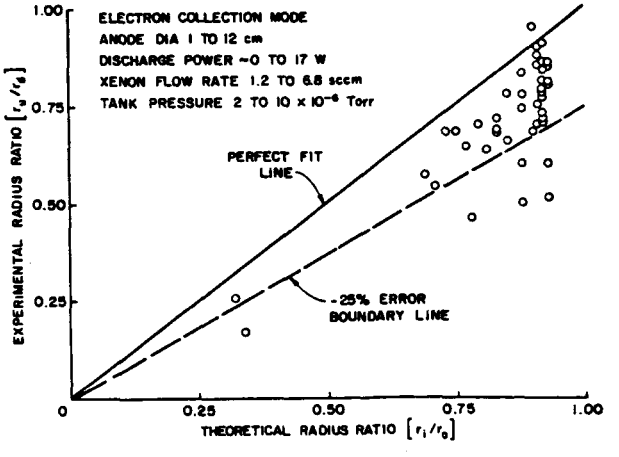

Fig. 15 Radius ratio comparison for hemispherical model

could not be explained on the basis of double-sheath development over a spherical surface less than 4π steradians in solid angle.

Limitations Observed at High Current Operating Conditions

The early experiments conducted on hollow cathode plasma contactors at Colorado State University involved electron collection currents that were small compared to the contactor anode current, J_{CA}, and the simulator anode current, J_{SA}. Use of a large diameter flat plate anode (especially the 7 and 12 cm dia configurations achievable with the apparatus of Fig. 2) changed this, however, and facilitated transition to the ignited electron collection mode where current levels that approached the contactor and simulator anode currents were measured. While operating in the electron emission mode and at high current, detailed current balances were made which showed the obvious, namely that electrons are emitted from hollow cathodes and collected by anodes. It was concluded from the current balances that ignited mode electron collection at a fixed simulator anode current, J_{SA}, caused the simulator electron emission current, J_{SE}, to be limited to $J_{SE} \leq J_{SA}$ when the simulator anode was connected to the tank in the manner shown in Fig. 1. Connecting the simulator cathode directly to the tank alleviated this problem and made it possible to emit large simulator electron currents from the cathode ($J_{SE} > J_{SA}$) while holding the simulator anode current constant. One might expect the electron current collection capability of the simulator would be limited when the tank connection is made to the simulator cathode, but test results show that the tank with its large surface area collects most of the electrons emitted by the contactor when it is operating in the electron emission mode. As a consequence test results measured for the contactor operating in the electron emission mode are essentially the same for both the tank/simulator cathode and tank/simulator anode connections.

Because electrons are emitted from the contactor hollow cathode in the emission mode and collected by the contactor anode in the collection mode the electron current being collected is also limited to $J_{CE} \leq J_{CA}$ when the contactor is connected in the manner shown in Fig. 1. On the other hand electron current being emitted does not pass through the anode power supply and/or the associated meter (J_{CA}) so it can exceed the contactor anode current. This means that the only way to realize operation at high electron collection currents using the configuration of Fig. 1 is to allow the contactor anode current (J_{CA}) to increase along with the current collected at the contactor anode. This has been done in the case of the data given in Fig. 16. This plot of electron emission current vs. contactor anode-to-simulated space plasma potential shows that a contactor electron collection current of 0.9 A can be achieved readily if the contactor anode current is also increased to 0.9 A.

It should be noted that contactor reversibility between high current levels of electron emission and electron collection is desirable in electrodynamic tether applications. The results just cited suggest this would require a high anode current level with attendant high power demand on the contactor anode power supply if either the contactor cathode was connected to the tether while the contactor was collecting electrons or if the contactor anode was connected to the tether while the contactor was emitting electrons. This problem could be alleviated, however, by connecting the end of the tether to the anode during periods of high current electron collection and switching this connection to the cathode during periods when tether operation was reversed and the contactor was emitting electrons. Thus it may be necessary to provide a tether switching capability to accommodate high current reversible tether operation.

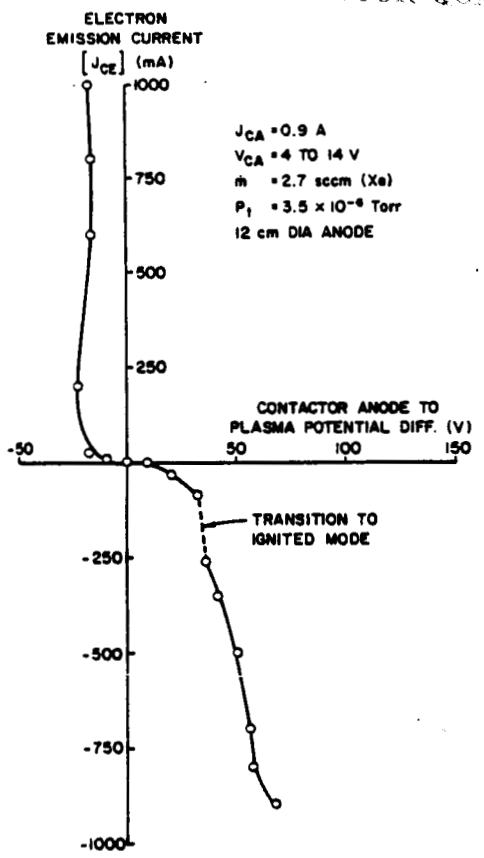

Fig. 16 Contactor anode-to-ambient plasma potential/current characteristic at high contactor anode current

Conclusions

The results presented have confirmed previous data that show substantial electron currents (~1 A) can be emitted under the influence of modest negative contactor bias potentials (~20 v below simulated plasma potential). These driving potential differences are about one-third of the contactor potential difference developed between the contactor and simulator anodes. In the electron collection mode of operation, substantial gains in the electron current that can be collected from the plasma are realized when the contactor is allowed to run in the ignited mode. When operating in this mode electron currents of several hundred milliamps can be collected at plasma-to-contactor anode potential differences of about 60 volts. This potential difference is two-thirds to one-half of the contactor anode-to-simulator anode potential difference which has typically been used to characterize the driving potential associated with contactor operation. Under conditions of electron collection a simple model which accounts for the development of a

space-charge-limited double-sheath can be used to achieve reasonable correlations with the experimental data. These results suggest that a space-charge-limited double sheath develops and limits the current that can flow between a contactor and a simulated space plasma under the influence of a given driving potential difference.

Because electrons which are the dominant charge carriers are emitted from a contactor hollow cathode and collected on its anode, it is desirable to have a large contactor anode. Such an anode facilitates electron collection in the ignited mode where the level of current collection can be enhanced over that obtained in the unignited mode. For a contactor operating on the end of a high current tether it may be desirable to switch the tether connection from the contactor anode to the contactor hollow cathode if it becomes necessary to reverse the direction of current flow in the tether as the contactor switches between the electron collection and electron emission modes of operation.

References

1. Hendrickson, R.A., "The Electron Echo Experiment Observations of the Charge Neutralization of the Rocket and Analysis of the Echos from Electrons Artificially Injected into the Magnetosphere," Cosmic Physics Tech. Report No. 160; also Ph.D. thesis, Univ. of Minn., Dec. 1972.

2. Cohen, H.A. and Lai, S., "Discharging the P78-2 Satellite Using Ions and Electrons," AIAA Paper 82-0266, AIAA 20th Aerospace Sciences Mtg., Orlando, FL, 1982.

3. Purvis, C.K., R.O. Bartlett and S.E. DeForest, "Active Control of Spacecraft Charging on ATS-5 and ATS-6," Proceedings of Spacecraft Charging Technology Conference, Feb. 1977, eds. C.P. Pike and R.R. Lovell, NASA TMX-73537, pp. 107-120.

4. Wilbur, P.J. and T.G. Laupa, "Plasma Contactor Design for Electrodynamic Tether Applications," Committee on Space Research Conference, Toulouse, France, 2 July 1986, Paper 1.5.5.

5. Keralake, W.R., Goldman, R., and Nieberding, R.G., "SERT II: Mission, Thruster Performance and In-Flight Thrust Measurements," J. Spacecraft and Rockets, vol. 8, no. 3, pp. 213-224, 1971.

6. Wei, R. and P.J. Wilbur, "Space-charge-limited Current Flow in a Spherical Double Sheath," J. Appl. Phys, v 60, 1 Oct. 1986, pp. 2280-2284.

7. Aston, G., "Ion Extraction from a Plasma," NASA CR-159849, June 1980, also Ph.D. thesis, Colorado State University, pp. 12-19.

DISTRIBUTION LIST

	Copies
National Aeronautics and Space Administration Washington, DC 20546 Attn:	
Mr. Edward J. Brazill, Code MT	1
Mr. Thomas D. Stuart, Code MK	1
Dr. Stanley Shawhan, Code ES	1
Dr. L.R. Owen Storey, Code ES	1
Mr. George Levine, Code MTF	1
Mr. Ivan Bekey, Code Z	1
Mr. John L. Anderson, Code RS	1
National Aeronautics and Space Administration Lewis Research Center 21000 Brookpark Road Cleveland, OH 44135 Attn:	
Technology Utilization Office, MS 7-3	1
Report Control Office, MS 60-1	1
Library, MS 60-3	2
Dr. M. Goldstein, Chief Scientist, MS 5-9	1
Mr. Dave Byers, MS 500-219	1
Mr. Jim Stone, MS 500-219	1
Mr. Vince Rawlin, MS 500-220	1
Ms. Carolyn Purvis, MS 302-1	1
Mr. Joseph C. Kolecki, MS 302-1	10
Mr. Michael Patterson, MS 500-220	10
National Aeronautics and Space Administration Lyndon B. Johnson Space Center Houston, TX 77058 Attn:	
Dr. James E. McCoy, Code SN3	1
National Aeronautics and Space Administration Marshall Space Flight Center Huntsville, AL 35812 Attn:	
Mr. J. H. Laue, Mail Code FA31	1
Mr. Chris Rupp, Mail Code PS04	1
Mr. James K. Harrison, Mail Code PS04	1
NASA Scientific and Technical Information Facility P.O. Box 8757 Baltimore, MD 21240 Attn:	
Accessioning Dept.	1

	Copies
Dept. of the Navy Office of Naval Research Universiy of New Mexico Bandolier Hall West Albuquerque, NM 87131 Attn:	
G. Max Irving	1
Procurement Executive, Ministry of Defense Royal Aircraft Extablishment Farnborough, Hants GU14 6TD ENGLAND Attn:	
Dr. D. G. Fearn	1
United Kingdom Atomic Energy Authority Culham Laboratory Abingdon, Oxfordshire OX143DB ENGLAND Attn:	
Dr. A. R. Martin (Rm F4/135)	1
Defense Nuclear Agency DNA/RAEV Washington, D.C. 20305-1000 Attn:	
Captain Daniel Allred	1
General Research Corporation Aerospace Systems Group 7655 Old Springhouse Road McLean, VA 22102 Attn:	
Mr. William A. Baracat	1
Intelsat M.S. 33 3400 International Dr. N.W. Washington D.C. 20008-3098 Attn:	
Mr. Rolland Schreib	1
Air Force Astronautics Lab Edwards AFB, CA 93523 Attn:	
LKDH/Lt. Robert D. Meya, MS 24	1
LKDH/Lt. Phil Roberts, MS 24	1
Jet Propulsion Laboratory 4800 Oak Grove Laboratory Pasadena, CA 91102 Attn:	
Technical Library	1
Dr. Paul Penzo, Code 1156-217	1
Dr. Stephen Gabriel	1

	Copies
TRW Inc. TRW Systems One Space Park Redondo Beach, CA 90278 Attn:	
Mr. Neal Holkower	1
Dr. Rob Stillwell	1
National Aeronautics and Space Administration Ames Research Center Moffett Field, CA 94035 Attn:	
Technical Library	1
Mr. Larry Lemke, Mail Code 244-4	1
National Aeronautics and Space Administration Langley Research Center Langley Field Station Hampton, VA 23365 Attn:	
Technical Library	1
Mr. George Wood, Mail Code 234	1
Hughes Research Laboratories 3011 Malibu Canyon Road Malibu, CA 90265 Attn:	
Dr. Jay Hyman, MS RL 57	1
Dr. J. R. Beattie, MS RL 57	1
Dr. J. N. Matossian, MS RL 57	1
Rocket Research Co. P.O. Box 97009 Redmond, WA 98073-9709 Attn:	
Mr. William W. Smith	1
Mr. Paul Lichon	1
Mr. Lee Parker 252 Lexington Road Concord, MA 01741	1
Department of Aeronautics and Astronautics Massachusetts Institute of Technology Cambridge, MA 02139 Attn:	
Dr. Daniel E. Hastings, Rm 37-441	1
Institute for Space and Aeronautical Science 4-6-1 Komaba, Meguro-ku, Tokyo, 153, JAPAN Attn:	
Prof. K. Kuriki	1
Prof. T. Obayashi	1

	Copies
Tokai University Kitakauame, Hiratsuka, Kanagawa, JAPAN Attn:	
Prof. K. Hirao	1
Physics Department Naval Postgraduate School Monterey, CA 93943-5000 Attn:	
Dr. Chris Olson, Mail Code 61-0S	1
Martin Marietta Aerospace P. O. Box 179 Denver, CO 80201	1
Attn:	
Dr. Kevin Rudolph, MS MO482	1
Systems, Science and Software P. O. Box 1620 LaJolla, CA 92038	1
Attn:	
Dr. Ira Katz	1
Dr. Victoria Davis	1
W. J. Schafer Assoc. Inc. 1901 North Fort Meyer Dr., Suite No. 800 Arlington, VA 22209 Attn:	
Dr. Herbert Cohen	1
Dr. Robert Vondra	1
Electric Propulsion Laboratory, Inc. St. Rt. 2, Box 3406A Tehachapi, CA 93561 Attn:	
Dr. Graeme Aston	1
Dr. John R. Brophy	1
Mr. Joe Carroll Energy Science Laboratories 11404 Sorrento Valley Rd., #112 San Diego, CA 92121	1
Instituto du Fisica dello Spazio Interplanetario Consiglio Nazionale dello Richerche Via G. Galilei 00044 Frascati, ITALY Attn:	
Dr. Marino Dobrowolny	1
Dr. Carlo Bonifazi	1
Dr. Luciano Iess	1
Mr. Giuliano Vannaroni	1

	Copies
Science Applications International Corp. 13400 B Northrop Way #36 Bellevue, WA 98005 Attn:	
Dr. Hugh Anderson	1
Starlab/SEL Stanford University Stanford, CA 94305 Attn:	
Dr. Peter Banks	1
Dr. Roger Williamson	1
Science Applications International Corp. Plasma Physics Division 1710 Goodridge Drive McLean, VA 22102 Attn:	
Mr. Edward P. Szuszczewicz	1
University of Alabama (Huntsville) Electrical and Computer Engineering Dept. Engineering Building Huntsville, AL 35899 Attn:	
Dr. Michael Greene	1